JOURNAL OF MADENAT ALELEM COLLEGE

REFEREED SCIENTIFIC JOURNAL Published
by the University College of Madenat al-elem , Iraq , Baghdad , AlKadmyia

Vol:4 No:2 year: 2012 ISSN: 2073-2295

كلية مدينة العلم الجامعة

Madenat Alel em Uni versity College

مجلة كلية مدينة العلم

العراق - بغداد - الكاظمية المقدسة

Journal of Madenat Al-elem College
(JMAC)

E-mail: Jmac2009m@yahoo.com

P.O,Box (9216) Tel:5238850

WWW.madenatalelem.com

INSTRUCTIONS to AUTHERS

Submitted articles to the Journal of Madinat Al-Elem University College can be published in all fields related to the Academic Departments of the College (Biology, Law, programming Engineering Sciences, and Computer Techniques Engineering).

Written request for publication and signing a consent form to publish must be for articles which have not been published or submitted for publication to other journals. Three copies with CD are needed. Manuscripts should be typed on: A4 white paper, double spaced, written in Times New Roman font size 14. Margins should be 3cm from top, bottom, left and right. The main title should be in: bold Times New Roman font size 14. Author names should be written in the following sequence: first name, middle name, the family name, followed by the names of departments and institutions of work. A footnote accompanies the first page stating the full address of correspondence author.

Articles need to contain the following items:

- Abstract in English and Arabic not more than 300 words.
- Article includes the following items: Introduction, Materials and Methods, Results and Discussion, Conclusion and References.
- References should be numbered in the text according to the sequence appeared in the text and listed in order.
- Tables and figures should be appropriately titled with size not exceed an A4 page.

The editor reserves the right to reject or accept any article submitted.

Contents

6 **Effect of The Height Potential Barrier for Charge Transfer At Liquid/Liquid Interface**

AL-Agealy.Hadi,J.,M., and AL-Saadi Adil.A.,M

18 **Measurements of Radon Concentrations Indwelling of Shrqat in Salah Dien / Iraq**

Shaker M. Marbut, Yasir K. Mohammad, Rajaa S. Najim

25 **Isolation and characterization of Staphylococcus aureus mutants sensitive to lysozyme by UV radiation**

Farah Tarik Abdulkareem, Dr. Hameed Majeed

38 **Measurement of Calcium, Inorganic Phosphate and Albumin levels in serum of Iraqi hypertensive male patients.**

Amal R. Farhan, Dr. Eham A.Ali ,Dr. Shatha M.J. Al-Khateeb

50 **Bioactivity of Bacillus species isolated from human feces**

Adnan, H. Abbas ,Jabbar, F. Al-maadhidi ,Mahdi, S. Al-Rubaie

62 **A New WP-MC/MCD-CDMA System Using Two-dimensional Spreading Code**

Natiq Abdullah Ali

74 **Cellular Mobile Base Stations Radiation at Baghdad**

Adheed Hasan Sallomi

86 **Study Of The Basic Parameters Characterized The (D-T) Hot Plasma Fusion Reaction In General Dense Plasma Focus Devices**

Assistant professor: Raad Hameed Majeed

101 **Secure Watermark Image Steganography by Pixel Indicator Based on Randomization**

M.Sc. Zena Ahmed, M. Hamid Mohammed Farhan

111 **Radiological Characterization of Destroyed Nuclear Reactor Tammuz-2 At Al-Tuwaitha Site**

Yousif M.Zayir AL-BAKHAT, Assim OleIwi Mahdi , Fouzey H. Kitah, Samir Nouri Marmardji , Anwar A.Ahmed , and Nabeel H. A. AL-Tameemi

124 **Determination of Uranium Concentrations in some Plants and Soils samples from Baghdad-Iraq using CN-85 Track Detector**

Essam M.R. Drweesh , Lutfi M.M. Salih , and Roaa T. Abdulla

Barrier for Charge Transfer at Liquid/Liquid Interface

Al-Agealy Hadi J.,M., and Al-Saadi Adil.A.,M.

Department of Physics, College of Education Ibn-Al-Haitham, University of Baghdad

Abstract

The height potential barrier $\Delta G^{++}(eV)$ of charge transfer at liquid/liquid interface was described and calculated on the base of the semi classical theory. It is a function of the reorganization energy, and driving force energy respectively. Results of the reorganization energy E_0 indicate that the charge transfer is more probable in liquid/liquid system which has more polarity parameter. Charge transfer in system has large dielectric constant are stronger than system that have small dielectric constant. The driving force energy for charge transfer is the energy that takes to bring the donor and acceptor together and drive the charge increases with the increase of absorption energy and decrease in wave length. Results of height barrier $\Delta G^{++}(eV)$ across liquid/liquid interface decreases with the decrease of the driving force energy and increasing of the absorption energies. The transition is so much small as a barrier has large values but in the low values of barrier, the transfer is most probable. The large height barrier exclusion transfer across liquid/liquid system and the charge suffering much resistant to transfer.

Key Words: height potential barrier, charge transfer, liquid/liquid interface.

تأثير ارتفاع بئر الجهد على انتقال الشحنة عبر وصلة سائل/سائل

هادي جبار مجبل العكيلي وعادل علي منصور السعدي

خلاصة

وصف ارتفاع حاجز جهد لانتقال الشحنة عبر وصلة سائل/سائل وحسبت على اساس النظرية شبه الكلاسيكية. حاجز بئر الجهد هو دالة لطاقة اعادة الترتيب وطاقة القوة الدافعة للالكترونات على التتالي. تشير نتائج طاقة اعادة الترتيب E_0 الى ان انتقال الشحنة اكثر احتمالا في نظام سائل/سائل الذي يملك معامل استقطابية عالية. انتقال الشحنة في نظام يملك ثابت عزل عالي اقوى من نظام يملك ثابت عزل صغير. طاقة القوة الدافعة لانتقال الشحنة هي التي تأخذ الواهب والمستقبل سوية وسوق الالكترونات يزداد مع زيادة الطاقة الممتصة وبتناقص الطول الموجي. نتائج حاجز الجهد ΔG^{++} عبر وصلة سائل/سائل يتناقص بتناقص القوة الدافعة وبزيادة الطاقة الممتصة. الانتقال يكون قليل لحاجز عالي الارتفاع ولحاجز ذو سطح قليل الارتفاع يكون الانتقال اكثر احتمالا. ارتفاع الحاجز العالي يمنع الشحنة لعبور الوصلة سائل/سائل والالكترون يعاني ممانعة اللانتقال.

الكلمات المفتاحية: ارتفاع بئر الجهد، أنتقال الشحنة عبر وصلة سائل/سائل.

Introduction

Charge transfer (CT) from a liquid donor state to an acceptor liquid state is one of the simplest conceivably reactions as chemical bond are neither formed nor broken. Charge transfer through molecular framework of vital important to a wide range variety of processes in physical chemistry, and biological [1]. For example charge transfer in primary step in photosynthesis and various chemical reactions. The studies of charge transfer in organic molecular systems have witnessed a rapid growth in recent years [2]. The charge transfer is of highly importance in bioenergetics and is an active field of research. Much attention has been devoted to studying the charge transfer at liquid /liquid interface and molecular transport reaction processes [3]. As a result ,the donor becomes oxidized and the

acceptor will be reduced .reactions which involve the transfer of an electron are called redox reactions .redox reactions play an important role in everyday life, for example, the sequence of reactions which sustain the metabolism in plants and animals consists entirely of redox reactions[4] .

The first observation of electron transfer reaction in solution goes back in the nineteenth century, when Humphrey Davy observed (1808) that passing ammonia over metallic potassium produces a fine blue color [5]. Since the late 1940 s, the field of electron transfer processes have grown enormously, both in chemistry and biology. The development of the field of the electron transfer experimentally and theoretically, as well as its relation to the study of other kinds of chemical reactions [6].

The classical transfer theory was initially generalized for the liquid |liquid coupling interface by Samec. Girault and Schifrin considered the electron transfer reaction as asides of steps, where the formation of a precursor complex of the reactants is followed by reorganization of the precursor, charge transfer and dissociation of the products [7].

The present study focus on the description and studying the charge transfer potential barrier height at liquid/liquid system; this will be calculated theoretically according to values of reorganization energy and the driving force energy.

Theory

The probability of charge transfer from donor liquid state to an acceptor liquid state is given by[8].

$$W_{DLAL}=\frac{2\pi}{\hbar}\,|T_{DA}|^2\quad \rho(E_{DL}-E_{AL}-\hbar\omega) \qquad \ldots\ldots\ldots\ldots\ldots\ldots\ldots\ldots\ldots\ldots(1)$$

Where $\hbar$ the plank constant divided by 2π, T_{DA} is the coupling matrix element, and $\rho(E_{DL}-E_{AL}-\hbar\omega)$ is the probability of finding the liquid-liquid system in the energy states E_{DL}, and E_{AL} are appreciable only when one or the other of the two terms is close to zero .

Assuming that $E_{DL} > E_{AL}$, then $\rho(E_{DL}-E_{AL}-\hbar\omega\ )$ is positive and the probability of transition may be enable to write [9].

$$\rho(E_{DL}-E_{AL}-\hbar\omega)=N\ exp\ \frac{-(E_A-E_D)}{K_BT} \qquad \ldots\ldots\ldots\ldots\ldots\ldots(2)$$

Where $E_A and, E_D$ are the energy of acceptor and donor state, k_B is the Boltzmann constant , ω is the frequency ,N is the normalized constant

,and T is the absolute temperature.

Note that the height barrier $\Delta G^{++}$for displaced harmonic oscillators is $\Delta G^{++}= E_A - E_D$, then the rate equation of electron transfer becomes.

$R_{et}= \frac{2\pi}{\hbar} |T_{DA}|^2 \rho(\Delta G^{++})$.....(3)

However the height barrier ΔG^{++} could be estimated with the Marcus theory [10] .

$\Delta G^{++}=\Delta G^{0++} - \frac{nF}{2}(\Delta\Phi - \Delta\Phi^0) + \frac{n^2F^2}{4E_0}(\Delta\Phi - \Delta\Phi^0)$ .....(4)

Where $\Delta G^{\circ++}$ is the height potential barrier (activation free energy) at equal the interfacial potential difference ($\Delta\Phi=\Delta\Phi^\circ$), $\Delta\Phi$,and $\Delta\Phi^\circ$ are the redox potential for donor and acceptor state, n is the number of electrons ,F is the Faraday constant ,and E_0 is total reorganization energy. The height barrier energy of reaction can be expressed as [11].

$\Delta G^{++}=$ -nf

($\Delta\Phi$- $\Delta\Phi^\circ$).....(5)

And the height potential barrier from classical Marcus theory is given by [12].

$\Delta G^{++}= \frac{E_0}{4} - \frac{\Delta G_0}{2} + \frac{G_0^2}{4E_0} = \frac{(E_0-\Delta G_0)^2}{4E_0}$ .....(6)

Where E_0 is contribution of the reorganization energy due to reaction ,and ΔG_0 is the driving force energy When the liquid/liquid system absorption photon light to excited and that's can be written as [13].

$\Delta G_0 = (h\nu - E_0)$.....(7)

Where ΔG_0 is the effective free energy (driving force)is given by [14].

$\Delta G_0 = h(c/\lambda) - E_0$.....(8)

Where h, is Planck constant, ν is the frequency, c is the velocity of light and λ is the wave length. The reorganization energy E_0 due to electron transfer reaction at liquid/liquid system can be written as [15].

$E_0 = \frac{(\delta e)^2}{4\pi\epsilon_0}\left[\frac{1}{2a_1}+\frac{1}{2a_2}-\frac{1}{R}\right]\left(\frac{1}{\epsilon_1^{op}+\epsilon_2^{op}} - \frac{1}{\epsilon_1^{S}+\epsilon_2^{S}}\right)$.....(9)

Where $R = a_1 + a_2$ is the separation distance between the two reactants and a_1, a_2 are the radii of ions ,ϵ_1^{op} ,ϵ_2^{op} , ϵ_1^{S}, and ϵ_2^{S} refers to the optical static dielectric constant of two liquid respectively. The radii of donor and acceptor can be estimated from the

apparent molar volume using spherical approach [16].

$$a_i = \left(\frac{3MW}{4\pi N_A \rho}\right)^{\frac{1}{3}} \quad \ldots\ldots\ldots\ldots\ldots\ldots\ldots\ldots\ldots\ldots (10)$$

Where a_i is the radius of donor or acceptor, NA Avogadro's number constant , MW is the molecular weight, and ρ is the mass density of liquid.

Results

The calculation of the rate constant of charge transfer depends on three main terms that's appearing in it; the reorganization energy, the electronic coupling, and the potential barrier height. The reorganization energy can be evaluated depending on the outer sphere model that is derived based on the electro statistics potential of the molecular donor and acceptor. The reorganization energy is needed to the reorientation of system before the transfer. The molecular parameters introduced in this model are the molecular weight MW, mass density ρ are taken from Table 1 and radius of molecule that's evaluated according the apparent molar volume using spherical approach in Eq.(10),the results are summarized in Table 1. The reorganization energy for water / liquid system can be calculated using Eq.(9) with inserting the values of radii of donor and accepter from Table(1), and dielectric constant ϵ optical dielectric constant ϵ_{op} from Table (2) and assume the distance $R = a_D + a_A$ between center to center for donor and acceptor knowing that $(\frac{e^2}{4\pi\epsilon} = 14.4\ eV)$ the results of reorganization free energy have been summarized in Table (2) .

The second step is to calculate the driving force energy (free energy) term at the liquid/liquid interface as a function of the reorganization energy ,and the absorption energy . The energy changes for the drive free energy of the charge to transfer from donor to acceptor involved the difference between the reorganization energy and absorption spectrum energy Eq.(8). The results of the reorganization energy in Table 2 can then be used to find the values of a driving force energy and barrier potential. The absorption energy in Eq. (8) can be roughly taking from the wave length in visible spectrum(4000A^o-7000$A°$) and transform energy equation $E = h\nu = \frac{hc}{\lambda}$,where h is Planck constant ,c is the velocity of light ,and λ is the wave length .

Since we have considered that the absorbed visible light is directed to the aqueous phase .we evaluated the

driving force energy for liquid/liquid system by inserting the values of the reorganization energy from Table 2, and absorption energy from spectrum in Eq. (8), results are listed in Table 3.

The height potential barrier $\Delta G^{++}(eV)$ using Eq.(6), by inserting the results of both reorganization energy from Table (2),and driving force energy in Table(3), with Math lab program. The results are formulated in Table (4).

Discussion

In this paper we calculate the height potential barrier t $\Delta G^{++}(eV)$ for charge transfer at liquid/liquid interface system depending on the results of the reorganization energies and the driving free energy (driving force ΔG_0).

The height potential barrier $\Delta G^{++}(eV)$ have been tested the probability of the transfer of charge from donor water to liquid acceptor state. Table (2) show that the reorganization energy for charge transfer at liquid/liquid system increases with increasing of the dielectric constant for acceptor in the system ,also an increases in the refractive index for acceptor liquid leads to decrease in the reorganization energies for system with the same refractive index (n) and dielectric constant for the donor. This indicate that the reorganization energy as a function of the polarity for system. The small polarity function results to decreasing the reorganization energy and vice versa .

Also the effective radius $R \approx (a_1 + a_2)$ for the interface system reduce to $E^o \approx 0.6932973949\ (eV)$: $0.8986405084\ (eV)$ for water/liquid . Although this values for $E_0(eV)$ might seem reasonable, it must be emphasized that Eq. (9) constitutes an oversimplification, and more elaborate Marcus -Hush model for $E_0(eV)$ should be used for quantitative purposes. Table(3) gives the results of the driving force energy for charge transfer is take term accounting for the attractive interactions between the tails of the donor state wave function and acceptor state wave function. Calculated results of the driving force energy as a function of the reorganization energy and the absorption energy visible spectrum ($4000A^o$-$7000\ A^o$) . Results in Table (3) of driving force ΔG_0(eV), show that the driving force energy take to bring the donor and acceptor together and it is the part of the work broken to derive the charge to transfer from donor to acceptor. The driving force energy to drive the charge increases with increasing of absorption energy and

decreasing in wave length. Table 4 gives the theoretical height barrier ΔG^{++} (eV) at liquid/liquid interface that obtained with the semi classical Marcus model given in Eq.(6) for different liquid/liquid system. Height barrier $\Delta G^{++}(eV)$ decreases with the decreasing of the driving force energy and with the of increasing the absorption energies .This indicate that the absorption energy divided to reorientation.

The system to transfer and the other enable to drive the charge to transfer due to height potential barrier from donor to acceptor. The height barrier $\Delta G^{++}(eV)$ values calculated from this model agree also with those observed rate constant [9]. Again, the transition is so much small as when the barrier is large . In the low values of barrier ,the transfer of electrons are most probable from donor to accepter .The large height barrier exclusion transfer across liquid/liquid system and the electron suffering much resistant to transfer . However, this excluded transfer could be significantly lower for high barrier and small concentrations of charge because of the hard (large height) barrier overlapping effect ignored in Eq. (6).

Conclusions

In summary the results calculation of the height potential barrier for charge transfer at liquid/liquid interface system are function of the reorganization energies and the driving free energy (driving force). The reorganization energy $E_0(eV)$ in indicate that the charge transfer is more probable in liquid-liquid system have more polarity parameter Not ably the charge transfer in system have large dielectric constant are stronger than system have small dielectric constant. The driving force energy for charge transfer is take term accounting for the attractive interactions between the tails of the donor state wave function and acceptor state wave function and depending on the reorganization energy and the absorption energy visible spectrum. It energy that take to bring the donor and acceptor together and drive the charge increases with increases absorption energy and decreasing in wave length. height barrier ΔG^{++} (eV) at liquid/liquid interface that decreasing with decreasing the driving force energy and increasing the absorption energies

This indicate the absorption energy divided to reformation the system to transfer and the other enable to drive the charge to transfer due to potential

barrier height from donor to acceptor. It can be concluded the transition is so much small as a barrier large values but in the low values of barrier, the transfer is most probable the large height barrier exclusion transfer across liquid/liquid system and the charger suffering much resistant to transfer .

References

1. Bumm, L.A.; Arnold,J.J.;Dunbar,T.D;Akara,D.L. and Weiss, P.S. (1999)"Electron Transfer Through Organic Molecules" J. Phys. Chem.8. Vol.103, 8122-8127.
2. Eranda, M.; and Francis, D.S (2007)"Design and Studies of Photoinduced Electron In Procesding"3rd Annual GR A Spsympsium,Wichita State University.
3. Xiaoquan, L.;Qin, W.and Xiuhui, L.(2007)" Review: Recent Applications Of Scanning Electrochemical Microscopy To The Study Of Charge Transfer Kinetics "AnalyticalChemical Acta 601,10-25
4. Hussein,K.M.(2011)"Study of the Electron Transfer at Metal/Semiconductor Interface By Using Quantum Mechanical Theories" M.Sc. Thesis University of Baghdad.
5. AL-Agealy,H.J. (2004)"Quantum Mechanical Model for Electron Transfer In Q-Switched Dye Used For Solid State Lasers" Ph.D. Thesis University of Baghdad.
6. Mohsin, A. H. (2009). "A Theoretical Model For Electron Transfer In Dye/Semiconductor System Interface With Verity Solvents" M.Sc. Thesis, Baghdad University.
7. Christoffer J.(2003)"Electro Deposition and Reactions at Liquid-Liquid Interfaces" Ph.D., Helsinki University of Technology Department of Chemical Technology Laboratory Of Physical Chemistry and Electro Chemistry.
8. Jan G. K And Andreas G., 2002."Semiconductors For Micro And Nanotechnology an Introduction For Engineers" Wiley-Vch Verlag Gmbh, Weinheim.
9. Al-Agealy H.J.M., and Hassooni M.A.,2011"Calculate of The Rate Constant Of Electron Transfer In [Tio]_(2-) Safranine Dye System".Ibn-Al-Haitham J.For Pure&Appl.Sci,Vol.24,No.3,PP 64-77.

10. Horita H.(2011)"Mechanistic study of electron transfer at oil/water interface" Ph.D. Thesis kobe university, kernel
11. Fre´de´ric, R.; David, F.; Hye; J. L.and Hubert, H. G.(2000) "Electrochemistry at liquid:liquid interfaces: methodology and potential applications"Electrochimica Acta 45.PP.(2647–2662).
12. Al-Agealy, H.J.M.and Zangana, H.A. (2010)"Electron transfer between ketone triplets and organic dyes in variety solvents"Journal of the College of Basic Education Vol.16,No.63,pp 61-68
13. Al-Agealy, H, J M..(2008)"photo induced electron transfer between metal lop or physic complex dihydroxy " Ibn –Al Hahtham J.for pure and appl. Sci. .Vol. 21,No.1, PP 34-44
14. Wibren D.,2002 "Electron Transfer in donor bridge acceptor system and derived material", Ph.D. Thesis, Debye Institute and University of Utrecht.
15. Adil,A.M.AL-Saadi (2012)"Interface charge transfer in liquid/liquid"M.Sc. Thesis college Ibn-AL-Haitham ,University of Baghdad.
16. Al-Agealy, H.J, and Hassoni M.A.(2010)"A Theoretical study of the effect of the solvent tyoe on the reorganization energies of dye /semiconductor system interface"Ibn-ALHaithem .J for pure &Appl.Sci.,Vol.23,No.3,pp 51-57
17. 17-Greenwood, N. N, and Earnshaw, A.(1997)"Chemistry of the Elements" 2nd edition ,Butterworth-Heinemann, Oxford, UK.
18. Silberberg,M.S.(2009),". Chemistry", Book, 5th edition, McGraw-Hill. Publisher.
19. West,R.C. (1995)."Handbook of chemistry and physics".76thed .CRC.press: Boca Raton.FL.
20. Paul,W; Derek, M.D.; David,J.G. Christopher, J.C.;and Donald, G.T .(2010)" Minnesota Solvent Descriptor Database", Department of, Chemistry and Supercomputer Institute University of Minnesota, Minneapoils.MN 55455-0431.

Table 1. The theoretical calculation values of radii a_i(A°) for water donor and acceptor liquid [17-18].

Liquid Type	**Molecule wt. (MW)$g.mol^{-1}$ [17-18]**	**Density (ρ) $g.cm^{-3}$ [17-18]**	**Calculated radii $a_i(A^0)$**
Water	18	1	1.92520792
Acetone	58.08	0.791	3.076121696
Formic acid	46.03	1.22	2.463847665
Bromoform	252.73	2.889	3.261043233
Chloroform	119.38	1.483	3.171881441
N-methylformamide	59.07	1.003	2.858087259
N,N dimethylformamide	73.09	0.944	3.13099322
Ethanol	46.0414	0.790	2.848135287
Haxanic acid	116.16	0.93	3.672073423
1,2 ethanediol	63	1.1151	2.818787796
n-hexadecane	226.44	0.733	4.96595975

Table 2. The reorganization free energy E_0 (eV) for charge transfer at water\liquid interface system.

Liquid Type	**Dielectric constant for acceptor ϵ_s[19-20]**	**Optical dielectric constant for acceptor ϵ_{op}[19-20]**	**Reorganization free energy E_0 (eV) [17-18]**
Water/Acetone	20.493	1.84633744	0.8516752339
Water/Formic acid	51.1	1.88073796	0.8986405084
Water/Bromoform	4.2488	2.56160025	0.6932973949
Water/Chloroform	4.7113	2.09062681	0.7858438989
Water/N,Methylformamide	181.59	2.05033761	0.8363805396
Water/N, Ndimeethylformamide	37.219	2.04633025	0.8075301745
Water/Ethanol	24.852	1.85259321	0.8635918533
Water/n-hexadecane	2.0402	2.05779025	0.8246426859
Water/Hexanic acid	2.6	2.00590569	0.8118435171
Water/1,2 Ethanediol	40.245	2.05005124	0.8244227082

Table 3. The driving force energy $\Delta G_o(eV)$for charge transport in water/liquid system.

	Driving force energy $\Delta G_o(eV)$									
Wave length λ $(A°)$	**Water-Bromoform**	**Water-n-hexadecane**	**Water-Chloroform**	**Water-N,Ndimethylformamide**	**Water-Haxanic acid**	**Water-1,2ethanediol**	**Water-n-methylformamide**	**Water-Acetone**	**Water-Ethanol**	**Water-Formic acid**
4000	2.4127	2.2813	2.3201	2.2984	2..2941	2.2815	2.2696	2.2543	2.2424	2.2073
4500	2.0676	1.9362	1.9750	1.9533	1.9490	1.9364	1.9245	1.9092	1.8973	1.8622
5000	1.7915	1.6601	1.6989	1.6772	1.6729	1.6603	1.6484	1.6331	1.6212	1.5861
5500	1.5656	1.4342	1.4730	1.4513	1.4470	1.4344	1.4225	1.4072	1.3953	1.3602
6000	1.3774	1.2460	1.2848	1.2631	1.2588	1.2462	1.2343	1.2190	1.2071	1,1720
6500	1.2181	1.0867	1.1255	1.1038	1.0995	1.0869	1.0750	1.0597	1.0478	1.0127
7000	1.0816	0.9502	0.9890	0.9673	0.9630	0.9504	0.9673	0.9232	0.9113	0.8762

Table 4. The results of height potential barrier $\Delta G^{++}(eV)$ for charge transport at water/liquid interface system.

Wave length λ (A^o)	Height Barrier $\Delta G^{++}(eV)$									
	Water-Bromoform	Water-n-hexadecane	water-Chloroform	Water-N,N dimethylformamide	Water-Haxanic acid	Water-1,2 ethanediol	Water-N,methylformamide	Water-Acetone	Water-Ehanol	Water-Formic acid
4000	3.4790	2.9246	3.0790	2.9865	2.9707	2.9253	2.8837	2.8315	2.7928	2.6837
4500	2.7488	2.3108	2.4249	2.3597	2.3472	2.3113	2.2784	2.2372	2.2067	2.1205
5000	2.2265	1.8717	1.9641	1.9113	1.9012	1.8721	1.8455	1.8121	1.7874	1.7175
5500	1.8400	1.5468	1.6232	1.5796	1.5712	1.5472	1.5252	1.4976	1.4771	1.4194
6000	1.5462	1.2998	1.3640	1.3273	1.3203	1.3001	1.2816	1.2584	1.2412	1.1927
6500	1.3174	1.1075	1.1622	1.1309	1.1249	1.1077	1.0920	1.0722	1.0576	1.0163
7000	1.1360	0.9549	1.0021	0.9750	0.9700	0.9552	0.9416	0.9245	0.9116	0.8763

Measurements of Radon Concentrations Indwelling of Shrqat in Salah Dien, Iraq

Shaker M. Marbut[+], Yasir K. Mohammad[++], and Rajaa S. Najim[++]

[+] University College of Madenat AL-Elem

[++] Dept. of Basic Science, College of Dentistry, Tikrit University

Abstract

High radon levels are present in granite and grandiosity rocks that spread in Makhol Mountains. Such materials are rich in uranium and widely used in the construction of dwelling in the Shrqat. In the present work, the concentration of radon was measured, by using CR-39 dosimeter. Results suggest that radon concentration range from 66.32 to 45.63 Bq/m^3. The maximum value 80.32Bq/m^3 and minimum value 24.2 Bq/m^3, with standard deviation 12.67Bq/m^3. The result provides a framework for future studies that include a large, broader survey of radon concentration in Salah Dein.

Keywords: Radon, granite rocks, grandiosity rocks, Makhol mountains.

قياس تركيز الرادون داخل المنازل في قضاء الشرقاط

شاكر محمود مربط وياسر خلف محمد ورجاء سهيل نجم

خلاصة

تحتوي صخور الكرانيت التي تنتشر على سلسلة جبال مكحول على مستويات عالية من غاز الرادون . حيث تعرف هذه المواد بأنها غنية باليورانيوم و هي شائعة الاستخدام في بناء المساكن في الشرقاط . تم في هذة الدراسة قياس تركيز غاز الرادون في داخل منازل الشرقاط باستخدام كاشف الحالة الصلبة المعروف باسم (CR-39) . و أشارت النتائج أن معدل تركيز الرادون في مكان الدراسة يتراوح بين (66.32-45.63 Bq/m^3) . وان أقصى تركيز هو ($80.32Bq/m^3$) وان ادني تركيز هو (24.2 Bq/m^3) مع متوسط انحراف معياري مقداره (12.67 Bq/m^3) و النتائج تشير الى ضرورة القيام بدراسة مستقبلية واسعة النطاق لمسح شامل لقياس تركيز الرادون في محافظة صلاح الدين.

الكلمات الدالة:

Introduction

Radon-222 is a radioactive gas with a half- life of 3.824 days. It is The immediate radioactive decay series products of radium (^{226}Ra), in the decay series of uranium(^{238}U) and thorium (^{232}Th). The half- life of thoron (^{220}Rn; radon isotop)is 55.6 sec which is much shorter than that of radon. Because of such a Short half-life of thoron, its emanation from building materials, as well as, its infiltration from the ground and further migration is restricted to a few centimeters only [1]. The process of the migration of Radon is a function of radioactivity concentration, and the porosity and permeability of the medium. Radon has long been known to contribute to risk of lung cancer. Radon and its daughter products emit alpha particles that are implicated in the cellular changes leading to lung cancer. Indoor Radon variations occur hourly, diurnally, and seasonally, and are influenced by numerous factors, including Radon infiltration rates, pressure differentials, soil characteristic weather conditions (e.g. rainfall, wind speed) and occupant behavioral [2]. The Radon concentration in air varies

in accordance with location, high level of the houses, material of the houses built, different room in the same house, and ventilation rate [3]. Radon exhalation rates in the areas, where uranium deposits and phosphate rocks is significant, and this is the main source of exposure to uranium. Long-term exposure to elevated levels of Radon increases ones risk of containing lung cancer. In Gaza , recent report of cancer registry unit shows that, the total reported diagnosed cases through the years 1998 -2002 were 2,404 {1.264 male, 1.140 female} cancer cases, number of these (31.4%) bronchus and lung cancer [4]. The purpose of this study is to gather information about the natural radiation and to evaluate the Radon concentration throughout. This is motivated by the concern about the possible consequences of long term exposure to higher concentration of Radon and its short-lived product in air. Since, it is known that Radon of its radioactive decay series products can cause lung cancer, and thus has become a public health concern [5]. Many countries have carried out surveys of prevailing indoor Radon levels [6, 7, 8, and 10]. A program of measurement of Radon concentration has been started in the country. This study will provide the basic data for any future study and project planning from the environmental point of view.

Methods and Material

Radon concentrations in the houses were measured using passive integral Solid-state track detectors CR-39 [9]. Were prepared and distributed inside the houses of the middle region of Shirqat. These houses are chosen to be representative of the whole region. Our sampling strategy was to distribute the dosimeters in houses located at different geographic parts of the region. Moreover, houses built of different materials, like (stones and concrete), (stone and zinc) and (stone and spouts). The detectors were placed in a room so as to avoid contribution of ^{222}Rn and its daughters, where the occupants of the house spend most of their time. Some of detectors were placed in bedroom and others in the living room. The detectors were left in the houses for a period of four months, (from May to Aug of 2009). Radon and its daughter's concentrations (C) throughout present work are determined by the following equation [11, 12]

$$C(Bq/m^3) = \frac{C_o(Bq/m^3)\, P\, t_o}{P_o t}$$

Where:

C_o: is the radon concentration of the calibrated chamber (90 KBq/m^3),

t_o: is the calibration time (48 hr),

P : is the measured tracks number density per cm^2 on -3q detector inside the dosimeters used in the study,

P_o: is the measured tracks number density per cm^2 on detectors of the calibrated dosimeters (95754 tracks/cm^3),

t: is the total exposure time in days for different places of the house (97days)

Results and Discussions

An overview of the Radon concentrations at houses on all camps is evaluated and given in table 1. The minimum and maximum values of Radon concentrations in the camps of each group measured in Bq/m^3 are also determined. The table also shows the average Radon concentrations (C) and the standard deviation (S.D) for each camp in location of the survey. Radon and its daughter's concentrations over the four locations in the middle region of Shrqat trip were varied between 66.32 up to 54.63Bq/m^3 and had a maximum value of 80.326 Bq/m^3. The average Radon concentration was 24.2 Bq/m^3 with average standard deviation of 12.67 Bq/m^3. Average Radon concentrations for each site were determined as follows: R Cost S camp 66.32 Bq/m3, camp R Cost N 61.16 Bq/m^3, L Cost S camp 45.63Bq/m^3, L Cost N camp 52.66 Bq/m^3. The average Radon concentrations of (a) and (b) camps were higher than (c) and (d) camps. The result also indicates that the difference between the minimum and maximum Radon concentrations in each camp is very high. This large variation in Radon values inside these camps is due mainly to the difference in the ventilation methods used different types of locations building and elevated floor of building. The types of building materials such as concrete, spouts, stone and concrete…. etc, are also influence the Radon concentration. Indicates that in (c) camp houses are built of stone and spouts where Radon concentration found higher than 1.32 times of these in (a) camp. It was found that Radon concentrations of (a) and (b) houses that built of stone and spouts higher than (c) and (d) houses that built of stone and concrete. This represents that houses built of spouts and stone are 1.4 times higher than of houses built of concrete and stone. The highest values were found in houses where the building substructure consisted of stone and zinc. Houses built of stone and

concrete had low Radon concentrations in all house locations. The ventilation method in these buildings can be understood to be better than other buildings. This indicates that the different materials of houses built are important parameters in determining Radon concentrations and shows that that the highest Radon concentrations are in bedrooms of (c) camp, and the lowest in living rooms in (b) camp. It also shows that highest percentage of Radon concentration is found in the bedrooms 41%, while kitchen 34% and living rooms 25%, within the same housing complex, have about the some Radon levels. The high Radon levels inside bedrooms are due also to the relatively of low ventilation. While living rooms of the houses have large windows, front of open area and well ventilation. In addition, there is an interactive effect between the Radon exposure and smoke cigarettes. Two agents have really causing and developing of lung cancer [12]. The Radon concentration of smoking people in (a) camp is very high comparing to other camps. Thus, higher Radon concentration and smoking together may cause lung cancer. Smokers should keep their exposure to Radon as low as possible. Smokers have many times the risk from Radon than non-smokers. If the house was tested in a frequently used basement, it may have measured a Radon level that is higher than actual level, stop smoking and spend most of your time upstairs [13]

Table 1. Radon concentrations in each camp.

Location	Symbol	No. of det	Ave. C(Bq/m^3)	Max. C(Bq/m^3)	Min. C(Bq/m^3)	S.D. (Bq/m^3)
Right Cost South	(a)	35	66.32	80.32	31.6	12.5
Right Cost North	(b)	29	61.16	76.14	32.2	12.5
Left Cost South	(c)	39	45.63	59.26	24.2	12.01
Left Cost North	(d)	34	52.66	70.60	34.4	13.7
Ave. value		137	56.44	71.58	30.55	12.67

Table 2. Comparison of the study and other studies.

Study	Syria[14]	Iraq[16]
80.32- 24.4	60.3-13.3	60.7-18.43

Table 3. Public recommended [15].

Authority	Dwelling know	Dwelling future
ICRP	400	200
CEC	400	200
WHO	200	200

Conclusions

Results indicate that Radon average concentration range from 30.55 up to 71.58 Bq/m^3 with a maximum value of 80.32 Bq/m^3, a sample of houses in all sites of camps. Despite the small number of building studied, the results provide a framework for future studies that include a larger, broader survey of Radon concentrations indoor and outdoor in Shrqat. Substantial research efforts are also requested all over Shrqat in air, water and soil to evaluate the average Radon concentration of whole country. Certainly, this study undertaken to provide a health oriented Radon assessment of the country to us in addressing long-tang management goals, particularly from the environmental point of view.

References

1. Ab-Murad K.M., and Al-Tamimi, M.H.,"Natural radioactivity due to radon in Some region, Jordan", Radiation Measurement, 39, 77-80, (2005).
2. Lbed, Veronique and Rannou, Aiain, and Tymen, Georges, *Heath Phys*., No. 65, p:172-178 (1992).
3. Durrani S. A. and Ilic R., Radon Measurements by Etched Track Detectors, Applications in Radiation Protection, Singapore: Earth Science and the Environment (1997).

4. Abu-Jarad A. and Al-Jarallah M., Radon in Saudi Houses, Radiat. Dosim., No.14, p: 243-249 (1986).
5. Soharabi M. and Solamanian A., Indoor Radon Levels in Some Regions of Iran, Nucl. Track Radiation Measurement, No. 15, p: 616 (1988).
6. J.AL-jundi and T.Haninger; "Radon-222 concentration in houses of Russaifa city Jordan " abhath AL-yarmouk : basic sci . and Eng . vol . 12 , (2003) , no 1, pp.181-190.
7. As'ad H. I., "Measurement of Radon Activity concentration in Iraqi Kurdistan Soil by Using CR-39 Nuclear Track Detectors, M.Sc. Thesis, Univ. of Salahaddin,(2004).
8. Khader B., Radon-222 Concentration in the Air of the Dwellings in Irbid Region- Jordan, Yarmouk Univ., Irbid M. Sc. Thesis, (1990).
9. A. Bozkurat and E. Kam; "indoor radon measurement in city of Edirne, Turky " sixth international conference of the Balkan physical union (2007) .
10. United States Environmental Protection Agency office of Air and Radiation, "A Citizen's guide to Radon," Indoor Environments Division 6609 J, EPA Document 402-k92-001, third edition, (2001).
11. R. Shweikani; "Variation of radon exposure in Damascus dwellings". Applied Radiation and Isotopes 70 785–789(2012).
12. David Pollard ,Radon Gas in Ireland "Radiological Protection Institute of Ireland"2010 .
13. S. Y. Hasan; " Measurement Of Indoor Radon Levels During Summer Season In AL-Hamdanya City – nenava Governorate"; Tikrit science journal ;3;16 pp;164-167;(2011).
14. R. Shweikani; "**Variation of radon exposure in Damascus dwellings**". Applied Radiation and Isotopes 70 785–789(2012)
15. 15. David Pollard ,Radon Gas in Ireland "**Radiological Protection Institute of Ireland**"2010
16. 16. S. Y. Hasan; " **Measurement Of Indoor Radon Levels During Summer Season In AL-Hamdanya City – nenava Governorate";** Tikrit science journal ;3;16 pp;164-167;(2011)

Isolation and characterization of *Staphylococcus aureus* mutants sensitive to Lysozyme by UV radiation

Farah Tarik Abdulkareem[+] and Hameed Majeed[++]

[+] Ministry of Sciences and Technology
[++] Al-Nahrain University

Abstract

Staphylococcus aureus, an opportunistic pathogen commonly found on human skin, were exposed to 1, 2, 3, 4 and 5 J/m^2 UV radiation; UV radiation was highly lethal and mutagenic. We detect the mutational effects of irradiation by culturing the isolates on lysozyme containing medium of isolate that was unable to grow in lysozyme and was affected by radiation. Four mutants were obtained and they were sufficiently effective for the isolation of macromolecules such as plasmid and deoxyribonucleic acids, from the cells after lysozyme-induced cell lysis.

Keywords: *Staphylococcus aureus*, UV radiation, lysozyme, mutation.

الحساسة لأنزيم اللايسوزايم عزل وتشخيص بكتريا المكورات العنقودية المطفرة

باستخدام الأشعة فوق البنفسجية

فرح طارق عبد الكريم و حميد مجيد

الخلاصة

تعد بكتريا المكورات العنقودية من الممرضات الانتهازية التي تتواجد عادة في جلد الإنسان. لقد تم تعريض هذه البكتريا الى 1 و 2 و 3 و 4 و5 جول/م^2 من الأشعة الفوق البنفسجية ووجد أن لها تأثير قاتل ومطفر على البكتريا وقد تم الكشف عن البكتريا المطفرة عن طريق زرع البكتريا على أوساط زرعيه تحتوي لايسوزايم. تم الحصول على أربع عزلات مطفرة واستخلاص الكروموسومات والبلازميدات بعد معاملتها بإنزيم اللايسوزايم وتشخيص هذي الطفرات ومقارنتها بالعزلة الأصلية.

الكلمات المفتاحية: بكتريا المكورات العنقودية، الأشعة الفوق البنفسجية، اللايسوزايم، الطفرة الوراثية.

Introduction

Staphylococci are Gram positive spherical bacteria that occur in microscopic clusters resembling grapes, it is a normal inhabitant of the skin and mucous membrane in the nose of healthy human [1].

Staphylococcus aureus, literally "Golden Cluster Seed" and also known as golden staph, is the most common cause of staph infections. It is a spherical bacterium, frequently living on the skin or in the nose of a person. Approximately 20–30% of the general populations are "staph carriers" [2].

S. aureus is, golden yellow colonies, often with β-hemolysis, when grown on blood agar plates , *S. aureus* is a facultative anaerobe and opportunistic pathogen [3].

Staphylococci cell walls are composed of teichoic acids, and wall-associated surface proteins. Stress-bearing murein represents continuous macromolecular units covering the whole cell [4].

The ability to evade host immune surveillance is a critical virulence determinant for any pathogen along with the capacity to defend against the immune defenses, and both of these aspects can be provided by the peptidoglycan ,a large polymer that provide much of the strength and rigidity to the bacterial cell wall. It consists a long glycan chains of alternating N-acetyleglucosamine (NAG) ,and N-actylmuramic acid (NAM) subunits [5].

The antibacterial nature of lysozyme was first witnessed by Sir Alexander Fleming (6). Because lysozyme is cationic, it closely adheres to bacteria through electrostatic interactions with negatively charged tiechoic and lipotiechoic acids and phospholipids on the bacterial surface this interaction can result in bacterial lysis by hydrolyzing the bond between NAG and NAM [7].

Although, lysozyme is known to be bactericidal to certain bacteria but its antimicrobial function is limited to certain gram positive bacteria owing to the differences found in their membrane structure [8].

S. aureus showed a remarkable ability to survive antibiotics treatment by developing new resistance mechanisms against them within a short time of its introduction. Some strains are now resisting most conventional antibiotics; it is worrisome that it seems to be there are no new antibiotics on the horizon and any recent antibiotic developments are merely a modification to existing drugs; *S. aureus* is known to be

notorious in their acquisition of resistance to new drugs [9].

Mutagenesis plays a central role in our lives. A low level of mutagenesis is advantageous, and ensures the survival of species by promoting evolution. Programmed mutagenesis of immunoglobulin genes promotes diversity and provides a dynamic defense against invading pathogens. However, many human diseases, including most cancers, arise as a consequence of mutations that occur either spontaneously, or are induced by copying errors in the genetic material during cell division, by exposure to ultraviolet or ionizing radiation [10].

Materials and methods

Bacterial Isolate

Staphylococcus aureus isolate used in this study was obtained from the Department of Biotechnology/College of Science/Baghdad University; it was isolated locally in 2007.

Media

Ready to use media

The following media were prepared according to the instruction of the manufacturing company; pH was adjusted to 7.0 and sterilized by autoclaving at 121ºC.

- Nutrient agar
- Nutrient broth
- Brain heart agar
- Brain heart broth

Laboratory prepared media [11].

- Luria – Bertani agar
- Luria broth

Antibiotic discs

The following antibiotic discs were used for antibiotic sensitivity test, Results of inhibition zone of *S. aureus* were then compared with those indicated in NCCLS (2002) [12] for *S.aureus*.

Buffers and solutions

Buffers and solutions used in this study were 12:

- Normal saline solution 0.85%
- Phosphate buffer solution (0.2M)
- Lysozyme Stock solution (500µg/ml)
- DNA extraction solutions
- Tris-EDTA buffer solution (TE)
- Sodium chloride Tris-EDTA buffer solution (SET)
- Sodium dodecyle sulphate solution (SDS) 10%
- Tris-borate Buffer solution TBE(1X)
- Agarose gel (0.7%)
- Ethidium bromide
- Loading buffer

Methods

Physical mutagenesis

Mutagenesis by UV irradiation was done (14) by subjecting fresh culture of *Staphylococcus aureus* suspended in phosphate buffer solution (pH7.0) to UV radiation in a dark place using the UV- transilluminator. The tray of the irradiation approximately 15X25 cm exposes sample in glass Petri dish and the distance between the UV source and irradiated suspension was 11 cm.

The suspension of *S. aureus* was prepared by inoculating 5 ml of L-broth with single colony of *S. aureus* overnight at 37ºC , cells were then precipitated at 3000 rpm for 15 min, and washed twice with normal saline and resuspended in 5 ml of phosphate buffer (pH 7), the cell suspension were poured in sterilized Petri dishes and subjected to 1, 2, 3, 4, and 5 J/m² UV of irradiation, then 0.1ml of cell suspension was taken after each treatment diluted to appropriate dilution and spread on brain-heart infusion agar plates, plates were then incubated over night at 37ºC to determine the viable count and survivals of *Staphylococcus aureus*. Lysozyme sensitive mutants were screened by replica plating on brain heart infusion agar plates containing 3.4µg/ml and 12.5µg/ml of lysozyme.

Plasmid profile

Total DNA of *S. aureus* was extracted alkaline lysis method and as follows [15]:

- Hundred ml of fresh culture of *S. aureus* in BHI broth was centrifuged at room temperature for b 5min.
- Cell pellets were resuspended in the same volume of SET buffer solution (pH 8), the cells were recenterifuged, suspended in 0.5ml ice-cold acetone, and kept on ice for 5 minutes.
- The cells were centrifuged again and residual acetone was removed with gentle stream of air.
- Bacterial pellets were resuspended in lysis buffer. Lysozyme was then added at final concentration 200µg/ml and incubated at 37°C for 30 minutes.
- Lysis was achieved by adding 0.4 ml of SDS (10%). Cellular debris was removed by centrifugation 12000rpm for 15min.
- The supernatant was then extracted twice with an equal volume of a mixture of chlorophorm- isoamyl alcohol (24:1 v/v).
- The DNA was precipitated with (0.6 v/v) isopropanol alcohol; the mixture was incubated at -20°C overnight and recentirfuged 12000rpm for 15 minutes.
- The supernatant was decanted and precipitate was washed with 70% ethyl alcohol, centrifuged again and

the precipitate was dried with gentle stream air.

- TE buffer (0.025 ml) was added for gel electrophoresis analysis.

Agarose gel electrophoresis

Agarose gels (0.7%) were run horizontally in Tris Borate- EDTA buffer (TBE 1 X), samples of extracted DNA were mixed with loading buffer in 1:10 ratio and added to the wells on the gel. Generally, gel was run for 2-3 h at 5 $v.cm^{-1}$ and the agarose gel was stained with ethidium bromide by immersing them in ethidium bromide solution (0.5 µg/ml) for 30-45 min, DNA bands were visualized by U.V in transilluminator cabinet, and photographed.

Characterization of lysozyme sensitive mutants

Antibiotic sensitivity test [11]

The disc diffusion method was used to test the antibiotic sensitivity of the bacterial isolate .A sterile cotton swap was applied in to the inocula (fresh culture for 18 hour) and the entire surface of the brain heart infusion agar plates was swabbed three times by rotating the plate approximately 60º after each streaking to ensure even distribution. Then the disc of antibiotics were applied on streaked plates and incubated at 37ºC. Inhibition zone was measured after incubation for 16 hour.

Protoplasts formation of *S. aureus* mutants by lysozyme

Protoplast formation of *S. aureus* involves the conversion of selected mutant cells into protoplast using lysozyme alone was achieved [16].

lysozyme sensitive mutant of *S. aureus* was obtained. Mutagenesis by UV radiation (S2) were selected by replica plating on brain heart infusion agar. Mutants were inoculated into 50ml of brain heart infusion broth and incubated over night at 37˚C with shaking till 0.50 optical density of the growth was achieved, then five ml of each growth culture were centrifuged at 3000rpm for 10min and resuspended in phosphate buffer (pH 7). Lysozyme was added to the cell suspension at final concentration of 50µg/ml and incubated at 37˚C with shaking 150rpm for 2 hours. The formation of protoplasts was observed by light microscope.

Temperature sensitive growth

Temperature sensitive growth of mutants *S. aureus* were tested and compared with the wild type [17].

Single colony of *S. aureus* (wild type) and the mutants cells (S2, S3, S4, S5) which were described previously

by replica plating, were inoculated into 50ml brain heart infusion broth over night at 37˚C, then 0.1ml of each culture spread on brain heart infusion agar and incubated over night at 30, 37, 40, 43 and 45˚C. Growth was observed and survivals were counted after each incubation.

Results and Discussion

Physical mutagenesis

DNA is one of the key targets of UV-induced damage; therefore, organisms have developed a number of repair mechanisms to counteract the DNA damage caused by UV. These repair mechanisms will however be unable to cope if the UV dose applied is higher than the repair capacity [18].

Results of subjecting fresh cultures of *S. aureus* to different doses of UV ray presented in Figure 1 showed lethal effect on bacterial cell; this can be noticed from reduction in the viable count of bacterial cells from $46x10^7$ CFU/ml at zero time to $13x10^7$ CFU/ml after exposure to UV ray decreases to 28.2%,6.9, 2.6 and 1.3% respectively as exposed to 1, 2,3and 4 $J/m^{2,}$ while the survivals was decreased to zero% after subjection to the final dose ($5J/m^2$) of UV ray. Results of treated cells with UV radiation showed that all of the selected colonies were able to grow on brain heart infusion agar containing 3.4µg/ml lysozyme. While results in Figure 2 showed that four of the total colonies were unable to grow on the medium containing 12.5µg/ml lysozyme. These colonies were probably affected by the mutagenic activity of UV radiation that may cause alterations in deoxyribonucleic acid (DNA) (19).

These results are due to pigmentation, since pigmented isolates were found to be more resistant to the effect of UV radiation (20).

In a previous study [21] it was found that with the proper mutation, *S. aureus* cells were rendered to lysozyme hydrolysis.

As shown in Figure 3, lysozyme sensitive mutants (S2, S3, S4, and S5) showed clear chromosomal and plasmid DNA bands on agarose gel. Which indicates lysis of these mutants; the wild type, on the other hand, was resistant to lysis by lysozyme. These results confirmed that lysozyme sensitive mutants isolated by chemical and physical mutagenesis have altered bacterial cell wall.

It appears that lysozyme sensitive mutants provide obvious economical advantages over the wild type strain for the preparation and study of macromolecules.

Characterization of lysozyme sensitive mutants

Antibiotic sensitivity test

Antibiotics sensitivity test was performed on wild type and mutants of *S. aureus* in order to reveal that the changes resulted from the effect of UV treatment on the antibiotics sensitivity pattern of the wild type, for this purpose twelve antibiotic discs were used in this test.

Results in Table 1 showed that the wild type of *S. aureus* was resistant to gentamycin, cephalothin, cefotaxime, erythromycin, penicillin, streptomysin, vancomycin, pipracillin and fucidic acid, while sensitive to impenem, amoxicillin and tetracycline. These results were constitute with other findings [22] which stated that *S. aureus* has become resistant to many commonly used antibiotics, only 2% of all *S. aureus* isolates were sensitive to penicillin, due to the penicillinase (a form of β-lactamase).

However, lysozyme sensitive mutants obtained after mutagenesis with UV radiation were variable in their resistance to these antibiotics; *S. aureus* mutants (S2, S3, S4, and S5) lost their ability to resist 4, 3, 3 and 3 different antibiotics respectively, these results may be due to the genetic alteration in different genes that express antibiotic resistance to *S. aureus*, occurred after mutagenesis with UV radiation [23].

Protoplast formation of *S. aureus* mutants by lysozyme treatment

Bacterial protoplasts and spheroplasts are osmotically fragile forms that lack rigid or partially rigid cell walls. A conversion of bacterial cells to protoplasts or spheroplasts achieved normally by the addition of lysozyme growth medium. Removing cell wall by lysozyme has been used with success on a variety of bacteria. However, protoplasts of *Mycobacterium smegmatis*, *S. aureus*, and *Clostridium pasteurianum* cells were not readily prepared by lysozyme alone [16].

lysozyme sensitive mutant of *S. aureus* isolated induced by UV radiation (S2) were treated with lysozyme at concentration of 50µg/ml, and incubated for 2 hours. The formation of protoplasts was observed by light microscope. Cells appeared as spherical bodies of various sizes and density. They were transparent and swollen in comparison with wild type. Figure 4 showed the morphological changes of *S. aureus* cells.

However, prolonged incubation may be necessary to cell division and loss of cell wall, which result in protoplast formation. As a result of this treatment, the cell contents would be enclosed only by a cell membrane.

Temperature-sensitive growth

Lysozyme sensitive mutants isolated by MNNG and UV mutagenesis might show temperature sensitive growth when incubated at elevated temperatures. *S. aureus* mutants were investigated for temperature sensitive growth and compared with the wild type(24).

Results in Table2 show the temperature sensitive growth of *S. aureus*. The wild type and mutants obtained after UV radiation (S4 and S5) showed growth at 30, 37, 40, 43 and 45˚C. While two of the mutants obtained after UV radiation (S2, and S3) were unable to grow at high temperature (above 40˚C), which suggested defects in cell surface structure and the membrane integrity as results of mutagenesis [25].

UV mutagenesis causes point mutation that produce defect in RNase. Temperature sensitive growth considered to be caused by simultaneous defect of RNase which is related to the synthesis and maintaining of the cell surface of this bacterium [26].

References

1. Cramton, S. E.; C. Gerke, N. F.; Schnell, W.; W. Nichols, and F. Götz. (1999). The intercellular adhesin (*ica*) locus is present in *Staphylococcus aureus* and is required for biofilm formation. Infect. Immun. 67:5427-5433.
2. Heyman, D. (2004).Control of Communicable Disease Manual 18th ed. Washington DC., American public Health Association.
3. Chambers, H.F. (2001). The changing epidemiology of *Staphylococcus aureus* Emerg. Infect. Dis. 7 (2): 178–182.
4. Höök, M. and Foster, T. J. (2000). Staphylococcal surface proteins, p. 386-391. *In* V. A. Fishetti, R. P. Novick, J. J. Feretti, D. A. Portnoy, and J. I. Rood (ed.), Gram-positive pathogens. ASM Press, Washington, D.C.
5. Boneca, I. G.; Dussurget , O. ;Cabanes, D. ;Nahori, M .A.; Sousa. S; Lecuit, M.; Psylinakis, E .; Bouriotis, V .;Hugot, J. P. and Giovannini, M. (2007).

Peptidoglycan molecular requirements allowing detection by Nod1 and Nod2. Proc. Natl. Acad. Sci. USA 104: 997-1002.

6. Cheetham, J. C.; Artymiuk, P.J. and Phillips, D.C. (1992) Refinement of an Enzyme Complex with Inhibitor Bound at Partial Occupancy. Hen Egg-white Lysozyme and Tri-N-Acetylchitotriose at 1.75Å Resolution J. Mol. Biol. 224-61.
7. Varki , A.; Cummings, Richard; Esko, Jeffrey; Freeze, Hudson; Hart, Gerald; and Marth, J. (1999) Essentials of Glycobiology, Cold Springs Harbor Laboratory Press, Plainview, New York
8. Cheetham, J. C.; Artymiuk, P.J. and Phillips, D.C. (1992) Refinement of an Enzyme Complex with Inhibitor Bound at Partial Occupancy. Hen Egg-white Lysozyme and Tri-N-Acetylchitotriose at 1.75Å Resolution J. Mol. Biol. 224-613.
9. Uwaezuoke, J. C. and Aririatu, L. E.(2004)) A survey of Antibiotic resistant *Staphylococcus aureus* strains from clinical sources in Owerri. J. Appl. Sci. Environ. Managt. 8(1):67-8.
10. Ellis, N.A.; Ciocci, S. and German, J. (2001). "Back mutation can produce phenotype reversion in bloom syndrome somatic cells". Hum. Genet. 108 (2): 167-173.
11. Atlas, R. M; Parks, L. C. and Brown, E. A. (1995). laboratory manual of experimental microbiology . Mosby-year book Inc. Wesline Industrial Drive, St. Louis, Missouri.
12. NCCL, National Committee of Clinical Laboratory Standard (2002). Performance standards for antimicrobial disk susceptibility tests. 4th ed. Vol (22)1.
13. Sambrook, J. and Russell , D. W. (2001). Molecular cloning a lab manual. 3rd ed. Cold spring harbor lab. Poes. Cold spring harbor, N.Y.
14. Chapple , M. R. ; Barbara, I. and Peter , R. S. (1991). Lethal and mutational effect of solar and UV radiation on *S. aureus* .Arch. microbial. (157)3:242-248.
15. Birnboim, H. C. and Doly, J. (1982). A rapid alkaline extraction procedure for screening recombinant plasmid DNA. Nucl. Acid. Res. 7:1513-1523.
16. Yabu, K. and Huempfner, H. R. (1974). Inhibition of growth of *Mycobacterium smegmatis* and of cell wall synthesis by D-serine. Antimicrob. Agents Chemother.6:1-10.

17. Inoue, R.; Kaito, C.; Tanabe, M.; Kamura, K.; Akimitsu, N. and Sekimizu, K. (2001). Genetic identification of two distinct DNA polymerases, DnaE and PolC, that is essential for chromosomal DNA replication in *Staphylococcus aureus*. Mol Genet Genomics 266, 564–571.
18. Danon, A.; Rotari. V. I.; Gordon ,A.; Mailhac, N. and Gallois, P. (2004) Ultraviolet-C overexposure induces programmed cell death in Arabidopsis, which is mediated by caspase-like activities and which can be suppressed by caspase inhibitors, p35 and Defender against Apoptotic Death. J. Biol. Chem. 279: 779-787.
19. Matsumura, Y. and Ananthaswamy, H. N. (2004), "Toxic effects of ultraviolet radiation on the skin ‹"Toxicology and Applied Pharmacology: 298-308‹
20. Sheagren, J. N. (1984) *Staphylococcus aureus* the president pathogen. N. Engel. J. Med.310:1368-1378.
21. Neuhaus, F. C. and Baddiley, J. (2003). A continuum of anionic charge, structure and function of D-alanyl-teichoic acid in gram positive bacteria. Microbiol. Mol. Bio. Rev. 67:686-723.
22. Maree, C.L.; Daum, R. S.; Boyle-Vavra S.; Matayoshi, K. and Miller, L. G. (2007). "Community-associated methicillin-resistant *Staphylococcus aureus* isolates causing healthcare-associated infections". Emerging Infect. Dis. 13 (2): 236–242.
23. De Jonge, B. L. M.; Chang, Y. S.; Gage, D., and Tomasz, A. (1992) Peptidoglycan composition of a highly methicillin resistant *S. aureus* strain. J. Biol. Chem. 267:11248–11254.
24. Hirasawa, T.; Wachi, M. and Nagai, K. (2000).A mutation in *cornyebacterium glutamicium* LtsA causes susceptibility to lysozyme, temperature sensitive and glutamate production. J. Bacteriol. 182:2696-2701.
25. Hsieh, P. C.; Siegel, S. A.; Rogers, B.; Davis, D. and Lewis, K. (1998).Bacteria lacking a multidrug pump: a sensitive tool for drug discovery. Proc. Natl. Acad. Sci. USA 95:6602–6606.
26. Kunst, F.; Ogasawara, N. ; Moszer, I. ; Albertini, A. M. and Alloni, G. (1997). The complete genome sequence of the Gram-positive bacterium *Bacillus subtilis*. Nature 390:249–256.

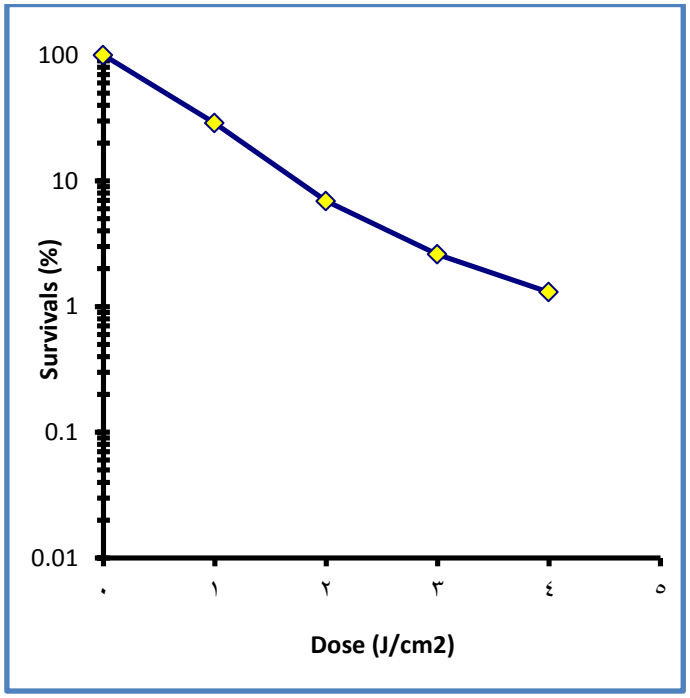

Figure 1. Survival curve for *S. aureus* after subjection to different doses of UV radiation (J/m^2).

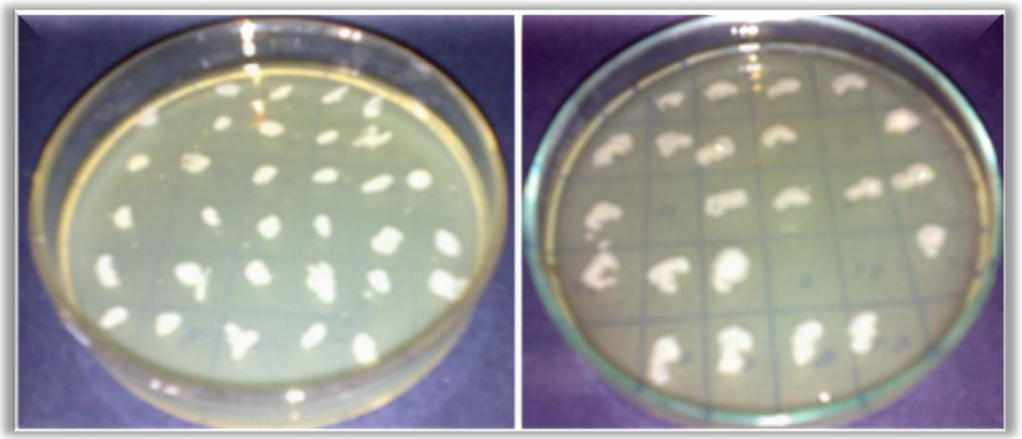

Figure 2. Screening lysozyme sensitive mutants of *S. aureus* after subjection to physical mutagenesis by UV radiation.

A: colonies plated on BHI agar (master plate).
B: colonies plated on BHI on agar containing 12.5µg/ml lysozyme.

Table 1: Antibiotic sensitivity of the wild type and mutants of *S. aureus* after subjection to UV mutagenesis and MNNG mutagenesis

`Antibiotic		Wild type	UV induced mutants			
Type	Conc. µg/ml		S2	S3	S4	S5
Gentamycin	10	R	S	R	R	R
Cephalothin	30	R	S	R	S	S
Cefotaxime	30	R	S	S	S	S
Erythromycin	15	R	S	S	S	S
Penicillin	10	R	R	R	R	R
Amoxicillin	25	S	S	S	S	S
Fucidic acid	10	R	R	R	R	R
Imipenem	10	S	S	S	S	S
Tetracycline	30	S	S	S	S	S
Pipracillin	100	R	R	R	R	R
Streptomycin	10	R	R	R	R	R
Vancomycin	30	R	R	S	R	R

R: Resistance S: Sensitive

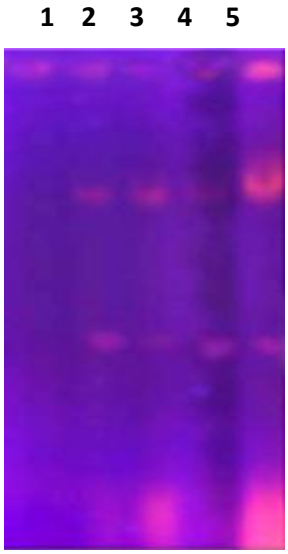

Lane 1: DNA extracted from wild type.
Lane 2: DNA extracted from lysozyme sensitive mutants S2.
Lane 3: DNA extracted from lysozyme sensitive mutants S3.
Lane 4: DNA extracted from lysozyme sensitive mutants S4.
Lane 5: DNA extracted from lysozyme sensitive mutants S5.

Figure 3. Genomic DNA extracted from *S. aureus* after subjection to mutagenesis by UV and MNNG on agarose gel (0.7%) electrophoresed for 2hours at 5v/cm.

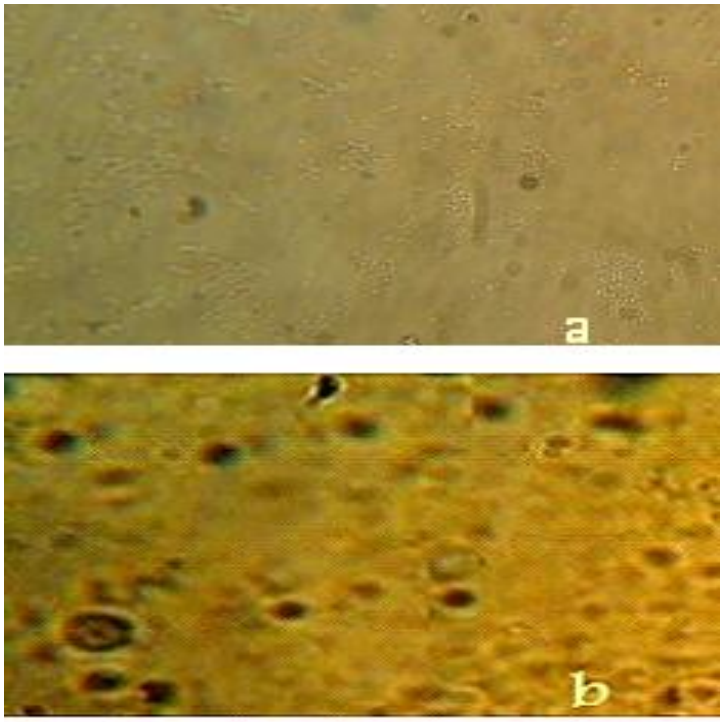

Figure 4: *Staphylococcus aureus* cells under light microscope.

a: wild type
b: lysozyme sensitive mutant S2 obtained after physical mutagenesis by UV radiation.

Table 2. Lysozyme sensitive mutants of *S. aureus* incubated at different temperatures.

Bacterial Isolate	Growth Temperature (°C)				
	30	37	40	43	45
WT	++	+++	++	+	+
S2	++	+++	++	-	-
S3	++	+++	++	-	-
S4	++	+++	++	+	+
S5	++	+++	++	+	+

+++ Very good growth ++ Good growth + Low growth - No growth
WT Wild type of *S. aureus*
S2, S3, S4, S5 Lysozyme sensitive mutants

Measurement of Calcium, Inorganic Phosphate and Albumin Levels in Serum of Iraqi Hypertensive Male Patients

Amal R. Farhan[+], Eham A. Ali[++], and Shatha M.J. Al-khateeb[++]

[+] Medical Laboratory Analysis, Medical Technical Institute, Foundation of Technical Education, Baghdad, Iraq. E-mail :f_fanar2004@yahoo.com
[++] Department of Clinical Biochemistry, College of Medicine, Al-Mustansiriya University, Baghdad, Iraq.

Abstract

Hypertension is a major health problem in adults, and contributes to cardiovascular disease. Malnutrition or deficiency in different nutrients found to be a risk factor for pathogenesis of essential hypertension. No clear association of calcium with blood pressure level could be identified. In this work serum calcium and albumin in hypertensive patients were compared with healthy control. Thirty uncomplicated, untreated, hypertensive, but otherwise have no other systemic diseases males, ranging in age from (26–55) years old, were entered into the study. Their blood pressure values were more than 95/140 mm Hg (seated posture). Control group consists of thirty healthy males with normal blood pressure and their age range is 22-46 years old. Serum calcium and serum albumin were measured calorimetrically using ready for use kits. Results showed a significant decrease ($p<0.05$) in serum calcium of patients group as compared with control group. No significant differences noticed between the two groups in serum albumin ($p>0.05$). Correlation coefficients between serum albumin and calcium in control group and patients group are 0.13, and 0.12, respectively. The ratio between mean serum albumin on mean serum calcium showed an increase in patients group (23.387) in comparing with control group (19.348). In this research we conclude that hypertensive patients have significantly lower serum total calcium than control group. Calcium supplements may be required as adjuvant treatment in addition to decrease NaCl in the diet to reduce excretion of calcium in urine. There is no significant difference between the two groups in serum albumin. In this work a new ratio (S. albumin/ S. calcium) is introduced as a useful marker for calcium state. No correlation was found between serum albumin and calcium in both groups indicating the need for estimating the free calcium in both groups. Further studies required for other biochemical parameters in larger patients sample size.

Keywords: hypertension, albumin, calcium, blood pressure.

قياس مستويات الكالسيوم والفوسفات اللاعضوي و الالبومين في امصال ذكور المرضى العراقيين المصابين بارتفاع ضغط الدم

آمال رشيد فرحان وايهام عامر علي وشذى محمد جواد الخطيب

الخلاصة:

ان ارتفاع ضغط الدم من المشاكل الصحية الرئيسية عند البالغين ويساهم في التسبب بأمراض القلب والشرايين. إن سوء التغذية ونقص بعض المواد الغذائية قد تكون من مسببات هذا المرض. لا توجد علاقة واضحة بين مستوى الكالسيوم في الدم ومرض ضغط الدم. في هذا البحث تم قياس تراكيز الكالسيوم والألبومين عند مرضى ضغط الدم ومقارنته بمستوياتهما عند الناس الأصحاء. لقد اشترك في هذه الدراسة 30 شخصا (ذكور فقط) مصابا بمرض ضغط الدم فقط وليس لديهم أمراض أخرى أعمارهم بين 26 و55 سنة. كان مستوى ضغط الدم لدى المرضى أعلى من 95/140 ملليمتر زئبق مقاسا بوضعية الجلوس. اخذ 30 شخصا سليما من المرض لغرض المقارنة أعمارهم بين 21 و44 سنة. كل المرضى لم تتم معالجتهم بأي دواء. تم قياس تركيزي الكالسيوم والألبومين بالطرق اللونية باستعمال العدد القياسية الجاهزة. أظهرت النتائج انخفاضا معنويا ($p<0.05$) في تركيز الكالسيوم في أمصال مرضى ضغط الدم مقارنة بمجموعة السيطرة بينما لا يوجد اختلاف معنويا ($p>0.05$) في تركيز الالبومين بين المجموعتين. كان معامل الارتباط بين تراكيز الكالسيوم والألبومين منخفضا لمجموعة المرضى ومجموعة السيطرة وبلغ 0.13 و0.12 ، على التوالي. ان قيمة نسبة معدل تراكيز الألبومين الى الكالسيوم (ألبومين/كالسيوم) هي نسبة عالية لدى مجموعة المرضى وتبلغ 23.387 مقارنة بمجموعة السيطرة 19.348. نستنتج من هذا البحث بان مرضى ضغط الدم لديهم تركيز اقل من الكالسيوم في المصل مقارنة بمجموعة السيطرة. لا يوجد اختلاف معنويا في تركيز الألبومين بين المجموعتين. وفي هذا البحث استحدثت نسبة جديدة هي نسبة معدل الألبومين الى معدل الكالسيوم في المصل كدليل مفيد لحالة الكالسيوم في الجسم. لا يوجد ارتباط بين تراكيز الألبومين والكالسيوم في مصول كلا المجموعتين مشيرا الى أهمية تقدير الكالسيوم الحر لدى المرضى بالإضافة الى الكالسيوم الكلي. يوصى بإضافة الكالسيوم كمساند الى برنامج علاج المرضى وتقليل تناول ملح الطعام لتقليل طرح الكالسيوم في الإدرار ودراسة مواد كيموحيوية أخرى لدى مرضى ارتفاع الضغط وبحجم عينات اكبر.

الكلمات الدالة: ارتفاع ضغط الدم، الألبومين، الكالسيوم، ضغط الدم

Introduction

Hypertension was defined as blood pressure greater than 140/90 mmHg. High blood pressure results from either an increased output of blood by the heart or, most often, increased resistance to blood flow in the arteries. In those with high blood pressure, the heart must work harder than normal to force blood through the arteries. Hypertension is a major health problem in adults, and contributes to cardiovascular disease. Hypertension, the most common cardiovascular disease, affect about 30% of Americans over age 50 and 50% by age 74 and only about 27% of American hypertensive have their blood pressure under control ,prevalence of hypertension is showing alarmingly steep rise due to rapid changes in diet and lifestyle. There are two types of hypertension; primary (essential hypertension) which accounts for 90%of cases and secondary hypertension which account for 10% of cases is secondary from other identifiable disorders ,about half of hypertensive are 'salt-sensitive', meaning that their blood pressure will decrease significantly when salt intake is restricted [1,2].

Positive family history of cardiovascular diseases and other atherosclerosis risk factors, obesity, high salt intake are known to be a major risk factor in hypertension, hypercholesteremia is a risk factor for atherosclerosis and subsequent hypertension [3].

Malnutrition or deficiency in different nutrients found to be a risk factor for pathogenesis of essential hypertension , such as zinc , vitamin C and deficiency in different other antioxidants [4].

There are many repots about alteration in the trace elements and other metals level and hypertension. Altered plasma status of copper, zinc, magnesium and calcium in hypertension has been reported [5]. Dietary intakes of potassium and magnesium have been reported to have favorable effects on blood pressure. Intake of these elements and calcium reduce blood pressure [6]. Cholesterol and nicotine are also risk factors for hypertension [7].

Current American guidelines recommend weight control, reduced intake of sodium chloride (salt), reduced alcohol consumption, and possibly increased dietary potassium as nutritional approaches to prevent and treat hypertension [8].

A relationship of calcium and magnesium intake with BP levels in the young has been studied, with variable

results. No clear association of potassium or calcium with BP level could be identified an Investigational effort to detect an independent effect of a dietary Action on BP level is complicated by the intercorrelation of multiple nutrients in the diet. A possible relationship between increase serum level of different substances including vitamin D and calcium, and cardiovascular disease was recorded [9,10].

In observational studies, significant inverse associations of blood pressure with intake of magnesium, potassium, calcium, fiber, and protein have also been reported [11]. However, in trials that tested these nutrients, often as dietary supplements, the reduction in blood pressure has typically been small and inconsistent [(12)]. Hence, in this study, serum calcium, inorganic phosphate, and albumin in hypertensive patients were compared with healthy control. In addition, serum albumin/serum calcium ratio was tested as indicator for calcium state in blood. The aim is obtaining a recommendation about using calcium supplements as a mean for treatment by altering serum calcium (if present).

Materials and Methods

Thirty uncomplicated, untreated, hypertensive, but otherwise have no other systemic diseases males were entered into the study. Their age expressed as mean ± standard deviation was (54.7±11.5) years old. Each hypertensive subject had a blood pressure measurement by conventional sphygmomanometry in excess of 90/140 mm Hg (seated posture), with the arm in the horizontal position after 5 min of quiet sitting, and had never received any antihypertensive treatment. The study was performed under out-patient conditions. Control group consists of thirty healthy males with normal blood pressure and their age range is between 22 and 46 years old. When the heart contracts (systole), blood pressure increases; when the heart relaxes (diastole), the pressure decreases. Average blood pressure reading for young adults in good physical condition are 110-120mmHg systolic over 70-80mmHg diastolic.

Five milliliters of venous blood samples were collected from cases without tourniquet. Sera were separated and measured immediately or, if necessary, stored at (-20° C) until analysis. Serum calcium measured by O-cresolphthalin complexion method [13] and serum albumin by bromocresol green method [14] using the procedures described by Randox® kits leaflets. The inorganic phosphorous was estimated in serum

using BioMerieux® kit. The method is colorimetric determination without deproteinization using a single reagent (ammonium hepta-molybdate) which reacts with serum phosphorous to form a phosphomolybdate complex in the presence of a reducing agent (ferrous sulfate). The colored complex is measured at 690 nm.

Results

The results of serum calcium and albumin in patients and control groups expressed as (Mean ± Standard deviation) in addition to the S.Albumin /S.Ca^{+2} ratios are represented in Table 1.

Serum calcium concentration was decreased in patients when compared with healthy control (1.84± 0.44, 2.27±0.22 mmol/L respectively) with P- value < 0.05.

The same result obtained when compare the level of serum albumin, there was decrease in this level in hypertensive patients when compared with healthy control, but this decrease was statistically not significant (P-value> 0.05), (41.55±7.72,44.76±5.74 g/ L respectively) .

The ratio between mean serum albumin on mean serum calcium showed an increase in patients group (23.387g/mmol) in comparing with control group (19.348 g/mmol).

Regarding the serum inorganic phosphate concentration, there was decrease in patients as compared with control (0.98±0.45, 1.17±0.14 mmol/L respectively) ,but this difference is not significant P- value > 0.05 .

Discussion

The decrease in serum calcium noticed in the present work is in accordance with other researches. In one research both serum and intralymphocytic concentrations of Na^{+}, and Ca^{+2} in hypertensive group were significantly higher than those in the normotensives [12]. Several experimental and clinical studies suggest that calcium depletion elevates blood pressure. Also the results support the studies related to the treatment of hypertension by mineral supplements including calcium [15].

Calcium load leads to the increment in Na excretion [16] and a reduced sodium intake reduced calcium excretion and *vice versa* and hence decreases in hypertension. The maintained natriuretic ability found in patients with higher salt sensitivity

could be mediated not only by the degree of underlying volume expansion but also by a well-known natriuretic effect of calcium (Ca^{+2}) through an increase in the renal tubular Ca^{+2} concentration [17].

Table 1. omparison between Calcium, Inorganic Phosphate and Albumin levels in serum of Iraqi hypertensive male patients and control group,represent as mean± SD.

	Patients (n=30)	Healthy Control (n=30)	P-value
S.Calcium(mmol/L)	1.84± 0.44	2.27 ± 0.22	2.063E-05
S.Albumin(g/L)	41.55 ±7.72	44.76 ± 5.74	0.09
S.Phosphate(mmol/L)	0.98 ± 0.45	1.17 ± 0.41	0.084
S.Albumin / S.Ca++(g/mmol)	0.98 ± 0.45	1.17 ± 0.41	

These changes in the blood pressure with low serum calcium level could possibly be attributed to some poorly known alterations in cell membrane transport mechanisms. Abnormal cellular ion transport resulting in altered membrane control over intracellular calcium may be related to essential hypertension [18]. The free intracellular calcium concentration determines the tension in vascular smooth muscle cells, thereby resulting in peripheral vascular resistance. Calcium has direct effect on peripheral vascular tone. Alternations in intracellular calcium are thought to be involved in the common pathway mediating the secretion and action of many hormones, including the presser action of catecholamine and angiotensin II [19]. Ionized serum Ca is reported to be lower in low-renin hypertensive patients and higher in high-renin hypertensive patients than in normal-renin hypertensive or in normotensives. Plasma renin activity in essential hypertension has a continuous negative correlation with serum Mg and a positive correlation with serum ionized Ca. Hence, plasma renin in hypertension may reflect (or contribute to) Ca and Mg flux changes across cell membranes [20].

Another notable factor which is indirectly involved in the pathogenesis of essential hypertension is altered lipid metabolism in the situation of low serum calcium level or decreased dietary calcium intake. Low calcium diet or low serum calcium stimulates increased production of 1,25-dihydroxyvitamin D which in turn,

stimulates adipocyte Ca2+ influx and, as a consequence, stimulates lipogenesis, suppresses lipolysis, and increases lipid accumulation; whereas increasing dietary calcium inhibits these effects and markedly accelerates fat loss. Many researchers even recommend a regular consumption of the recommended daily levels of dietary calcium to combat with hypertensive disorders [21]. Jolma P et al. [22] found that calcium supplementation reduced blood pressure in hypertensive individuals during chronic nitric oxide synthase inhibition and abrogated the associated impairments in endothelium-dependent and endothelium-independent arterial relaxation. High calcium diet had been found to enhance the vasorelaxation in nitric oxide-deficient hypertension.

The research observations may elucidate the mechanism(s) by which oral Ca^{+2} supplementation decreases blood pressure in patients with salt-sensitive hypertension [23]. Significant inverse correlation of blood pressure with the increase intake of some metals including calcium and different other nutrients have been frequently recorded. More recently the Dietary Approach to Stop Hypertension (DASH) [24] clinical trial in adults with high, normal, and untreated stage I hypertension demonstrated that significant BP reduction occurred on a diet high in fruits and vegetables and low-fat dairy products. Diets with high fiber content of, which may have impeded calcium absorption [25] while there is also some evidence that other diet nutrients, including potassium, calcium, and magnesium, are inversely related to BP levels, the BP level is higher in those with diets lower in potassium, calcium, magnesium, and vitamins. These results suggest that diets deficient in multiple nutrients may contribute to the development of hypertension in adolescents having risk factors for cardiovascular disease. These observations are consistent with the dietary benefits on BP level observed in the DASH trial [24]. Indeed, several studies suggest that the effect of Na intake on blood pressure is determined by the adequacy of other minerals, such as Ca^{+2} , Mg^{+2} and K^{+} . [26].

The presser effect of NaCl seems to be expressed in subjects with the lowest intake of these minerals [21]. The natriuretic effect of Ca^{+2} may be mediated either through increases in serum and/or renal tubular Ca^{+2} concentrations. In one research, oral intake of calcium lactate tablet increased Urinary excretion of calcium and could reduce their average blood pressure and prevent them from

hypertension for those with mild and moderate hypertension and in high risk with higher blood pressure [27].

The results of this research revealed additional evidence to the fact that the retention in calcium excretion and subsequent maintenance in serum calcium is good for hypertension.

The kidney plays a key role in the maintenance of mineral ion homeostasis, particularly that of calcium (Ca^{+2}). Urinary calcium (UCa^{+2}) excretion depends on the filtered load of Ca^{+2} and on several other factors, including PTH levels, sodium (Na^{+}) excretion, serum concentrations of Ca^{+2} and magnesium (Mg^{+2}), Ca^{+2} intake and absorption, and acid-base status [28]. The effect of NaCl loading is hypercalciuric and hence decreases in serum calcium. In those who are salt sensitive and in whom dietary calcium is suboptimal dietary replenishment of calcium may reduce blood pressure. Volume expansion with saline causes a decline in Na^{+} and Ca^{+2} reabsorption by the kidney proximally and distally, thereby resulting in an increase in the excretion of both cations. Untreated hypertensive patients had a higher prevalence of hypercalciuria in patients with essential hypertension. It was concluded that hypercalciuria is a frequent finding of untreated essential hypertension [29].

Hypertensive subjects have been shown to present an increase in urinary calcium excretion despite a lower dietary calcium intake ; this apparent paradox has been referred to as a renal calcium leak, and several studies have clearly suggested that urinary calcium excretion was significantly higher in salt-sensitive subjects compared with those who were salt-resistant [15].

The results also indicate that there is no significant difference in the serum inorganic phosphate in patients and control groups. Hence the change in calcium may not dependent on the changes in serum inorganic phosphate only but may involve the free ionic calcium in addition to the bound calcium. In one hypertension research unit, the plasma Aldosterone concentration and parathyroid hormone are high. At the same time we found calcium metabolism alterations: high urine calcium excretion, low serum ionic calcium [30]. These alterations may explain the indifference in serum albumin and decrease in serum calcium in hypertensive patients noticed in our research. In only one study proteinuria (macroalbuminuria) was found to correlate positively and very significantly with both systolic and diastolic blood pressure, but this study needs more confirmation because we didn’t find any corresponding results.

Serum albumin may be affected if there is renal damage [31] and our patients group has no renal complications as mentioned in the subjects and methods paragraph, while another study revealed a positive association was found between serum albumin and blood pressure, since albumin in contrast to high blood pressure is consider to be cardio protective, probably effect cardiovascular risk by unrelated mechanisms.

In the present work, the ratio between serum albumin and serum calcium ratio may be more useful indicator for any change in calcium even it has not noticed statistically. The ratio need more studies in different other diseases related to calcium metabolism to knowledge evaluate its advantages as predictor for these diseases.

Conclusion

Hypertensive patients have significantly lower serum total calcium than control group. There is no significant difference between the two groups in serum albumin and inorganic phosphate. In this work, a new ratio (S.albumin/ S. calcium) is introduced as a useful marker for calcium state. There is a need for estimating the free calcium in both groups. Calcium supplements may be required as adjuvant treatment in addition to decrease NaCl in the diet to reduce excretion of calcium in urine. Further studies required for other biochemical parameters in larger patients sample size.

References

1. Kearney PM, Whelton M, Reynolds K, Muntner P, Whelton PK, He J; Global burden of hypertension: analysis of worldwide data; Lancet. 2005 Jan 15-21; 365(9455):217-23.
2. Popkin BM, Horton S, Kim S, Mahal A, Shuigao J: Trends in diet, nutritional status, and diet-related noncommunicable diseases in China and India: the economic costs of the nutrition transition. Nutr Rev. 2001 59 :379 –90.
3. Al-Hazimi AM, Syiamic AY.Relationship between plasma angiotensinII, leptin and arterial blood pressure. Saudi Med J. 2004 Sep;25(9):1193-8.
4. Shashi A. Chiplonkar, Vaishali V. Agte, Kirtan V. Tarwadi, Kishor M. Paknikar, Uma P. Diwate,; Micronutrient Deficiencies as Predisposing

Factors for Hypertension in Lacto-Vegetarian Indian Adults Journal of the American College of Nutrition, (2004) 23 (3): 239-247.

5. Patki PS, Singh J, Gokhale SV, Bulakh PM, Shroti DS, Patwardhan B: Efficacy of potassium and magnesium in essential hypertension: a double blind,placebo controlled,crossover study.Br Med J 1990,301:521-523.
6. Saladin K.S., Porth C.M. (1998): Anatomy & Physiology : The Unity of Form & Function .1 st Edition . McGrawHill.p:709.
7. Falkner B., Sherif K., Michel S.; Harvey Kushner, Dietary Nutrients and Blood Pressure in Urban Minority Adolescents at Risk for Hypertension. Arch Pediatr Adolesc Med. 2000;154 (9):918-922.
8. Gillman MW, Oliveria SA, Moore LL, Ellison RC. Inverse association of dietary calcium with systolic blood pressure in young children. JAMA. 1992;267:2340-2343.
9. Rajasree S, Rajpal K, Kartha CC, Sarma PS, Kutty VR, Iyer CS, Girija G. Serum 25-hydroxyvitamin D3 levels are elevated in South Indian patients with ischaemic heart disease. Eur J Epidemiol. 2001;17(6):567-71.
10. Burgaz A, Byberg L, Rautiainen S, Orsini N, Håkansson N, Ärnlöv J, Sundström J, Lind L, Melhus H, Michaëlsson K, Wolk A Confirmed hypertension and plasma 25(OH)D concentrations among elderly men J Intern Med. 2011;269:211-8.
11. Obarzanek E, Velletri PA, Cutler JA. Dietary protein and blood pressure, JAMA 1996;275:1598-1603.
12. Li J, Wang J, Chen X, Tong S, Fang J, Yu H. Cross-sectional survey of intralymphocytic and serum elements in hypertensive patients. Chin Med J (Engl). 1999 Jul;112(7):641-5.
13. Doumas B.T., Watson W.A., Biggs H.G., Clin.Chim.Acta. 1971;31:87.
14. Corns C., Ludman C. Ann. Clin.Biochem. 1987, 24, 345.
15. (2AA) Kamlesh Jha and Poonam Kumari, Serum Calcium in Essential hypertension and its Co-relation with Severity of the Disease. Advanced Studies in Biology, Vol. 3, 2011, no. 7, 319 - 325
16. PCoruzzi, L. Brambilla, V. Brambilla, M. Gualerzi, M. Rossi, G. Parati, et al: Potassium Depletion and Salt Sensitivity in Essential Hypertension. J Clin Endocrinol Metab 2001 Vol. 86, No. 6 2857-2862
17. Lin PH, Ginty F, Appel LJ, Aickin M, Bohannon A, Garnero P, Barclay D, et al.

The DASH diet and sodium reduction improve markers of bone turnover and calcium metabolism in adults. J Nutr. 2003 Oct;133(10):3130-6.

18. DC Hatton and DA McCarron; Dietary calcium and blood pressure in experimental models of hypertension. A review Hypertension, Vol 23,513-530.
19. K. Sudhakar, M. Sujatha, S. Ramesh Babu, P. Padmavathi and P. P. Reddy, serum calcium levels in patients with essential hypertension and their First degree relatives. Indian Journal of Clinical Biochemistry, 2004, 19 (1) 21-23.
20. Resnick, Lawrence M .; Laragh, John H.;Sealey ,Jean E .; Alderman,Michael H.Divalent Cations in Essential Hypertension-Relations between Serum Ionized Calcium,Magnesium,and Plasma Renine Activity.New-Engl-J-Med. Boston, Mass.;Massachusetts Medical Society. Oct 13,1983.v. 309(15)p.
21. Zemel MB, Thompson W, Milstead A, Morris K, Campbell P Calcium and dairy acceleration of weight and fat loss during energy restriction in obese adults. Obes Res. 2004 Apr;12(4):582-90.
22. Jolma P, Kalliovalkama J, Tolvanen J-P, Kööbi P, Kähönen M, Hutri-Kähönen N, Wu X, Pörsti I. High-calcium diet enhances vasorelaxation in nitric oxide-deficient hypertension. Am J Physiol Heart CircPhysiol 2000:279(3):H1036-H1043.
23. McCarron DA. Role of adequate dietary calcium intake in the prevention and management of salt-sensitive hypertension. Am J Clin Nutr. 1997;65:712S–716S) .
24. Appel LJ, Moore TJ, Obarzanek E, et al for the DASH Collaborative Research Group. A clinical trial of the effects of dietary patterns on blood pressure. N Engl J Med. 1997;336:1117-1124.
25. National Research Council. Diet and health: implications for reducing chronic disease risk. Washington, D.C.: National Academy Press, 1989:301.
26. Folaranmi OM and Adesiyan AA. Comparative study of plasma electrolytes (Na, K, Cl, and HCO3) and urea levels in HIV/AIDS and pulmonary tuberculosis infected subjects. Biokemistri 2004, 16 (1): 29-36.
27. Pan Z, Zhao L, Guo D, Yang R, Xu C, Wu X. [Effects of oral calcium supplementation on blood pressure in population] Zhonghua Yu Fang Yi Xue Za Zhi. 2000 Mar;34(2):109-12. (English abstract).

28. Haenni, A. Reneland, R., Lind, L. and Lithell, H. (2001). Serum aldosterone changes during hyperinsulinemia are correlated to body mass index and insulin sensitivity in patients with essential hypertension. J. Hypertens., 19, 107- 112.

29. Tasić N, Nesović M, Djurić D, Kanjuh V [Changes in calcium levels in blood and urine during various regimens of table salt intake in patients with essential arterial hypertension]. Srp Arh Celok Lek. 2002 Jan-Feb;130(1-2):7-1

30. John P. Forman, Naomi D.L. Fisher, Emily L. Schopick, and Gary C. Curhan. Higher Levels of Albuminuria within the Normal Range Predict Incident Hypertension. J Am Soc Nephrol, Published online June 25, 2008 DOI:

31. Ravjit Kaur Sabharwal , Parduman Singh , M M Arora ,B L Somani and Vivek Ambade.Incidence of Microalbuminuria in Hypertensive Pateints.Indian Journal of Clinical Biochemistry ,2008⁄23(1) 71-75.

Bioactivity of *Bacillus* Species Isolated from Human Feces

Adnan, H. Abbas[+], Jabbar, F. Al-Maadhidi[++], and Mahdi, S. Al-Rubaie[+]

[+]Ministry of Science and Technology, Baghdad, Iraq
[++]Madenat Alelem University College, Baghdad, Iraq

Abstract

In the present study, twenty isolates of *Bacillus* genus according to morphological feature of colonies and the presence of spores by light microscopy, were obtained from 15 samples of human feces, after heat-treated and killed all vegetative cells. These spore-former isolates were characterized at the species level biochemically by the use of API 50 CHB kit and identified as *Bacillus insolitus, B. laterosporus, B. polymyxa* and *B. bodius* with proportion ratio rate 40, 20, 35 and 5% of the total, respectively. Eighty five percent of *Bacillus* isolates were formed biofilm, which have protective and adhesive properties and could be responsible for an increased antibiotics resistance. Seventy five percent of *Bacillus* species isolated from human feces were produced inducible extracellular Levansucrase and responsible for synthesis of fructan polymers (levan), described as useful prebiotics due to the capacity of the β-linked fructose units. Five *Bacillus* species were showed positive result for Exopolysaccharides production. *Bacillus* species resistant to Ampicillin (AP), Chloramphenicol (C), Nitrofurantoin (NI), Gentamicin (GM), Carbenicillin (PY), Nalidixic acid (NA), Methenamine Mandelate (MM), and Cotrimoxazole (TS), reached 20, 100, 60, 0.0, 5, 95, 5 and 70%, respectively.

Keywords: *Bacillus* species, Human feces, Classification, Biofilm. Levansucrase, Exopolysaccharides, Antibiotic susceptibility.

الفعاليات الحيوية لأنواع بكتريا *Bacillus* المعزولة من براز الإنسان

عدنان حنون عباس و جبار فرحان المعاضيدي ومهدي صالح الربيعي

الخلاصة

جمعت في هذه الدراسة عشرين عزلة من جنس *Bacillus* حسب الصفات الشكلية للمستعمرات وتمييز السبورات بواسطة المجهر الضوئي، من 15 عينة براز إنسان بعد قتل الخلايا الخضرية بالمعاملة الحرارية. شخصت العزلات المكونة للسبورات كيميائيا باستخدام العدة API 50 CHB إلى *B. insolitus* ,*Bacillus laterosporus* ,*B. polymyxa* و*B. Bodius* بالنسب المئوية 40 و20 و35 و5 %، على التوالي. وجد أن 85% من عزلات *Bacillus* مكونة للفلم الحيوي الذي يمتلك خاصية الوقاية والالتصاق وقد يكون مسؤولا عن زيادة المقاومة للمضادات الحيوية. كما وجد ان 75% من أنواع *Bacillus* المعزولة من براز الإنسان منتجة لأنزيم Levansucrase المفرز خارج الخلية والمسؤول عن تخليق بوليمرات الفركتوز (الليفان) الموصوفة كمادة غذائية مفيدة للمعززات الحيوية. تبين أن خمسة أنواع من *Bacillus* منتجة للمواد البوليمرية الخارجية إضافة إلى مقاومتها للمضادات الحيوية التالية (AP) Ampicillin، (C) Chloramphenicol، (NI) Nitrofurantoin، (GM) Gentamicin، (PY) Carbenicillin، (NA) Nalidixic acid، (MM) Methenamine Mandelate، (TS) Cotrimoxazole، بالنسب المئوية 20، 100، 60، 0.0، 5، 95، 5 و 70 ، على التوالي.

الكلمات المفتاحية : أنواع بكتريا *Bacillus* ، براز الإنسان، التصنيف، الفلم الحيوي، ليفان سكريز، متعدد السكريات الخارجي، المقاومة للمضادات الحيوية.

Introduction

Bacteria belonging to the genus *Bacillus* species are commonly associated with soil, and as such are isolated almost ubiquitously from soil, water, dust, and air. The dominant bacteria found in the small and large intestines are species of Lactobacilli, Streptococci, Enterobacteria, Bifidobacteria, Bacteroides, Clostridia and *Bacillus* species. For example, in a

study of human faeces, *Bacillus* species were isolated in numbers of between 5 × 10^3 and 5 × 10^6 CFU g^{-1} feces [1].

Biofilm are formed by adhesion of cells to surfaces through an exopolymeric matrix. This matrix is important both in the formation and structure of the biofilm, and also on the protection of the cells since it may prevent the access of antimicrobials and xenobiotics to the cells inside the biofilm and confer protection against environmental stresses such as UV radiation, pH shifts, osmotic shock and desiccation [2, 3]. Bacterial strains that do not produce (exopolymeric substance or extracellular polysaccharide or exopolysaccharide) (EPS) present lower adhesive abilities than slime producing strains. EPS is particularly valuable after the initial phase of adhesion in organisms, conferring protection against phagocytosis, interference with the cellular immune response, reduction of antibiotic potency [4, 5] and may protect the cell against unfavorable environmental conditions like oxygen tension, toxic compounds, temperature or high osmotic pressure, and may contribute to the uptake of metal ions [6].

Fructosyloligosaccharides are described as useful probiotics due to the capacity of the β-linked fructose units to pass the gastrointestinal tract undigested. In the colon, they stimulate selectively the growth of beneficial gut bacteria, like Bifidobacteria or Lactobacilli [7]. In addition, fructan, like levan, are employed in the food and non-food industry as viscosifier, stabilizer, emulsifier, gelling, or water-binding agent. Fructooligosaccharides are produced by fructosyltransferases, like Levansucrase. Levansucrase (EC 2.4.10) synthesize levan composed of β-2, 6 linked fructose residues [8].

The functions of intestinal microbiota may include diverse actions in the gastrointestinal tract including nutritional fermentation, participation in the host's immune defense system against pathogens as a probiotic and production of metabolites or enrich metabolites such as glycans, amino acids, xenobiotics, vitamin K, folate and short-chain fatty acids [9].

One action of probiotics is that they can produce antimicrobial substances as direct antagonists against intestinal pathogens. Probiotics may exert their effective antagonistic activity alone or synergistically. Recent studies have indicated that the antagonistic activities against intestinal pathogens are produced by antimicrobial substances from several probiotics strains [10].

The aim of this study is to screen susceptibility of *Bacillus* species human feces for Biofilm, Levansucrase, Exopolysaccharides production and their resistant to antibiotics.

Materials and Methods

Bacterial strains

Spore-forming *Bacillus* isolates were obtained from laboratory of Bacteriology, Department of Biology, Ministry of Science and Technology, Baghdad, Iraq.

Biofilm assay

To test biofilm production overnight, cultures were used to inoculate liquid MSgg medium (100mM l^{-1}MOPS pH 7.0, 0.5% glycerol, 0.5% glutamic acid, 5mM potassium phosphate pH 7.0, 50µgm l^{-1} tryptophan, 50 mgm l^{-1} phenylalanine, 2 mM l^{-1} $MgCl_2$, 0.7 mM l^{-1} $CaCl_2$, 50µM l^{-1} $FeCl_3$, 50µM l^{-1} $MnCl_2$, 2µM l^{-1} thiamine, 1µM l^{-1} $ZnCl_2$) [11]. Cells grown at 37°C without shaking for up to 48h. Cells forming a solid layer at the liquid-air interface were considered as biofilm producers.

Levansucrase production

Screening on solid medium

Bacillus isolates were activated on Luria-Bertani (LB) broth (10gm Bacto-tryptone, 5gm Bacto-yeast extract, 10gm NaCl, completed to one liter of distilled water and pH was adjusted to 7.0), incubation was done at 37°C for 18h, one tenth micro liter of culture suspension was streaked on sucrose mineral salt agar and incubated at 37°C for 48h.

Enzyme production

The following medium was used as cellular production medium [12] for Levansucrase production and had the following composition (g/L): yeast extract 2.5gm, sucrose 200gm, $MgSO_4$ 0.2gm and K_2HPO_4 5.5gm. The medium was completed by addition one liter of distilled water, after adjusted the pH to 7.8.

Enzyme assay

Cells were harvested by centrifuge at 5000 rpm for 10min at 4°C and the supernatant was used as enzyme source. Sucrase activity was assayed by analyzing the reducing sugar liberated during sucrose hydrolysis. The reaction mixture [250µl of enzyme extract and 250µl of 1M sucrose in acetate buffer (50mM, pH 5.0)] was incubated at 30°C for 30min. Reducing sugar

released was determined according to Somogyi [13].

One unit of Levansucrase activity was expressed as the amount of enzyme required to liberate 1µmol of reducing sugar from sucrose in 1min under experimental conditions.

Production of Exopolysaccharides

The cultures were streaked on Yeast Malt Glucose agar (YMG) agar plates (Composition per liter: 10.0gm glucose, 3.0gm yeast extract, 3.0gm malt extract, 5.0gm peptone, agar 15gm, and pH was adjusted to 7.0). After incubating at 30°C for 48h the plates were examined for the presence of mucous colonies [14].

Antibiotic susceptibility testing

Antibiotic susceptibility testing was performed by the disc diffusion method [15]. The test was performed on Muller Hinton agar using antibiotic impregnated discs. The following eight antibiotic discs were used in the test: Ampicillin (AP), Chloramphenicol (C), Nitrofurantoin (NI), Gentamicin (GM), Carbenicillin (PY), Nalidixic acid (NA), Methenamine Mandelate (MM), Cotrimoxazole (TS). After 18 hours of incubation at 37°C, the strains were characterized as susceptible or resistant based on the zone of inhibition created around the discs.

Results and Discussion

Identification of spore-former Bacilli from human feces

Twenty isolates of *Bacillus* genus according to morphological feature of colonies and the presence of spores by light microscopy, used in this study (Table 1) were *B. insolitus, B. laterosporus, B. polymyxa and B. bodius* with (40, 20, 35 and 5)% of the total, respectively.

Biofilm production

Results showed that 85% of strains belong to *B. insolitus, B. polymyxa* and *B. laterosporus* with (17 out of 20) formed biofilm (Fig. 1). This is an interesting observation since biofilm have protective and adhesive properties and have been associated with a longer persistence of Bacilli in the gastrointestinal tract (GIT) of animals, then prevent the access of antimicrobials and xenobiotics to the cells inside the biofilm and confer protection against environmental stresses such as UV radiation, pH shifts, osmotic shock and desiccation [17]. In fact, the host immune system is, in general, capable of rapidly kill non-adherent bacteria. The slow growth rate observed in biofilm and/or transport limitations of nutrients, metabolites and oxygen between the

surface and the interior of the biofilm could be responsible for an increased antibiotic resistance over planktonic cells [18].

Fructan polymers production

In this study 75% of *Bacillus* species isolated from human feces were secreted inducible extracellular Levansucrase, appeared as mucoid consistence of bacterial colonies on sucrose mineral salt agar by using sucrose as carbon source (Table 2). A large amount of levan was produced when the bacteria were cultivated using sucrose, but the yields varied with the sucrose concentration. Enzymes responsible for the synthesis of fructan polymers of the levan type are generally referred to as fructosyltransferases (FTF) or Levansucrase. They catalyse the transfer of the fructosyl unit of sucrose to a number of acceptors including sucrose, water (resulting in hydrolysis) and fructan polymer [19]. So fructosyloligosaccharides are described as useful prebiotics due to the capacity of the β-linked fructose units to pass the gastrointestinal tract undigested. In the colon, they stimulate selectively the growth of beneficial gut bacteria, like *Bifidobacteria* or Lactobacilli [7].

Exopolysaccharides production

Out of 20 isolates only five were showed positive result for Exopolysaccharides on YMG agar (Fig. 2). Microorganisms synthesize large spectrum multifunctional polysaccharides including intracellular polysaccharides, structural polysaccharides and extracellular polysaccharides (EPSs). Exopolysaccharides generally consist of monosaccharide and some non carbohydrate substituent's (such as protein, nucleic acids, lipids, acetate, pyruvate, succinate, and phosphate). Microbial EPS plays an important task in interaction between bacteria and their environment [20]. EPS showed higher stability against enzymatic degradation, capability for metal removing, and heat stable. It may find possible applications in the industrial fields and in biotechnological processes [21].

Antibiotic resistance

The antibiotic resistance pattern showed that *Bacillus* species isolated from human feces were resist to Ampicillin (AP), Chloramphenicol (C), Nitrofurantoin (NI), Gentamicin (GM), Carbenicillin (PY), Nalidixic acid (NA), Methenamine Mandelate (MM), Cotrimoxazole (TS), with proportion ratio rate (20, 100, 60, 0.0, 5, 95, 5 and

70)%, respectively (Table 2). *Bacillus* specie showed multiple drug resistance (MAR) against four tested antibiotics (More than 50%) appeared with Chloramphenicol (C), Nitrofurantoin (NI), Nalidixic acid (NA) and Cotrimoxazole (TS). Regardless of whether the resistance is mediated by excessive or multiple exposures to antibiotics by other mechanisms, the antibiotic resistant bacteria may have public health significance. The selective process leading to the emergence and maintenance of bacterial resistance to antibiotics are mainly brought about by incorrect or abusive utilization of the drugs [22].

Table 1. Strains of *Bacillus* spp. isolated from feces [16].

Strains	Species
AS1	*Bacillus insolitus*
AS2	*Bacillus laterosporus*
AS3	*Bacillus insolitus*
AS4	*Bacillus laterosporus*
AS5	*Bacillus laterosporus*
AS6	*Bacillus polymyxa*
AS7	*Bacillus laterosporus*
AS8	*Bacillus insolitus*
AS9	*Bacillus insolitus*
AS10	*Bacillus polymyxa*
AS11	*Bacillus insolitus*
AS12	*Bacillus polymyxa*
AS13	*Bacillus polymyxa*
AS14	*Bacillus polymyxa*
AS15	*Bacillus bodius*
AS16	*Bacillus polymyxa*
AS17	*Bacillus insolitus*
AS18	*Bacillus insolitus*
AS19	*Bacillus polymyxa*
AS20	*Bacillus insolitus*

*Species assignment was based on the results of the API 50 CHB kit.

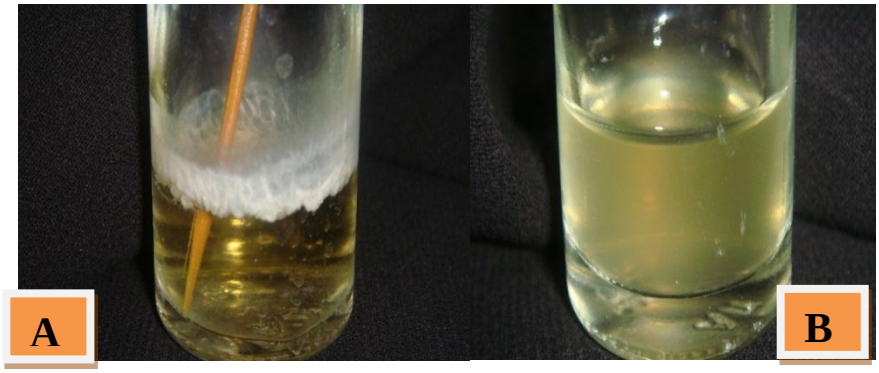

Figure (1) Biofilm production, (A) positive, (B) negative

Table 2. *Bacillus* species levansucrase production

Strains	Species	Levansucrase production	Levansucrase activity Unit / ml
AS1	*Bacillus insolitus*	+	92.096
AS2	*Bacillus laterosporus*	-	-
AS3	*Bacillus insolitus*	+	92.153
AS4	*Bacillus laterosporus*	-	-
AS5	*Bacillus laterosporus*	-	-
AS6	*Bacillus polymyxa*	+	90.893
AS7	*Bacillus laterosporus*	-	-
AS8	*Bacillus insolitus*	+	93.264
AS9	*Bacillus insolitus*	+	88.453
AS10	*Bacillus polymyxa*	+	89.553
AS11	*Bacillus insolitus*	+	92.886
AS12	*Bacillus polymyxa*	+	97.216
AS13	*Bacillus polymyxa*	+	95.945
AS14	*Bacillus polymyxa*	+	91.855
AS15	*Bacillus bodius*	-	-
AS16	*Bacillus polymyxa*	+	92.577
AS17	*Bacillus insolitus*	+	94.158
AS18	*Bacillus insolitus*	+	93.092
AS19	*Bacillus polymyxa*	+	92.096
AS20	*Bacillus insolitus*	+	94.432

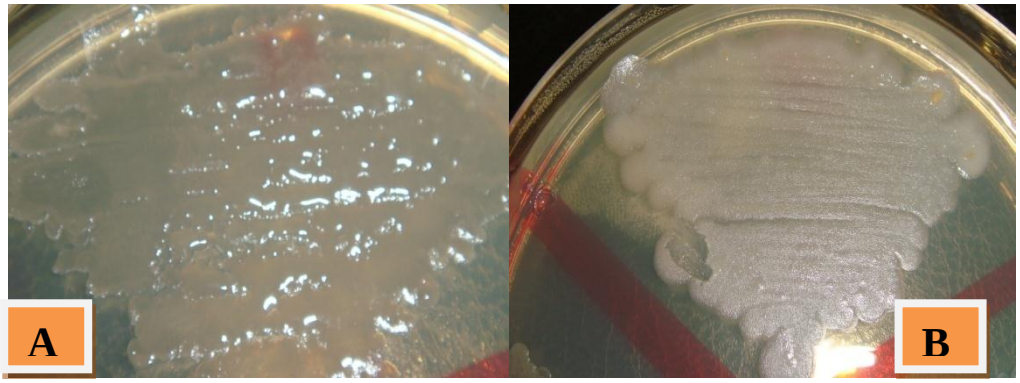

Figure 2. Exopolysaccharides production
(A) positive, (B) negative

Table 3. Antibiotic susceptibility testing for human feces *Bacillus* species

Strains	Species	Antibiotics (mm)							
		AP	C	NI	GM	PY	NA	MM	TS
AS1	*Bacillus insolitus*	10	18	10	S	S	30	S	30
AS2	*Bacillus laterosporus*	S	20	17	S	S	20	S	27
AS3	*Bacillus insolitus*	S	15	18	S	S	15	S	25
AS4	*Bacillus laterosporus*	S	18	8	S	S	13	S	S
AS5	*Bacillus laterosporus*	S	13	15	S	S	22	S	30
AS6	*Bacillus polymyxa*	12	30	S	S	S	20	S	25
AS7	*Bacillus laterosporus*	15	28	S	S	S	15	S	20
AS8	*Bacillus insolitus*	10	28	S	S	10	20	S	25
AS9	*Bacillus insolitus*	S	17	S	S	S	25	S	27
AS10	*Bacillus polymyxa*	S	15	13	S	S	17	S	20
AS11	*Bacillus insolitus*	S	15	10	S	S	10	S	17
AS12	*Bacillus polymyxa*	S	17	S	S	S	26	S	26
AS13	*Bacillus polymyxa*	S	17	S	S	S	17	S	S

AS14	*Bacillus polymyxa*	S	15	S	S	S	23	S	S
AS15	*Bacillus bodius*	S	19	10	S	S	S	S	15
AS16	*Bacillus polymyxa*	S	17	S	S	S	17	S	S
AS17	*Bacillus insolitus*	S	25	12	S	S	17	S	10
AS18	*Bacillus insolitus*	S	19	10	S	S	19	S	17
AS19	*Bacillus polymyxa*	S	17	12	S	S	16	S	S
AS20	*Bacillus insolitus*	S	25	13	S	S	20	8	S
Proportion ratio rate of antibiotic resistance %		20	100	60	0.0	5	95	5	70

R: Resistance, S: Sensitive, AP : Ampicillin, C: Chloramphenicol,
NI : Nitrofurantoin, GM : Gentamicin, PY: Carbenicillin,
NA: Nalidixic acid, MM: Methenamine Mandelate, TS: Cotrimoxazole

References

1. McFarlane, G. T. ; Cummings, J. H. and Allison, C. (1986). Protein degradation by human intestinal bacteria. J. Gen. Microbiol., 132, 1647–1656.
2. Davey, M. E. and Toole, G. A. (2000). Microbial biofilm: from ecology to molecular genetics, Microbiol. Mol. Biol. Rev., 64: 847-67.
3. Flemming, H. C. (1993). Biofilm and environmental protection. Water Sci. Technol., 27 : 1-10.
4. Costerton, J. W. (1999). Introduction to biofilm. Intern. J. Antimicrob. Agents, 11 : 217-21.
5. Costerton, J. W. ; Stewart, P. S. and Greenberg, E. P. (1999). Bacterial biofilm: a common cause of persistent infections. Science, 284 : 1318-22.
6. Cerning, J. (1990). Exocellular polysaccharides produced by lactic acid bacteria. FEMS. Microbiology Reviews 87, 113-130.
7. Salminen, S. ; Isolauri, E. and Salminen, E. (1996). Clinical uses of probiotics for stabilizing the gut mucosal barrier: successful strains and future challenges. Antonie Van Leeuwenhoek 70 : 347–358.

8. Van Hijum, S. A. ; Szalowska, E. ; Vander Maarel, M. J. and Dijkhuizen, L. (2001). Biochemical and molecular characterization of a Levansucrase from *Lactobacillus reuteri*. Microbiology 150 : 621–630.

9. Hooper, L. V. ; Midtwedt, T. and Gordon, J. I. (2002). "How host microbial interactions shape the nutrient environment of the mammalian intestine", Annu. Rev. Nutr., 22, 283-307.

10. Verdenelli, M. C. ; Ghelfi, F. ; Silvi, S. ; Orpianesi, C. ; Cecchini, C. and Cresci, A. (2009). "Probiotic properties of *Lactobacillus rhamnosus* and *Lactobacillus paracasei* isolated from human faeces", Eur. J. Nutr., 48, 355-363.

11. De Kievit, T. R. ; Gillis, R. ; Marx, S. ; Brown, C. and Iglewski, B. H. (2001). Quorum sensing genes in *Pseudomonas aeruginosa* biofilms: their role and expression patterns. Appl. Environ. Microbiol., 67 : 1865–1873.

12. Yanase, H. ; Fukushi, H. ; Ueda, N. ; Maeda, Y. ; Toyoda, A. and Tonomura, K. (1991). Cloning, sequencing and characterization of the intracellular invertase gene from *Zymomonas mobilis*. Agric. Biol. Chem 55 : 1383–1390.

13. Somogyi, M. J. (1952). Notes on sugar determination. J. Biol. Chem., 195 : 19-23.

14. Ganguly, R. S. ; Manjrekar, S. D. ; Shree, S. A. and Bhadekar, R. K. (2012). Evaluation of marine microorganisms for characteristic presence of novel biomolecules. Romanian Biotechnological Letters, Vol. 17, No.(3) : 7279-7286

15. National Committee for Clinical Laboratory Standard (NCCLS). (1998). Performance standards for anti microbial susceptibility testing, Third Information Supplement Villonova PA : 108 pp.

16. Al-Rubaie, M. S. ; Abbas, A. H. ; Hamza, I. S. ; Abbas, A. K. ; Fachary, S. S. and Abdelhameed, F. F. (2012). Biofilm and Levan production by *Bacillus* species isolated from human feces. International Journal for Sciences and Technology, Vol. 7, No. 3 : 71– 77.

17. Davey, M. E. and O'Toole, G. A. (2000). Microbial biofilms: from ecology to molecular genetics, Microbiol. Mol. Biol. Rev., 64 : 847-67.

18. Donlan, R. M. and Costerton, J. W. (2002). Biofilms: survival mechanisms of clinically relevant microorganisms. Clin. Microb. Rev., 15 : 167-93.

19. Perez-Oseguera, M. A. ; Guereca, L. and Lopez-Munguia, A. (1996). Properties of levansucrase from Bacillus circulans. Appl. Microbiol. Biotechnol., 45 : 465–471.

20. Decho, A. W. (1990). Microbial exopolymer secretions in ocean environments: their role (s) in food webs and marine processes. Oceanogr Marine Biology, Annual. Review, 28 : 73-153.

21. Shadia, M. A. ; Hoda, A. H. ; Foukia, E. M. and Amber, S. G. (2012). Acidic pH-shock induces the production of an exopolysaccharide by the fungus *Mucor rouxii*: utilization of beet-molasses. New York Science Journal, 5 (2) : 52-61.

22. Anderson, J. D. (1968). The ecology of transferable drug resistance in the Enterobacteriaceae. Ann. Rev. Microbiol., 22 : 131-281.

A New WP-MC/MCD-CDMA System Using Two-dimensional Spreading Code

Natiq Abdullah Ali

Technical College of Management, Baghdad, Iraq
E-mail: apdr_natiq@yahoo.com

Abstract

The Fourth Generation (4G) of wireless communication networks is able to handle much higher data rates in the range of 1Gb, the WLAN environment and 100 Mb in cellular networks. Also, the 4G can support various multimedia services such as voice, data and video, which require multirate transmission and large bandwidth. In this paper, the Wavelet Packets (WP), Multicarrier (MC), Multicode (MCD) and multiuser (MU) are combined together in Code Division Multiple Access (CDMA) communication system to yield a novel communication system that is WP-MC/MCD/MU/CDMA. Besides, the wireless communications networks require multirate transmission. Therefore, to improve the system performance in multirate transmission, the two-dimensional spreading codes with different length are used in the proposed system. The overall transceiver system is simulated and modeling using Matlab R2008a. The proposed system is evaluated under the Additive White Gaussian Noise (AWGN) and Rayliegh channels. The Bit Error Rate (BER) results show that the proposed system gives improvement in the performance as compared with the currently systems and is reliable and good candidate for the 4G cellular mobile systems.

Keywords: OFDM, MC, CDMA, spreading codes**,** WP**,** MCD, MU.

نظام *WP-MC/MCD-CDMA* جديد باستخدام الرمز المنتشر ثنائي الأبعاد

ناطق عبدالله علي

خلاصة

إنّ الجيلَ الرابعَ (4G) مِنْ شبكاتِ الاتصال اللاسلكي قادر على مُعَالَجَة نِسَبِ بياناتِ عالية جداً، وبمدى 1Gb في أنظمة الـ WLAN و100 Mb في الشبكاتِ الخلويةِ. وأيضاً، الـ 4G يُمْكِنُ أَنْ يَدْعمَ خدماتَ متعددة الأوساطَ مثل الصوتِ والبياناتِ والفيديو، واللذان يَتطلّبانِ إرسالَ متعدّدَ وسعة نطاق كبيرةَ. في هذاالبحث، الـ (WP)، (MC) ، (MCD) ، (MU) أستخدمت سوية لتصميمنظام اتصال مبتكرِ الذي هو WP-MC/MCD/MU/CDMA. إضافةً إلى ذلك، تَتطلّبُ شبكةَ الاتصالات اللاسلكية إرسالَ متعدّدَ. لذا، ولتَحسين أداءِ النظامَ في الإرسالِ المتعدّدِ، فقد تم استخدام تقنية الـ two-dimensional codes spreading بأطوال مختلفِة في النظامِ المُقترَحِ. إنّ النظامَ المقترح تم تنفيذه باستخدام الـ Matlab R2008a. إنّ النظامَ المُقترَحَ نفذ باستخدام قناة الـ AWGN وقناة الـ Rayliegh. بينت نسبة خطأِ القطعةَ BER بأنّ النظامَ المُقترَحَ قدم تحسيناً في الأداءِ كما هو مُقارن بالأنظمةِ المُقترَحةِ حالياً ومرشّحُ موثوقُ وجيدُ لأنظمة الـ 4G والأنظمة الخلوية.

الكلمات المفتاحية: OFDM، MC، CDMA، الرموز المنتشرة، WP، MCD، MU

1. Introduction

The future wireless mobile communication systems will be required to support high speed transmission rate. The high data rate requires broad frequency bands. Unfortunately in broadband wireless channel, the severe frequency-selectivity due to the more number of resolvable multiple paths fading degrades the BER performance [1].

The growth of wireless applications and spectral limitations are serious concerns for both the military and civilian communities. "A special spectrum task force set up by Federal Communications Commission (FCC) revealed that in many bands spectrum access is a more significant problem than physical scarcity of the spectrum" [2].

Wireless connectivity of mobile devices and notebook computers is the hallmark feature of the next generation of network infrastructure. A major challenge to the traffic capacity of such

systems is the complex characteristics of the mobile channel encompassing multipath propagation [3].

The demand for high data rate wireless multi-media applications has increased significantly in the past few years [4].

2. Multiple Access Techniques

In communication systems, there are three types of multiple access technique namely Time Division Multiple Access (TDMA), Frequency Division Multiple Access (FDMA) and Code Division Multiple Access (CDMA). TDMA and FDMA are techniques that use time and frequency slots to share system resources, while CDMA uses orthogonal code sequences to share resources in both frequency and time. When CDMA is compared with TDMA and FDMA, we can see that CDMA is an excellent resource sharing technique since it uses the entire spectrum and time slots. Compared to FDMA in which the spectrum is divided into several sub-bandwidths, and compared to TDMA in which the time duration is divided into several time slots [5,6].

There are three types of multiple access schemes based on the combination of CDMA and Orthogonal Frequency Division Multiplexing (OFDM). These are (a) Multicarrier (MC)-CDMA; (b) Multicarrier Direct Sequence (MC-DS)-CDMA, and (c) Multitone (MT)-CDMA. The signals of these systems can be easily transmitted and received using the Fast Fourier Transform (FFT) without increasing the complexities of the transmitter and receiver and have the attractive feature of high spectral efficiency due to minimally densely spaced subcarrier [4].

3. OFDM

Orthogonal Frequency Division Multiplexing (OFDM) has recently gained a lot of attention and is a potential candidate for 4G systems [7]. OFDM is very efficient in spectrum usage and is very effective in a frequency selective channel. By taking advantage of recent improvements in Digital Signal Processing (DSP) and Radio Frequency (RF) technologies, OFDM can provide higher data rates and is a very good choice for service providers to compete with wire-line carriers. A variation of OFDM which allows multiple accesses is Multi-Carrier CDMA (MC-CDMA) which is essentially an OFDM technique where the individual data symbols are spread using a spreading code in the frequency domain [7].

Multicarrier (MC) modulation, in particular orthogonal frequency division multiplexing (OFDM), has been successfully applied to various digital communications systems. OFDM can be efficiently implemented by using the discrete Fourier transform (DFT). Furthermore, for the transmission of high data rates its robustness in transmission through dispersive channels is a major advantage. For MC-CDMA, spreading in frequency and/or time direction is introduced in addition to the OFDM modulation. MC-CDMA has been deemed a promising candidate for the downlink of future mobile communications systems [8].

4. MC-CDMA

Broadband wireless access for evolving mobile internet and multimedia services are driving a surge of research on future wireless communication systems, which have to be highly spectral efficient in order to support multi-user access and high data rates. Therefore, MC-CDMA formed by combining orthogonal frequency division multiplexing

OFDM with Code Division Multiple Accesses (CDMA) became significant research topics. The former is well suited for high data rate applications in frequency selective fading channels and the later is a multiplexing technique where number of users is simultaneously available to access a channel. With its capability of synchronous transmission, MC-CDMA is suitable for downlink of cellular communication systems. High data rate MC-CDMA systems can additionally employ MIMO techniques like the Alamouti codes [1,9,10].

Using a given spreading code, the MC-CDMA transmitter spreads the original data stream over different subcarriers in frequency domain. MC-CDMA scheme is robust to frequency selective fading. For MC-CDMA system, there are some detection techniques such as Equal Gain Combining (EGC), Orthogonal Restoring Combining (ORC), Maximum Ratio Combining (MRC) and MMSE. The MMSE scheme can achieve better performance [1].

The MC-CDMA proved to be a suitable technique for the downlink transmission. Uplink transmission, due to the more complex propagation conditions, introduces additional problems which result in harder applicability of MC-CDMA in uplink [11].

5. The Proposed System Model

In this section, a Wavelet Packets (WP) based Multicarrier (MC)/Multicode (MCD) CDMA communication system denoted as WP-MC/MCD-CDMA is proposed, described and semi-modeled analytically.

The framework for evaluating the performance of the system is presented in terms of the signal power, noise power, and the throughput of the system. The proposed system model is described as, Transmitter, Channel and Receiver.

Transmitter System Model

The transmitter model of WP-MC/MCD-CDMA system assuming K users transmitting information simultaneously is shown in Fig. (1). The data $d_k(t)$ for the k^{th} user is a random complex sequence given by [4,6,7]:

$$d_{hj}(t) = \sum_{i=-\infty}^{\infty} d_{hj}^{i} \prod_{T/H}\left(t - \frac{iT}{H}\right) \quad \ldots (1)$$

Where $\prod_x(\cdot)$ represents a rectangular pulse of duration x. and J is the number of substreams in the multicode part,

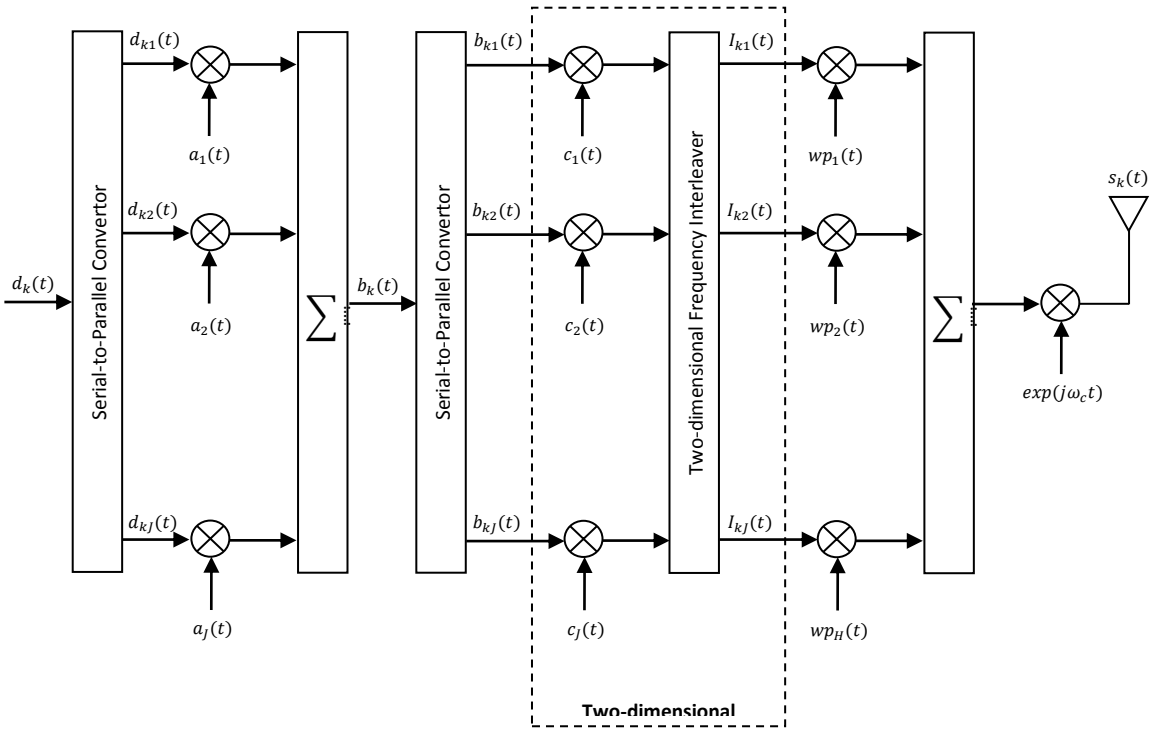

Fig. 1. The Proposed Transmitter Model [4].

After the S/P conversion, the data substreams are coded by a set of orthogonal signals $a_j(t)$ to reduce the Inter-Substream Interference (ISSI) resulting from the interference between the J substreams themselves. The orthogonal signal coding the j^{th} substream is given by

$$a_j(t) = \sum_{i=0}^{N_c-1} a_j^i \prod_{T_c}(t - iT_c) \quad \ldots\ldots (2)$$

where N_c is the code length, T_c is the chip duration, and a_j has a chip rate $1/T_c$. Note that a_j^i and $d_{kj}^i \in \{\pm 1\}$ with probabilities $P(1) = P(-1) = 0.5$ (equal probabilities).

In order to maintain orthogonality of the coding signals, the maximum number of substreams J is limited to N_c . The coded substreams are added and the resulting signal $b_k(t)$ is given by [5]

$$b_k(t) = \sum_{j=1}^{J} a_j(t)\, d_{kj}(t) \quad \ldots\ldots (3)$$

This signal is again S/P converted into H superstreams $b_{kh}(t)$ and is given by

$$b_{kh}(t) = \sum_{j=1}^{J} d_{kjh}(t) a_j(t) \quad , \quad h = 1, \ldots\ldots, H \ldots\ldots (4)$$

where $d_{kjh}(t)$ with period T, is the data symbol of k^{th} user, r^{th} substream of the h^{th} superstream.

The modulation of the superstreams by the PN sequence corresponding to the k^{th} user, and is given by [5,6]

$$c_k(t) = \sum_{i=0}^{N_n-1} c_k^i \prod_{T_n}(t - iT_n) \quad \ldots\ldots (5)$$

where N_n is the length of the PN code sequence and $c_k^i \in \{\pm 1\}$ with probabilities $P(1) = P(-1) = 0.5$.

Each of the spreading superstreams will be used to modulate a wavelet packets $w_{ph}(t)$, where the h^{th} wavelet packet is given by [3,4]

$$wp_h(t) = \sum_i w_h(t - iT_n) \quad \ldots\ldots (6)$$

Assuming identical power for all user, the transmitted signal $s_k(t)$ is given as [4,6]

$$s(t) = \sqrt{2p}\sum_{h=1}^{H} Re\,[b_{kh}(t)c_k(t)wp_h(t)\exp(j\omega_c t)] \quad \ldots\ldots\ldots\ldots\ldots (7)$$

Channel Model

The channel is considered a conventional multipath channel with equivalent transfer function $h(t)$ given by [5,6]:

$$h(t) = \sum_{l=1}^{L} A_{kl}\, e^{j\theta_{kl}}\delta(t-\tau_{kl}) \quad \ldots \quad \ldots\ldots\ldots\ldots\ldots\ldots\ldots\ldots\ldots (8)$$

where L is the number of the propagation paths, $A_{kl}$is the path gain of the path l for user k, τ_{kl} is the time delay of path l for user k, uniformly distributed over the symbol duration θ_{kl} is the phase of path l for user k uniformly distributed over the interval [0, 2π].

The output of the channel $y(t)$ for the k^{th} user is given by [5,6]

$$y(t) = s(t) * h(t) \quad \ldots\ldots\ldots\ldots\ldots\ldots\ldots\ldots\ldots\ldots\ldots\ldots\ldots\ldots\ldots\ldots\ldots\ldots (9)$$

Receiver System Model

At the receiver, the signal is detected using the single user detection method. The received signal is demodulated by the carrier, despread by a user specific code sequence, multiplied by the wavelet packets and correlated over a period T to recover the super bitstream, which is then P/S converted. The output signals of the P/S converter is again despread by each code in multicode part to recover the J parallel data streams before correlated over a period T. Finally, the correlated outputs from J paths is P/S converted torecover the original data bit.The receiver is assumed to be a synchronous receiver, designed to detect the first substream of the first user's first wavelet packet for the signal propagating via the first path. The receiver system model is shown in Fig. 2.

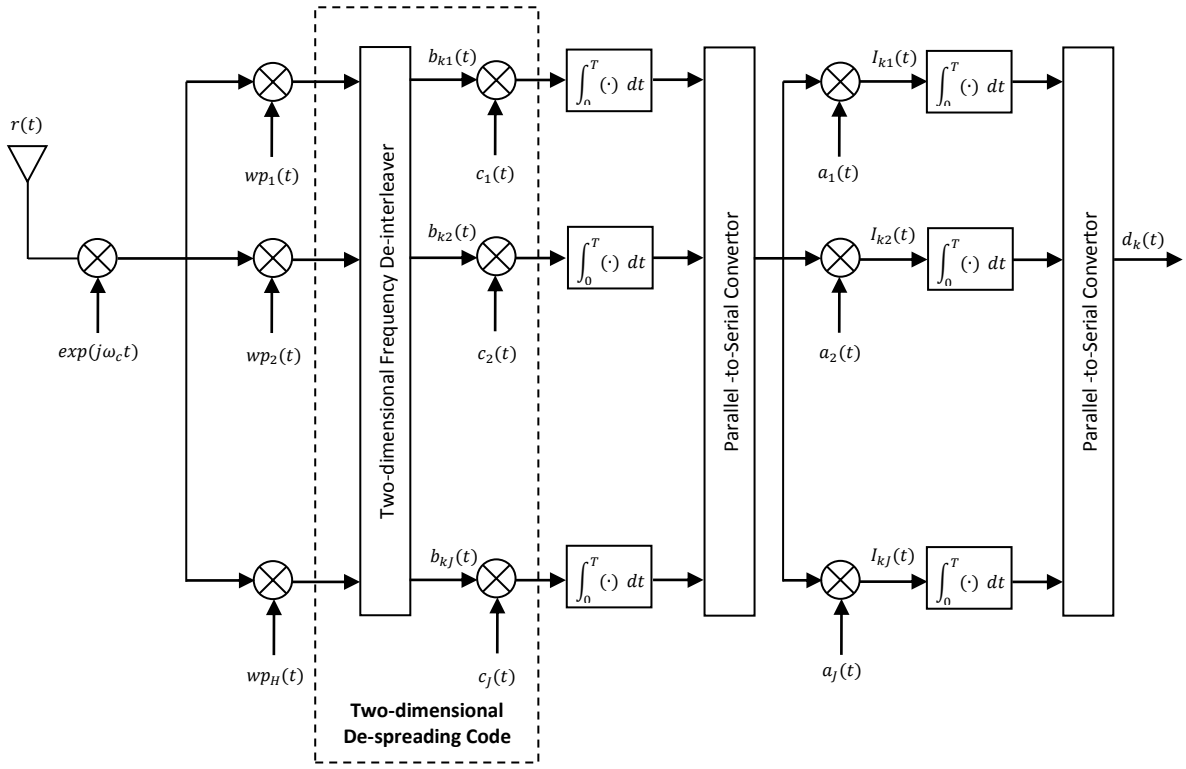

Fig. 2. The Proposed Receiver Model.

6. Results and Discussions

The Signal-to-Interference-Noise-Ratio (SINR) performance for the proposed system is presented and discussed in this section. Also, the performance of the proposed system is compared with the currently proposed systems.

The effects of some parameters on the system performance such as the number of users K, the number of multicodes substreams J, family of wavelet packets,the length of the filter of wavelet packet, and their superstreams numbers H were investigated.

Also, SINR performance of the proposed system is compared with WP-MC/MCD-CDMA system proposed in [4]. The BPSK modulation is used in the simulation. The parameters listed below are used in the simulation.

Wavelet packets Daubechies 3 dB, number of wavelet packets superstreams $H = 4$, Period for the encoder $T = 10^{-6} sec$, The delay time

$\rho = T_n/10$, Length of PN code $N_1 = 2$, Number of user $K = 30$, Local mean power $\Omega = 10\,dB$, Number of multipath $L = 3$, Number of multicode substreams $J = 4$, Path gain for target user $10\,dB$, Sum of amplitude levels of all multipath components Q, $MIP\ Q = L\ Q = L = 3$.

In the case of delay range, the same channel is used for all systems compared. This means all systems have the same propagation delay in the same communication environment.

6.1 SINR Performance Comparison

In this section, the proposed system WP-MC/MCD-CDMA is compared with the system proposed in [4]. These systems will be compared by the SINR and bit error rate performance. Here assume that the two systems use BPSK modulation. Fig. (3) illustrates the SINR performance of the two systems.

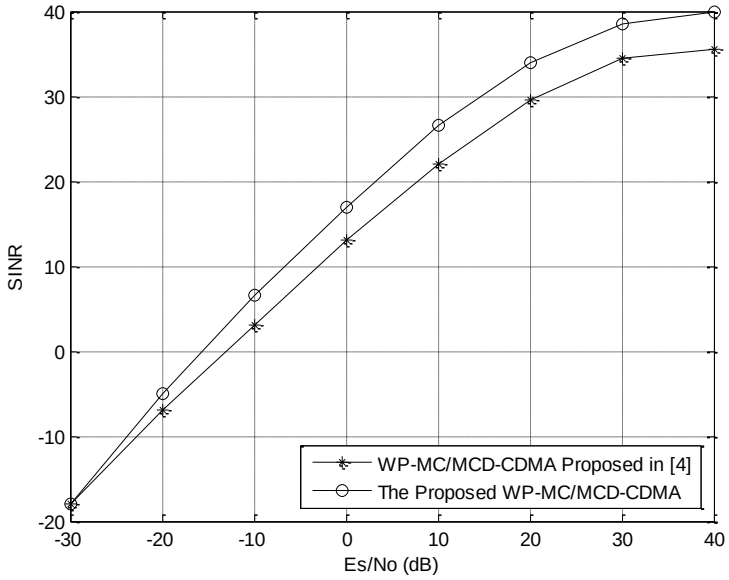

Fig. 3. SINR performance for the two systems for BER of 10^{-4} .

All the parameters used in this simulation are given in section (6). As it is shown from the figure, the proposed system outperforms the system in [4] and has the highest SINR. This is due to use of various lengths of two dimensional spreading codes. Besides, the using of wavelet packets results in lower side lobe energy leakage and is negligible. As shown in Fig. 3 the E_s/N_o = 20 dB for the system in [4] and is equal to 35 dB for the proposed system, i,e, gives 15 dB gain. In this case, the proposed system

provides better performance by minimizing the interference between substreams with several carriers.

Also, using multicarrier in this system increases the bandwidth of the signal and can suppress the effect of narrowband signal.

6.2 BER Performance Comparison

In this sub-section, the BER performance of the proposed system is compared with that proposed in [4]. In order to give fair results, the same parameters used for this simulation are the same as that used in the previous simulation. Figure (4) illustrates the BER performance for the two systems. The BPSK modulation scheme is also used in the simulation. It can be noticed from the figure that the proposed system has the lowest BER and it outperforms the other one. This is because of using multicode scheme with multicarrier can decrease inter-carrier interference. As shown in Fig. (4), the proposed system gives 20 dB E_s/N_o gain as compared with the system proposed in [4] at BER $= 10^{-4}$.

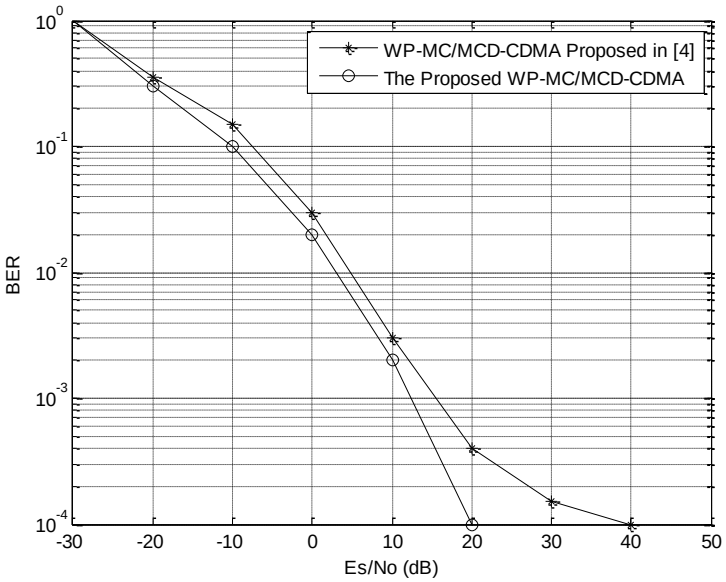

Fig. 4. The BER performance for the two systems.

6.3 Outage Probability Performance Comparison

The outage performance of WP-MC/MCD-CDMA system is compared with the CDMA based system given in [4]. For this simulation, $E_s/N_o = 10\ dB$ is used and the other parameters are the same as that presented in

section (6). Figure (5) illustrates the outage probability performance for the two systems. The BPSK modulation is also used in this part of simulation.

Notice that the new proposed system WP-MC/MCD-CDMA is outperformed the one proposed in [4]. This is also due to the using of two dimensional spreading codes.

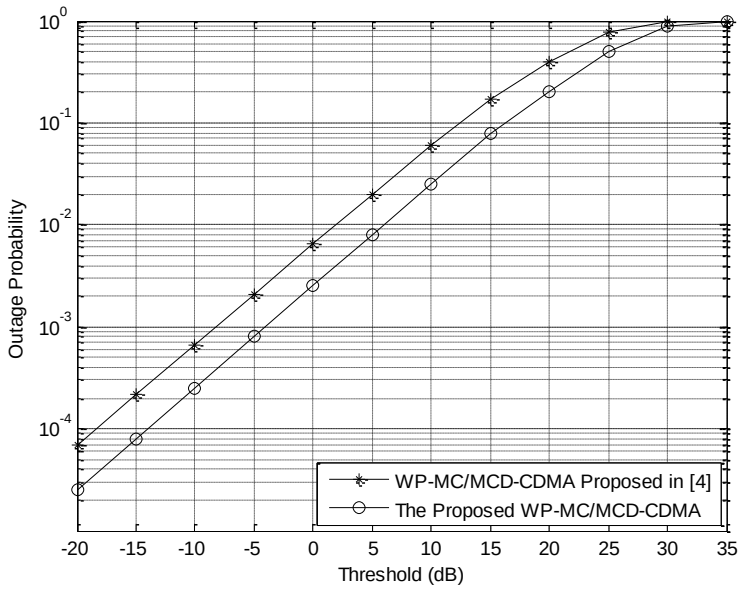

Fig. 5. The outage probability performance for the two systems.

7. Conclusions

This paper handles a proposed transmission and receiving schemes for 4G systems, namely WP-MC/MCD-CDMA. Simulations compare the error and E_s/N_o performance of the proposed system in a cellular environment. Through the using of spreading codes, the BER of the multi users system is improved according to the values of SINR. In such a way, that the average user throughput is maximized. Simulation results have also shown that spreading codes yields in general a significant improvement of the throughput at higher SINRs, while enabling satisfactory throughput at low SINRs. Moreover, the application of spreading codes results to be particularly advantageous when the mobile Rayliegh channel is considered.

References

1. T. Luo, G. Wu, and Shaoqian; ***"DS-CDMA and MC-CDMA with Per-User*** *MMSE Frequency Domain Equalization"*; International Journal of Hybrid Information Technology; Vol. 1; No. 3 July; 2008.
2. V. hakravarthy, S. Nunez, and P. Stephens; ***"TDCS, OFDM, and MC-CDMA"***; IEEE Radio Communications; September 2005.
3. A. Muayyadi and M. Abu-Rgheff; *"Wavelet-based Multicarrier CDMA System and its Corresponding Multi-user Detection"*; IEE Proc.Comm., Vol. 150, No. 6; December 2003.
4. M. Akho-Zahieh; *"Design and Analysis of Multicarrier Multicode Wavelet Packets Based CDMA Communication Systems with Multiuser Detection"*; Ph. D. Thesis; The Graduate Faculty of the University of Akron; 2008.
5. K. Fazel; *"Multi-Carrier and Spread Spectrum Systems From OFDM and MC-CDMA to LTE and WiMAX"*; Second Edition; John Wiley and Sons, Ltd; 2008.
6. J. Woo Lee; *"Performance Analysis of a Multicode Multi-carrier CDMA Communication System"*; M. Sc. Thesis; The Graduate Faculty of the University of Akron; December, 2004.
7. R. Venkatasubramanian; *"Beamforming for MC-CDMA"*; M.Sc. Thesis; The Faculty of Virginia Polytechnic Institute and State University; 2003.
8. G. Auerl, S. Sand and A. Dammann; *"Special Issue on Multi-Carrier Spread-Spectrum Analysis of Cellular Interference for MC-CDMA and its Impact on Channel Estimation"*; European Transaction on Telecommunications Euro. Trans. Telecomms.; 2004.
9. N. Kumaratharan and M. Padmavathy; *"Performance Improvement of MC-CDMA System Through DSTBC Site Diversity"*; Journal of Theoretical and Applied Information Technology; 2008.
10. RuiDinis; *"Analytical Evaluation of Nonlinear Effects in MC-CDMA Signals"*; IEEE Transaction on Wireless Communications, Vol. 5, No. 8; August 2006.
11. I. Cosovic1 and M. Schnell; *"Time Division Duplex MC-CDMA for Next Generation Mobile Radio Systems"*; 10th Telecommunications forum TELFOR'2002, Belgrade, Yugoslavia, Nov. 26-28; 2002.

Cellular Mobile Base Station Radiation at Baghdad

Adheed Hasan Sallomi

adalameed@yahoo.com

Abstract

Growing demand for mobile communication services results in a continuous increase in the number of base stations over a limited area, accompanied by public concern about the possible health and ecological effect of these systems. The main contribution of this paper is the usage of an empirical radio wave propagation model based on practical measurements in some ASIACELL sites in the city of Baghdad to measure the received signal power at the ground level in the vicinity of base stations and to determine the power- distance gradient value. The extracted power gradient value was used to examine the electromagnetic energy levels due to the base station transmitters. The calculated values of the power density levels in the vicinity of base stations were compared with the widely employed safety guidelines to ensure compliance with these standards. It was found that the exposure levels produced by the base station are too low compared with the exposure standards.

Keywords: Cellular Mobile Radiation Effects, Mobile Channel Modeling, RF safety limits.

الاشعاع المنبعث من محطات الأجهزة الخلوية عند مدينة بغداد

عضيد حسن سلومي

خلاصة

أدى الطلب المتزايد على خدمات الاتصالات المتنقلة إلى زيادة مستمرة في عدد المحطات الرئيسية في منطقة محددة وقد ازداد معها القلق الشعبي من الآثار الصحية والبيئية المحتملة لتلك المنظومات. إن الإسهام الرئيسي لهذا البحث هو استخدام نموذج تجريبي لانتشار الموجات الراديوية اعتمدت فيه القياسات العملية في بعض مواقع شركة آسيا سيل ضمن مدينة بغداد كنموذج لقياس قدرة الإشارة المستلمة على الأرض قرب المحطات الرئيسية ولحساب مقدار اضمحلال الطاقة مع المسافة. تم استعمال مقدار اضمحلال الطاقة مع المسافة لغرض فحص مستوى الطاقة الكهرومغناطيسية المنبعثة من مرسلات المحطات الرئيسية. تمت مقارنة مستويات كثافة القدرة المحسوبة قرب المحطات الرئيسة مع معايير الأمان الراديوي الأكثر استخداما للتأكد من تطابقها مع تلك المعايير. وجد بان مقدار التعرض للإشعاع أقل بكثير من المعايير المحددة.

الكلمات المفتحاية: التأثيرا ت الاشعاعية للموبايل الخلوي، نماذج قنوات الموبايل، حدود سلامة RF

I. Introduction

Electromagnetic radiation can be described as waves of electric and magnetic energy moving together through propagation mediums. Electromagnetic waves are classified into ionizing, and non-ionizing radiations depending on their frequencies.

Ionizing radiations are Extremely High Frequency (EHF) electromagnetic waves that have enough energy to produce ionization and break the atomic bonds, such as X-rays and gamma rays. Non-ionizing radiations are electromagnetic waves that have weak photon energies to result in ionization, such as the radio waves that are used for providing various types of

communication at radio frequencies (RF) [1, 2].

As the population continues to grow and so does the number of people using mobile phones(subscribers), more and more base stations are going to be installed. The large number of base stations in areas where people live and work, has raised the public concern regarding the probable effects due to exposure to the radiation emitted by base stations [3]. At the same time, there is less concern over the mobile phones themselves, although the (RF) exposures from these phones are greater as the common position of use (the head of the user), receives the highest exposure [2].

In order to avoid any probable biological and health effects from short- and long-term exposure to RF radiation, several guidelines and standards have been issued by many national and international organizations. These guidelines are expressed in terms of field intensities, the power density in the far-field zone of the radiation source, or in terms of the energy absorbed by an element of biological body mass, i.e., called the specific absorption rate (SAR) [4, 5].

This paper is composed of four sections: section II provides a brief review of the cellular communication systems including a description of the based geometry for power density calculations at the ground levels. In section III the most widely- employed RF safety limits specified by the international health organizations are summarized. Section IV presents the power exponent radio wave propagation model that is applied to evaluate the power- distance gradient and power density levels to assess compliance with the maximum permissible exposure limits. The final section provides a summary and conclusion.

II. Cellular Telephone Network Radiations

Cellular mobile communication networks were developed by replacing a single high power transmitter that is located to achieve a large coverage area in radio-TV broadcasting systems with a single, low-power transmitter. In order to increase the number of simultaneous calls in cellular mobile communication networks, a large area is divided into a large number of small areas (cells), that is covered by a single base station, and the frequency of a cell is reused to another cell after skipping several cells.

Base stations are connected to one another by the Mobile Switching Center (MSC), which is connected to

the fixed communication system i.e., the Public Switched Telephone Network (PSTN). From the MSC the calls can be terminated into other cellular phones or conventional land-line phone.

To evaluate the power density at any location, it is necessary to understand how signals propagate in the particular environment.

In free space, at the far-field regions, the power density (S) from an isotropic point source may be thought of as the effective isotropic radiated power (EIRP) divided by the surface area of a sphere with radius r. In practice, Effective Radiated Power (ERP) is used instead of EIRP to denote the maximum radiated power due to radiation of P_t watts by a distant antenna with a gain of G_t . It can be given as [6, 7].

$$S = \frac{ERP}{4\pi r^2} = \frac{P_t G_t}{4\pi r^2} \qquad (1)$$

Eq.1, implies that the power density from a transmitting antenna is inversely proportional to the second power of distance ($S \propto 1/r^2$), where r is the distance between the radiation center of the antenna and the exposure point in the far-field zone.

In urban environments, the Line of Sight (LOS) path between the base station and the mobile units is mostly blocked as the height of the mobile unit antennas may be smaller than the surrounding structures. The received signal and the power density is inversely proportional to the power of the distance, which varies depending on the propagation medium. Such relationships take the form $S \propto (1/r^{\gamma})$, where γ is the path loss exponent value which is typically between 2 and 6[8]. Larger values of power exponent correspond to faster decrease in power density as the distance becomes larger.

At ground level, RF exposure is inversely proportional with the distance measured from the antenna to the point at which the power density exists. Eq.1, computes the main beam (on-axis) power density at the free-space conditions, and the off-axis power density will be considerably less.

The power density at the ground level can be determined in terms of the effective radiated power, the heights of the transmitting antenna and exposure point, and the horizontal distance from the tower to the point of exposure(d), using the geometry shown in Fig.1. The power density can be given as[4]

$$S = \frac{P_t G_t}{4\pi r^2} = \frac{P_t G_t}{4\pi \left\{ \sqrt{(h_b - h_m)^2 + d^2} \right\}^{\gamma}} \quad (2)$$

where h_b denotes the height of the base station antenna above the ground, and h_m is the exposure point height.

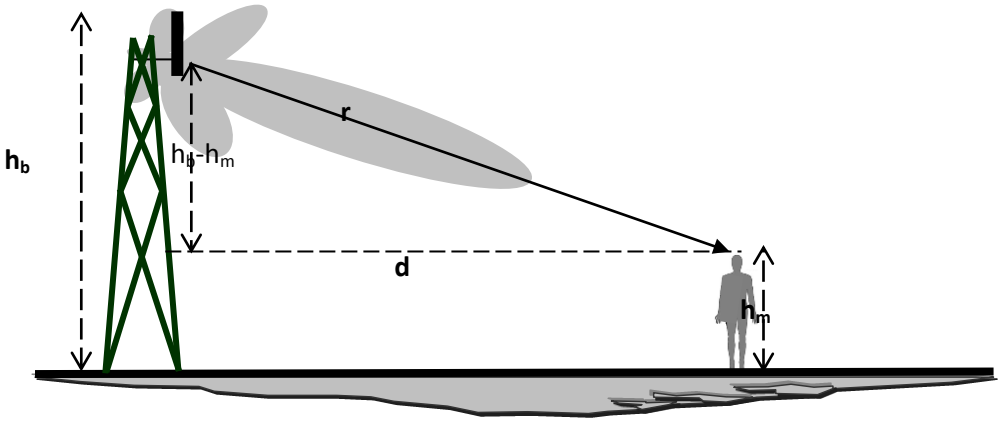

Figure 1. Power Density Calculation at Ground Level

III. RF Safety Standards

Many international authorities provide the Maximum Permissible Exposure (MPE) levels that protect the public from RF radiations. These safety limits are usually given in terms of the maximum possible exposure of electric and magnetic fields, or power density. The most widely respected standard levels of (RF) radiation are those recommended by the American National Standards Institute and the Institute of Electrical and Electronics Engineers (ANSI/IEEE), and the International Commission on Non-Ionizing Radiation Protection (ICNIRP). The ANSI/IEEE standard is recognized as an American National Standard, while the exposure standards recommended by ICNIRP has been adopted by more than 80 countries. These guidelines cover a wide range of RF frequencies as shown in Table 1 [2, 7, 9].

Table 1. ANSI/IEEE - ICNIRP Exposure Limits [2] [7] [9].

Frequency f (MHz)	Electric Field E (V/m)	Magnetic Field H (A/m)	Power Density S (mW/cm^2)
ANSI/IEEE GULDE LINES			
100-300	27.5	0.0729	0.2
300-3000	--	--	f(MHz)/1500
ICNIRP GULDE LINES			
400-2000	$\mathbf{1.375}\sqrt{f}$	$\mathbf{0.0037}\sqrt{f}$	f(MHz)/ 2000
2000-300000	61	0.16	10

The authority who is responsible for the most RF telecommunications services in the United States is the Federal Communications Commission (FCC). The FCC guidelines include standards for mobile base stations antennas are the same as the (ANSI/IEEE) guidelines[2].

The Global System for Mobile Communication (GSM) is the most popular system for mobile communications in the world. The GSM systems operate in either the 900 MHz or 1800 MHz band[4]. ASIACELL utilizes the GSM-900 to provide cellular communication services in Iraq, and the base stations transmitted RF signals are within the frequency band of 900MHz. Therefore, the Maximum Permissible Exposure (MPE) limits are between 0.45-0.6 mW/cm^2 based on ICNIRP and ANSI/IEEE guidelines respectively.

IV. Propagation Channel Modeling

The propagation channel is the main contributor to many of the problems and limitations that be set mobile radio systems. RF engineers use mobile radio channel models to predict the mean signal strength and the level of RF energy that will be emitted by the base station at any point in the coverage area.

The complexity of signal propagation in urban areas makes it difficult to obtain a single model that characterizes the power level accurately across a range of different environments. Accurate radio wave propagation models can be obtained from empirical measurements. The power exponent model (Log-Distance model) is an empirical model that is widely used to predict the power transfer between a transmitter and a receiver depending practical measurements of the received power at different distances from the base station transmitting antenna in cellular system. It takes into account the decrease in energy density due to the radio wave spreading, as well as the energy loss in terms of an empirical path loss exponent (γ)[10][6].

The received signal power at any distance, i.e., $P_r(d)$ is proportional to the distance between transmitter and receiver d, raised to a certain exponent(γ), which is referred to as the power exponent value or the distance-power gradient; that is,

$$P_r(d) = P_r(d_o).\left(\frac{d_o}{d}\right)^{\gamma} \qquad for \quad d > d_o$$

Where $P_r(d_o)$ is the received power at a reference distance d_o.

As this model depends on real measurements, it can be used to derive empirical relationships for signal propagation and the effect of cellular mobile base station radiation can be examined by using this model.

Power Exponent Model Application

The received power measurements had been done at different distances from the base station transmitter in three different sites in the City of Baghdad by using the Cell Track software that has been installed in a cellular mobile phone. The received power has been measured by using this program, then the least squares approach is applied to calculate the accurate power exponent value. For each site (base station), N number of measurements had been taken. Least mean square error (LMS) as a numerical optimization schemes is applied to minimize the error in power exponent value calculation. The problem is formulated as finding the minimum of [6][10],

$$F(\gamma)=\sum_{i=1}^{N}(e_i)^2=\sum_{i=1}^{N}\left[Measured\ P_r(d_i)-Calculated\ P_r(d_i)\right]^2$$

$$F(\gamma)=\sum_{i=1}^{N}(e_i)^2=\sum_{i=1}^{N}\left[p_{ri}-(p_r(d_o)-10\,\gamma\,Log_{10}(\frac{d_i}{d_o}))\right]^2 \qquad (4)$$

where e_i is the error between the measured and calculated values of the received signal power, and P_{ri} is the received power as measured in i-th measurement at the distance d_i.

Table 2, shows the obtained measurements at different distances from the base station of three sites in the city of Baghdad. Fig.2, shows one of the tested sites.

Applying eq.4, using the obtained measurements for the first site,

$$F(\gamma)=\sum_{i=1}^{N}(e_i)^2=[-51+51+0]^2+[-54.37+51+1.249\gamma]^2+[-55.65+51+2.218\gamma]^2+$$
$$[-59+51+3.679\gamma]^2+[-63+51+4.259\gamma]^2+[-63.88+51+4.7712\gamma]^2+$$
$$[-65.64+51+5.228\gamma]^2+[-67.97+51+6.02\gamma]^2$$

Differentiating F(γ) relative to γ and setting it to zero yields

$$\frac{dF}{d\gamma}=670.4254+248.987\,\gamma=0$$

$$\gamma=2.692709$$

The values of γ for the other two sites were calculated by the same method to be 2.758, and 2.754. The average value of the power exponent value was calculated to be 2.735.

Table 2. Empirical Data for Three Sites (Practical Measurements)

Distance (d) m	Received Power (Pr (d)) d Bm	Distance (d) m	Received Power (Pr(d)) dBm	Distance (d) m	Received Power (Pr(d)) dBm
SITE-1		**SITE-2**		**SITE-3**	
do = 60	Pr(do) = -51.00	do = 40	Pr(do) = -50	do = 50	Pr(do) = -51.6
80	-54.37	120	-63.2	100	-60
100	-55.65	160	-66.33	150	-64.1
140	-59.00	200	-68.65	200	-68
160	-63.00	220	-70	300	-72.3
180	-63.88	-	-	350	-76
200	-65.64	-	-		-
240	-67.97	-	-		-

By using the extracted value of γ, the power density caused by a transmitting antenna of 20W, with a gain of 18dBi was calculated at a point of 1.5 m height. The calculated power density values were 0.00119 mW/cm^2, 0.0032 mW/cm^2, 0.001215 mW/cm^2, 0.000325 mW/cm^2, at 20m, 40 m, 60 m and 100 m away from the base station respectively. It can be noticed that the exposure levels produced by the base station is too low compared with the exposure limits even in close proximity to the antennas, because the mobile phone base stations are low power system. Unsafe power density levels can be reached due to high transmitter power, high antenna gain, very close proximity to the transmitting antenna.

In cases where exposure levels might pose a problem, there are various techniques can be applied to avoid excessive radiated power density absorbed by the general public who are exposed to the electromagnetic radiation emitted by cellular base stations.

Figure 3, shows that increasing the base station antenna height (h_b), results in radiation exposure reduction as the signal path to the exposure point will be increased. In Figure 4, the power density against the transmitting antenna height is drawn for a point 1.5 m above the ground, 50 m away from the base station. From the Fig., it can be noticed that the power density can be significantly reduced by increasing the transmitting antenna height.

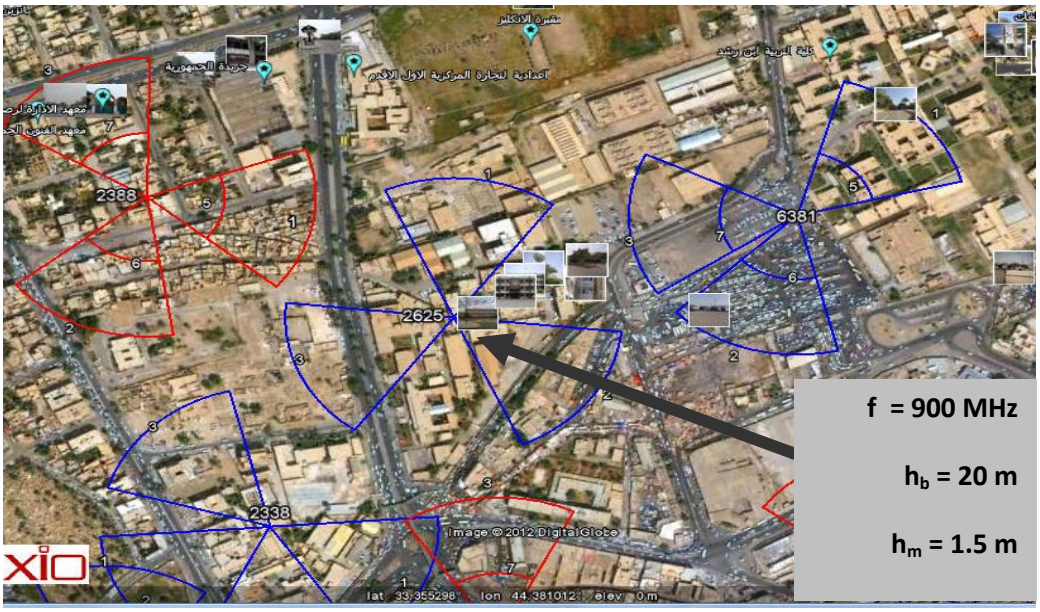

Figure 2. Site No. 1 in the City of Baghdad

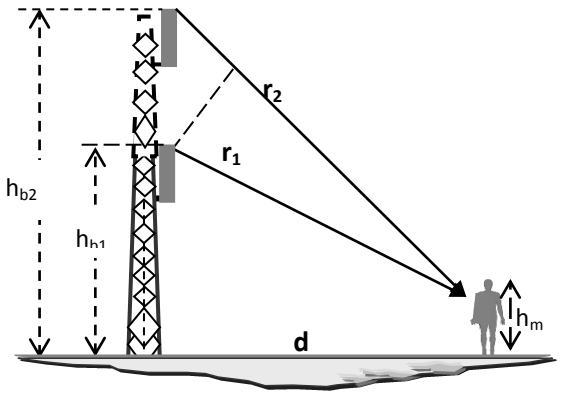

Figure 3. Effect of Antenna Height Height Relation

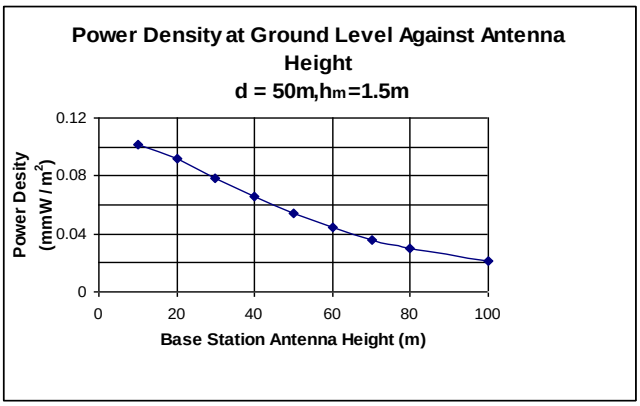

Figure 4. Power Density-Antenna

Conclusions

Cellular base stations are one of the main sources of RF radiation that may affect the public health. Depending on empirical measurements taken in some sites in the city of Baghdad, the power exponent value was found to be 2.735 without line of sight between transmitter and receiver.

The power density levels calculated in the examined ASIACELL sites located in Baghdad are much lower than the exposure limit recommended by ANSI/IEEE and ICNIRP that are 0.6 mW/cm^2 and 0.45 mW/cm^2 respectively.

References

1. Cleveland, Robert F., and Ulcek , Jerry L., " Questions and Answers about Biological Effects and Potential Hazards of Radiofrequency Electromagnetic Fields", Issued by (Federal Communications Commission Office of Engineering & Technology), August. 1999.
2. Dawoud, M. ," High Frequency Radiation and Human Exposure", Proceedings of the International Conference on Non-Ionizing Radiation at UNITEN (ICNIR 2003).
3. Abdelati, M., "Electromagnetic Radiation from Mobile Base stations at Gaza", Journal of The Islamic University of Gaza (Natural Sciences Series) Vol.13, No.2, 2005, PP 129-146.
4. Sallomi, A. H., "Safety Distance and power Density Calculations for GSM Communication Systems", Journal of Engineering and Development, Vol.15, No.2, June,2011, PP 63-73.
5. Ahma L., Ibrani M., and Hamiti, "Computation of SAR Distribution in a Human Exposed to Mobile Phone Electromagnetic Fields", PIERS Proceedings, Xi'an, China, March, 2010, PP 1580-1582.
6. Rappaport, T. S., "Wireless Communications Principles and Practice", Prentice Hall, Upper Saddle River NJ, Second Edition, 2002.
7. Seybold, John S., "Introduction to RF Propagation", John Wiley & Sons, INC., First Edition, 2005.

8. Koivo, H., and Elmusrati, M., "System Engineering In Wireless Communications", John Wiley & Sons, Ltd., First Edition, 2009.
9. Kitchen, R., "RF and Microwave Radiation Safety Handbook", Second edition, Reed Educational and Professional Publishing Ltd, 2001.
10. Goldsmith, A., "Wireless Communications ", Cambridge University Press, First Edition, 2005.

Study of the Basic Parameters Characterized the (D-T) Hot Plasma Fusion Reaction In General Dense Plasma Focus Devices

Raad Hameed Majeed

Department of Physics, University of Baghdad,
College of Education (Ibn al-Haitham),

Abstract

Plasma focus devices can be considered (PFD) as a strong source for the elementary charge particles, neutrons, protons, and soft x-rays are the main reason for its importance in many experimental applications. The dependency of the basically hot plasma parameters such as reactivity, reaction rate, and energy of the emitted neutrons, upon the total cross section of D-T fusion reaction still up to now the essential factor governed the primary calculations, and accuracy, for both experimental and theoretical studies. Formulism describing the physical behavior of a given experiment still varies from others experiments and indeed, a theoretical modification for the empirical formulas plays a rule to achieve compatible results.

Keywords: plasma focus, neutron yield, hot plasma parameters, d-t reaction, total cross section, fusion power.

رعد حميد مجيد

خلاصة

تعزى كثرة التطبيقات العملية لاجهزة بؤرة البلازما الكثيفة الى خصوصية هذه الاجهزة باعتبارها مصدر للجسيمات الاولية المشحونة (النيوترونات والبروتونات) اضافة الى الاشعة السينية. اعتمادية العوامل الاساسية للبلازما الحارة كالفعالية، معدل التفاعل، وطاقة النيوترونات المنبعثة على المقطع العرضي الكلي للتفاعل لاتزال حتى وقتنا الحاضر من اهم العوامل المؤثرة والمحكمة لدقة الحسابات النظرية والعملية وعملية التوافق مابينهما. العلاقات التجريبية التي توصف سلوك المقطع العرضي الكلي تختلف من تجربة الى اخرى وبالتالي وجد من الضروري اجراء تحوير او تطوير لمثل هذه العلاقات كي يتم البلوغ الى توافق معقول بين النتائج النظرية والعملية.

Introduction

The relevance and importance of a plasma focus devices(PFD), as intense source of neutrons are due to essentially the low costs and dimensions of the device itself, to its high performance in term of neutrons emitted per discharge and to the type of spectra of the emitted neutrons. For instance a D-T filled advance plasma focus (APF) with capacitor bank energy of about 200 KJ can give about 10^{14} neutrons per discharge, these being emitted almost point wisely and almost mono energetically at about $14\ MeV$ [1] .

Plasma focus devices operated with D-T fuels suitable to generate a neutron yield about $Y_n = 10^{15}$, during a 1-year run, an overall fluencies affecting materials to the order of $0.1\ to\ 1.0$ displacement per atom (DPA) (1 DPA is equal to a mean neutrons flux of 4.5×10^{16} neutron $m^{-2}s^{-1}$ for 1 year) for such testing purposes, at a very low cost relative to other methods currently being considered [2].

The main technological problems are indeed related to the stability of the discharge repetition rates, which nowadays can reach $10 - 15\ Hz$ and can be sustained for times of the order of magnitude of the hour. If the technology related to these performances could be improved somehow, PF devices will be highly competitive as neutrons sources in the future. Therefore, great theoretical and experimental efforts should be directed towards a better characterization of the energetic and angular distribution of the emitted neutrons, in other words towards a better characterization of the neutronics of PF machines. This means that the fusion doubly-differential cross sections are to be more correctly evaluated, and the models giving the corresponding fusion reaction rates more precisely set-up, as well as the description of the plasma dynamics in the pinch zone of the PF [1].

Generally, several parameters like the initial pressure, insulator length [3], and capacitor bank energy [4], are effective to the various products of the PF device. However, the results are collected in an important factor called the drive parameter, which is defined as $S = \left(\frac{I}{a}\right)/\sqrt[2]{P}$, in which I, a, P is the maximum current flowing into the pinch, anode radius, and the initial filling gas pressure at the optimized neutron regime, respectively [5]

Theoretical models

Presently two main classes of models for the evaluation of fusion reaction rates are used, namely.

1- The "BEAM-TARGET" MODEL
2- The "MAXWELLAIN REACTIVITY". MODEL

The beam target model was introduced by Bernstein and Comisar [6] in the late `60s to early of `70s .It is presently the most largely accepted model. This model assumes that the colliding ions in the pinch zone of the PF can be divided into two sub-populations of "beam ions" and "target ions". The target ions are assumed in many calculations to be at rest; axially only moving target ions have also been considered. The fusion reactions are assumed to happen in so a small zone called the pinch region. Reaction rates are then calculated as being the production term of the collision of the Boltzmann equation for the interaction of the two sub-populations. In doing this, one has to know the energetic and angular dependence of the beam ions distribution functions. Bernstein and Comisar were the first to perform beam-target reactivity calculations assuming energetic and angular dependence for the beam ions distribution functions which were dictated by a few experimental studies [6, 7].

In more recent years there have been a lot of efforts for both in the direction of theoretical and experimental determine the ions, neutrons beams distribution function. The consistence of these results has been checked using the beam-target model, and considerable improvements have made since the times of Bernstein and Comisar [1].

By definition the reaction rate $\boldsymbol{R}$ for reaction $\boldsymbol{i}$ in a space independent problem is given by [1].

$$\boldsymbol{R = n_D\, n_T \iiint f(\vec{v}_D) F(\vec{v}_T)\, g\, \frac{d\sigma_i}{d\Omega}\, d\Omega d\vec{v}_D d\vec{v}_T} \qquad (1)$$

Where $n_D \; and \; n_T$ are the beam and target ions densities with unit-normalized distribution functions $f \; and \; F$ respectively; g is the modulus of the relative velocity between beam and target ions and $\frac{d\sigma_i}{d\Omega}$ is the doubly differential cross section.

In the Bernstein – Comisar formalism one can introduce the dummy variable E by use of a Dirac Delta distribution, so that

$$R = n_D\, n_T \iiint f(\vec{v}_D) F(\vec{v}_T)\, g\, \frac{d\sigma_i}{d\Omega}\, \delta(E - E_n) d\Omega d\vec{v}_D d\vec{v}_T\, dE \qquad (2)$$

Where E_n *is* the emitted neutron energy in the case of axially moving target ions. By the laws of energy and momentum conservation, and from the general basic fundamental equation of calculating the energy for the charged particles from any nuclear reaction given below [8].

$$\sqrt[2]{E_3} = v \pm \sqrt[2]{v^2 + \omega} \qquad (3)$$

Where $v = \frac{\sqrt[2]{M_1 M_3 E_1}}{M_3 + M_4} \cos\theta$ *and* $\omega = \frac{M_4 Q + E_1 (M_4 - M_1)}{M_3 + M_4}$ (4)

For the case of the binary D-T reaction,

$$^2_1D + {}^3_1T \rightarrow {}^1_0n\ (14.1\ MeV) + {}^4_2He\ (3.5\ MeV) \qquad (5)$$

Where

$$E_3 = E_n\ , M_1 = M_d\ , M_2 = M_t\ , M_3 = M_n\ , M_4 = M_{He}\ , E_1 = E_d$$

And $Q_{value} = 17.6\ MeV$ is the Q-value of the above D-T fusion reaction, E_d is the deuteron bombarding energy.

Substituting the values for the quantities $v, \omega, M_1, M_2, M_3, M_4, E_1, Q$ as it is described above in equation (3), and taken into account some mathematical analysis steps to get or deduced a formula for evaluating the energy of the emitted neutrons that given below.

$$E_n = \frac{20\,Q + 12\,E_d}{25}\left[\sqrt[2]{1 - \gamma^2 \sin\theta} + \gamma\cos\theta\right]^2 \qquad (6)$$

Where $\gamma^2 = \frac{2\,E_d}{20\,Q + 12\,E_d}$ (7)

Equation (5), explain the relationship between the energy of the emitted neutrons from the D-T fusion reaction with the energy of bombarding deuterons and reaction angle $E_d\ , \theta$, respectively.

A most important quantity for the analysis of nuclear reaction is the *cross section*, which measure the probability for the occurrence of a nuclear reaction. The cross section $\sigma_{12}(v_1)$ is defined as the number of reactions per target nucleus per unit time

when the target is hit by a unit flux of projectile particles that is by one particle per unit target area per unit time. Actually, the above definition applies in general to particles with relative velocity v, and is therefore symmetric in the two particles, since we have $\sigma_{12}(v) = \sigma_{21}(v)$.

Cross section can also express in terms of the center of mass energy, and we have $\sigma_{12}(\epsilon) = \sigma_{21}(\epsilon)$. In most cases, however, the cross section are measured in experiments in which a beam of particles with energy , measured in the laboratory frame, hits a target at rest. The corresponding beam-target cross section $\sigma_{12}^{bt}(\epsilon_1)$ is related to the center-of-mass cross section $\sigma_{12}(\epsilon)$ by

$$\boldsymbol{\sigma_{12}(\epsilon) = \sigma_{12}^{bt}(\epsilon_1)} \qquad (8)$$

With $\boldsymbol{\epsilon_1 = \epsilon \cdot (m_1 + m_2)/m_2}$

If the target nuclei have density n and are at rest or all move with the same velocity, and the relative velocity is the same for all pairs of projectile-target nuclei, then the probability of reaction per unit times is obtained by multiplying the probability per unit path times the distance travelled in the unit time, which gives $n_2\, \sigma(v)v$.

Another important quantity is the ***reactivity***, which defined as the probability of reaction per unit time per unit density of target nuclei. It is just given by the product $\sigma\, v$. In general, target nuclei moves, so that the relative velocity v is different for each pair of interacting nuclei. In this case, we compute an ***averaged reactivity***.

$$\boldsymbol{\langle \sigma\, v \rangle = \int \sigma(v) v\, f(v) dv}, \qquad (9)$$

Where $f(v)$ is the distribution function of the relative velocities, normalized in such a way that $\int_0^\infty f(v)dv = 1$.

Both controlled fusion fuels and stellar media are usually mixtures of elements where species `1` and `2` have number densities $n_1, n_2, respectively$. the volumetric reaction rate, that is the number of reactions per unit time and per unit volume is then given by

$$\boldsymbol{R = \frac{n_1\, n_2}{1+\delta_{12}} \langle \sigma\, v \rangle = \frac{f_1\, f_2}{1+\delta_{12}}\, n^2 \langle \sigma\, v \rangle} \qquad (10)$$

Where n is the total nuclei number density, f_1 and f_2, are the atomic fraction of species "1" and "2", respectively. The Kronecker symbol δ_{12}(with $\delta_{12} = 1, if\ i = j\ and\ \delta_{12} = 0\ eleswhere$) is introduced to properly take into account the case of reaction between like particles. Equation 7 show a very important feature for fusion energy research: the volumetric reaction rate is proportional to the square of the density of the mixture. For feature reference, it is also useful to recast it in terms of the mass density ρ of the reacting fuel

$$\boldsymbol{R_{12}} = \frac{\boldsymbol{f_1 f_2}}{\boldsymbol{1+\delta_{12}}} \frac{\boldsymbol{\rho^2}}{\boldsymbol{\bar{m}^2}} \boldsymbol{\langle \sigma\, v \rangle} \qquad (11)$$

Where $\bar{m}$ is the average nuclear mass.

Here, the mass density is computed as $= \sum_j n\, m = n\bar{m}$, where the sum is over all species. We also immediately see that the specific reaction rate is proportional to the mass density, again the role of the density of the fuel is achieving efficient release of fusion energy [8].

Main controlled fusion reaction

The most important main controlled fusion reactions necessary as power source applications that recently used in many interested countries which supported huge efforts are listed in table (1).

Table 1. Main controlled fusion reactions [9].

Reaction	$\sigma(10\ keV)$ $barn$	$\sigma(100\ keV)$ $barn$	σ_{max} $barn$	$\in_{max}$ keV
$D + T \rightarrow \alpha + n$	2.72×10^{-2}	3.43	5.0	64
$D + D \rightarrow T + p$	2.81×10^{-4}	3.3×10^{-2}	0.096	1250
$D + D \rightarrow {}^3He + n$	2.78×10^{-4}	3.7×10^{-2}	0.11	1750
$T + T \rightarrow \alpha + 2n$	7.90×10^{-4}	3.4×10^{-2}	0.16	1000
$D + {}^3He \rightarrow \alpha + p$	2.20×10^{-7}	0.1	0.9	250

In our work, we concentrate on study the reaction between the hydrogen isotopes, deuterium and tritium, which are the most important fuels for controlled fusion research, namely, the D-T reaction.

$$D + T \rightarrow \alpha\,(3.5\ MeV) + n\,(14.1\ MeV)$$

The D-T reaction has the largest cross section, which reaches its maximum (about 5 barns) at the relatively modest energy of $64\ keV$ (see fig. 1). Its $Q = 17.6\ MeV$ is the largest of this family of reactions. It is to be observed that the cross section of this reaction is characterized by a broad resonance for the formation of the compound ^5He nucleus at $\epsilon \cong 64\ keV$ [9].

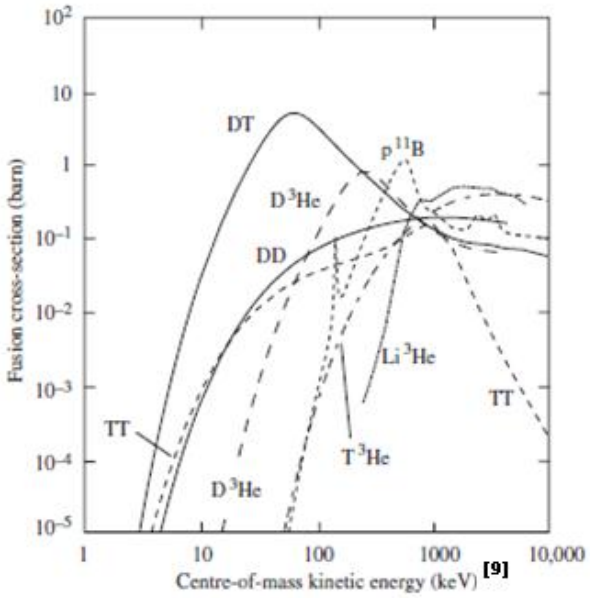

Figure 1. Fusion cross sections for the main controlled fusion reactions

Calculation and Results

The calculations are concentrated on the D-T fusion reaction, because of its huge applications in power source due to their high energy release, such as fusion reactors, (Tokomak), and others small systems like the dense plasma focus devices (DPF).

Clearly, as it is described previously, in order to calculate such hot parameters, i.e., reactivity, reaction rate, and the energy of emitted neutrons are all controlled by the cross section, which represents the essential factor in the calculations. A widely used parameterization of fusion reaction cross section is [9]

$$\boldsymbol{\sigma \approx \sigma_{goem} \times \mathcal{T} \times \mathcal{R}} \qquad (12)$$

Where σ_{goem} is a geometrical cross section, $\mathcal{T}$ is the barrier transparency, and $\mathcal{R}$ is the probability that nuclei come into contact fuse. The first quantity is of the order of the square of the de-Broglie wavelength of the system:

$$\boldsymbol{\sigma_{goem} \approx \lambda^2 = \left(\frac{\hbar}{m_r v}\right)^2 \propto \frac{1}{\epsilon}}, \qquad (13)$$

Where $\hbar$ is the reduced Planck constant and m_r is the reduced mass. Equation 9 concerning the barrier transparency, and its often well approximated by [9].

$$\boldsymbol{\mathcal{T} \cong \exp\left(-\sqrt{\frac{\epsilon}{\epsilon_G}}^2\right)} \qquad (14)$$

Which is known as the Gamow factor, where

$$\boldsymbol{\epsilon_G = \left(\pi \alpha_f Z_1 Z_2\right) 2 m_r c^2 = 986.1\, Z_1{}^2 Z_2{}^2 A_r \quad keV} \qquad (15)$$

Is the Gamon energy, $\alpha_f = \frac{e}{\hbar c} = \frac{1}{137.04}$, is the fine structure constant commonly used in quantum mechanics, $A_r = m_r/m_p$

The reaction characteristics $\mathcal{R}$ contains essentially all the nuclear information's of the specific reaction. it takes substantially different values depending on the nature of the interaction characterizing the reaction. It is largest for reaction due to strong nuclear interactions; it is smaller by several orders of magnitude for electromagnetic nuclear interactions; and still smaller by as many as 20 orders of magnitude for weak interactions. For most reactions, the variation of $\mathcal{R}(\epsilon)$ is small compared to the strong variation due to the Gamon factor. In conclusion the cross section is often written as [9].

$$\boldsymbol{\sigma(\epsilon) = \frac{S(\epsilon)}{\epsilon} \; exp\left(-\sqrt{\frac{\epsilon}{\epsilon_G}}^2\right)} \qquad (16)$$

Where the function $S(\epsilon)$ is called the astrophysical S factor, which for many important reactions is a weakly varying function of the energy [9]. Plasma reactivity calculations require reaction cross sections for energies well below those at which direct measurement are practicable [10]. A more convents or suitable formula for calculation the total cross section for D-T or others main controlled fusion reactions (listed below), which has a compatible agreement results with the really experimental results is given by.

$$D + D \rightarrow T\,(1.011) + P\,(3.022)\ \ probability(50\%)$$
$$D + D \rightarrow He\,(0.820) + n\,(2.449)\ \ probability(50\%)$$
$$P + T \rightarrow {}^3He + n - 0.764$$
$$D + T \rightarrow {}^4He\,(3.561\ MeV) + n\,(14.029\ MeV)$$
$$T + T \rightarrow {}^4He + 2n + 11.332\ MeV$$
$$D + {}^3He \rightarrow {}^4He\,(3.712\ MeV) + P\,(14.641\ MeV)$$
$$T + {}^3He \rightarrow {}^4He + n + P + 12.096\ MeV \qquad probability(59\%)$$
$$T + {}^3He \rightarrow {}^4He\,(4.800\ MeV) + D(9.520\ MeV) \qquad probability(41\%)$$
$${}^3He + {}^3He \rightarrow {}^4He\,(0.820\ MeV) + 2p + 12.860\ MeV$$

$$\sigma(\epsilon) = \frac{S(\epsilon)}{\epsilon}\ exp\left(-\frac{R}{\sqrt[2]{\epsilon}}\right)\ \ with\ R = \pi\left(\frac{e^2}{\hbar c}\right)\sqrt[2]{2mc^2}\ Z_1Z_2 \qquad (17)$$

Where the cross section is expressed in centre of mass units, $\in = \frac{1}{2}mv^{\,2}$, $m = m_1m_2/(,m_1 + m_2)$ and v is the relative velocity of the interacting particles which have masses $m_1 and\ m_2$ and charges $Z_1 and\ Z_2$ respectively.the constants $e, \hbar\ and\ c$ have their usual meaning. $S(\epsilon) = A\exp(-\beta\ \in)\ \ and\ the\ parameters\ A, \beta\ and\ R$ are given in table (2). Note that laboratory energies may be used if the substitution $\in = \left(\frac{m}{m_1}\right)\in_{lab}\ has\ to\ be\ considered$ [10].

Table 2. Low energy cross section parameterization [10].

Reaction	$A(\ barns - keV)$	$\beta \quad (keV^{-1})$	$R \quad (keV^{1/2})$
$D - D_p$	52.6	-5.8×10^{-3}	31.39
$D - D_n$	52.6	-5.8×10^{-3}	31.39
$D - T$	9821	-2.9×10^{-2}	34.37
$T - T$	175	9.6×10^{-3}	38.41
$D - {}^3He$	5666	-5.1×10^{-3}	68.74
$T - {}^3He$	2422	4.5×10^{-3}	76.82
${}^3He - {}^3He$	5500	-5.6×10^{-3}	153.70

By testing equation 14, for the D-T fusion reaction and in order to arrive results gives high agreement with the corresponding experimental published results, we find that it

is very necessary to introduce a correction factor related to each deuterons energy ($\in$) in the above equation, and these case are completely described in table 3.

Theoretically, the energy of the emitted neutrons from the D-T fusion reaction can be exactly determined from equation (6) as a function of both the incident deuteron energy $E_d$and the reaction angle θ. The calculated results are completely described in Table 4.

Finally, the reactivity as a function of the temperature, obtained by numerical integration of the following equation with the best available cross section for the reactions of interest to controlled fusion.

$$\langle \sigma v \rangle = \left[\left(\frac{m_1 + m_2}{2\pi k_B T} \right)^{3/2} \int dV_c \, exp\left(-\frac{m_1 + m_2}{2k_B T} V_c^2 \right) \right] \times \left(\left(\frac{m_r}{2\pi k_B T} \right)^{3/2} \int dV_c \, exp\left(-\frac{m_r}{2k_B T} V^2 \right) \sigma(v) v \right)$$

The term in square bracket is unity, being the integral of a normalized Maxwellain, and we are left the integral over the relative velocity. By writing the volume element in velocity space as $= 4\pi v^2 dv$, and using the definition of center of mass energy ϵ , we finally get

$$\langle \sigma v \rangle = \frac{4\pi}{(2\pi m_r)^{1/2}} \frac{1}{(k_B T)^{3/2}} \int_0^\infty \sigma(\in) \in exp(-\in / k_B T) d$$

For the D-T fusion reaction, which is by far the most important one for present fusion research, the following expression is used to calculate the reactivity [8]. And the present calculated results are completely described in figure 3.

$$\langle \sigma v \rangle = 9.10 \times 10^{-16} \, exp\left(-0.572 \left| ln \frac{T}{64.2} \right|^{2.13} \right) \quad cm^3/s \qquad (18)$$

Discussion and Conclusion

Clearly, from the results about the total cross section for the D-T fusion reaction calculated by equation (17), it is appear a common shift from the published experimental results and one can interpreted that by some physical reasons that directly correlated with the fundamentals parameters deal with the system or device designing, geometrical dimension for the cathode and anode, and the operating factors, such as the fuel pressure, initial power, and we can added another reason deal with the construction time for building the experiment, in which that any system are exactly differ in all covering physical conditions with the recent ones. In other words, it is necessary to available a given empirical formula for each systems (experimental devices). Therefore, we concluded that it is important and necessary to modify the formula for the total cross section for the D-T fusion reaction by introducing a fixed correction factor for certain deuteron energy/or energy intervals to avoid the disagreement between the theoretical and experimental results.

From Table 1 and Table 3, we see that our calculated results about the total reaction cross section, after introducing the correction factors are more compatible with the published results [9]. Also, from Figure 3, the calculated results about the D-T fusion reaction reactivity by using equation (18) give or reflect a physical behavior that are more suitable with the corresponding published results, and this case can be interpreted for the reason of the cross section data are available in the reactivates equation. Finally it's useful to suggest the recommendation of the modified formulas instead of the previously described ones to be applied in the recently systems.

From Table 4, it is clear that the energies of emitted neutron, which calculated by our expressed formula at incident reaction angle of 90 degree are of quite agreement with the recommended value of (14.029 MeV), and this case can be interpreted as, there exist a small percentage of incident deuterons are scattered from its original direction, and all the really occurring physical experimental phenomenon's can be explained at this angle instead of others angles.

References

1. Federico Rocchi and Marco Sumini," Characterization of neutron emission from a D-D filled plasma focus", M&C 2001 Salt Lake City, Utah, USA, September 2001 .
2. Sor Heoh Saw and Sing Lee, "Scaling the plasma focus for fusion energy considerations", Int. J. Energy Res., vol. 35. Pp.81-88,2011.
3. M. Zakaullah, T.J. Baig, S. Beg, and G. Murtaza, "Effect of insulator sleeve length on neutron emission in a plasma focus", Phys. Let. A,Vol.137, no. 1/2, pp. 39-43, may 1989.
4. A. Talaei and S. M. Sadat Kiai, "Study the influence of the bank energy on the dynamical pinch in plasma focues', J. Fusion energy, vol.28, no. 3, pp. 304-313, sep. 2009.
5. T. Zhang, R. S. Rawat, S. M. Hassan , J. J. Lin, S. Mahmood, T. L. Tan, S. V. Springham, V. A. Gribkov, P. Lee, and S. Lee, "Drive parameters as a design consideration for Mather and Fillippov types of plasma focus,"IEEE Tran. Plasma Sci., vol. 34, no. 5, pp. 2356-2365, oct. 2006.
6. Bernstein, M.J, Comisar, G.G., "Neutron energy and flux distribution from a crossed-field acceleration model of plasma focus and Z-pinch discharges",the physic of fluids, 15, 4, pp 700-707, 1972.
7. Tiseanu, I., Mandache, N., Zambreanu, V.,"Energitic and angular distribution of the reacting deuterons in a plasma focus", plasma phys. Control. Fusion, Vol. 36, pp417-432, 1994.
8. Robly D.Evans , "The atomic nucleus", Mcgraw-Hill book company, inc., 1955.
9. Stefano Atzeni, Juroen M., " The physics of inertial ", Oxford University press, 2004.
10. O.N. Jarvis, www.Kayelaby.npl.co.uk, "Table of physics and chemical constants", Chapter 4, section 4.7.4, 2011.
11. T.A. Heitemes, G.A. Moses, J.F. Santarius, "Anaylsis of an improved fusion reaction rate model for use in fusion plasma simulation", fusion technology

institute, university of Wisconsin,1500 engineering drive, Madison, WI 53706, UWFDM- Report, 2005.

Table 3. The recommended correction factors necessarily for calculations the D-T fusion reaction cross section.

Energy $\in$ keV	Correction factor	Cross section $\sigma(\epsilon)$ barns
5	1.080	5.1779×10^{-4}
10	1.081	2.7020×10^{-2}
20	0.50	0.2015
30	0.35	0.5148
40	0.30	1.0253
50	0.32	2.0754
60	0.31	3.4198
64	0.375	5.0144
70	0.255	4.4785
80	0.150	4.0166
90	0.085	3.3684
100	0.0598	3.3427

Table 4. The calculated energy of emitted neutrons as a function of the reaction angle.

E_n MeV	$\theta = 0$ deg		$\theta = 45$ degre		$\theta = 60$ degre		$\theta = 90$ degre
14.0842	E_d keV	E_n MeV	E_d keV	E_n MeV	E_d keV	E_n MeV	E_d keV
14.0882	10	14.2979	10	14.2350	10	14.1906	10
14.0923	20	14.3915	20	14.3020	20	14.2391	20
14.0963	30	14.4646	30	14.3546	30	14.2773	30
14.1004	40	14.5272	40	14.3997	40	14.3102	40
14.1044	50	14.5830	50	14.4400	50	14.3397	50
14.1084	60	14.6341	60	14.4769	60	14.3668	60
14.1125	70	14.6815	70	14.5113	70	14.3922	70
14.1165	80	14.7260	80	14.5436	80	14.4160	80
14.1205	90	14.7682	90	14.5743	90	14.4387	90
14.1246	100	14.8084	100	14.6036	100	14.4604	100
14.1286	110	14.8469	110	14.6317	110	14.4813	110

14.1326	120	14.8840	120	14.6587	120	14.5015	120
14.1366	130	14.9198	130	14.6849	130	14.5210	130
14.1407	140	14.9545	140	14.7103	140	14.5399	140
	150	14.9882	150	14.7349	150	14.5584	150

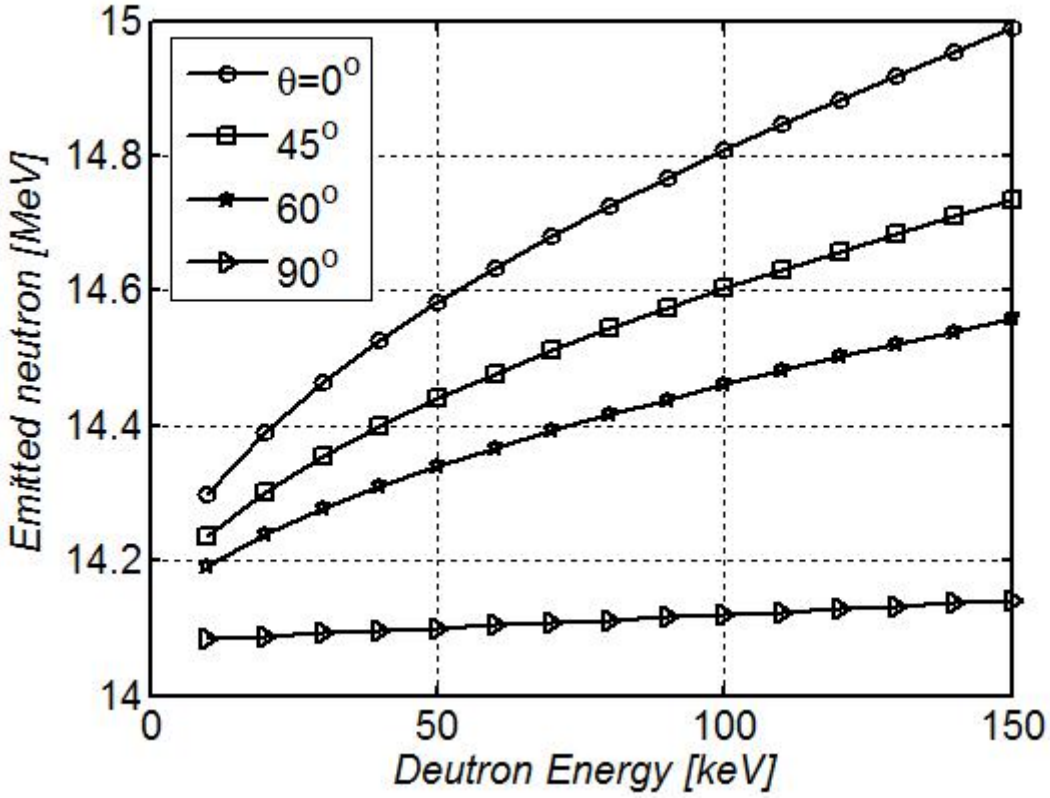

Figure 2. Variation of the emitted neutron energy versus the incident deuteron energy

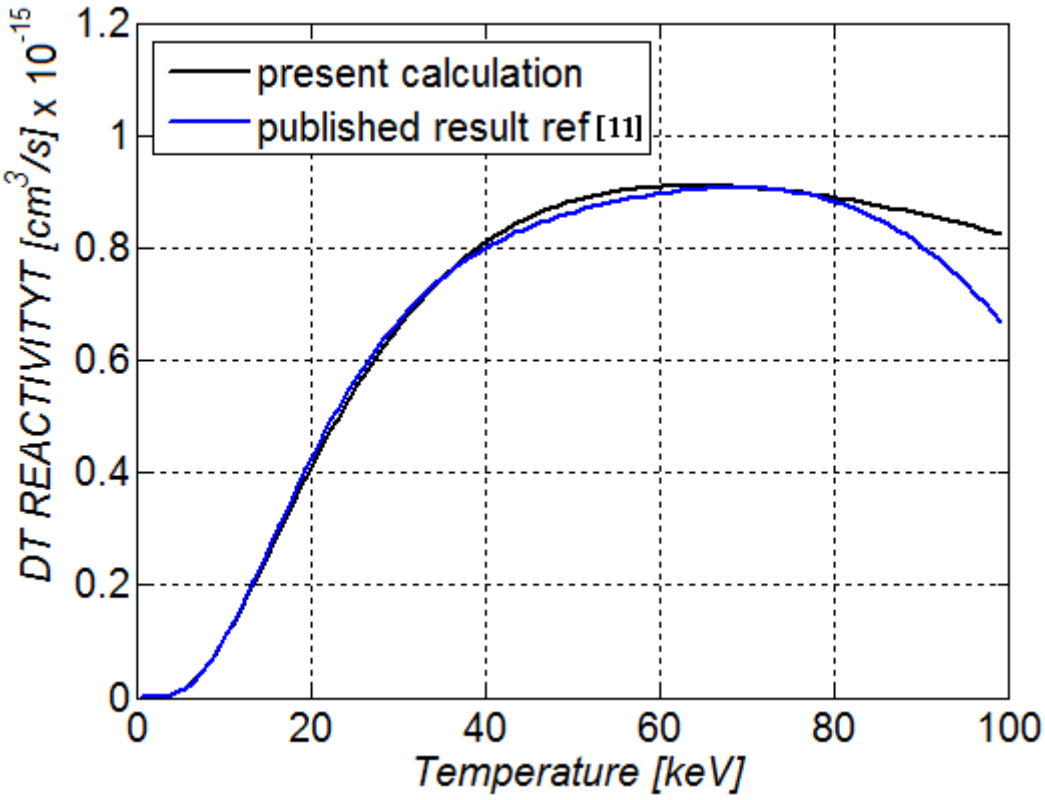

Figure 3. Variation of the D-T Reactivity versus the incident deuteron temperature

Secure Watermark Image Steganography by Pixel Indicator Based on Randomization

Zena Ahmed[+] and M. Hamid Mohammed Farhan[++]

College of Electrical and Electronics Technique
[+] E-mail:zena782004@yahoo.com
[++] E-mail:hamd_farhan@yahoo.com

Abstract

Steganography is the art of hiding the fact that communication is taking place, by hiding information in other information. In this paper have being investigated a method to RGB image steganography based on pixel indicator technique and triple-A algorithm. They uses the same principle of Least Significant Bit (LSB), where the secret is hidden in the least significant bits of the pixels, with more randomization in selection of the number of bits used and the color channels that are used. This randomization is expected to increase the security of the system and also increase the capacity of information. These techniques can be applied to RGB images where each pixel is represented by three bytes (24 bit) to indicate the intensity of red, green, and blue in that pixel. This work showed attractive results especially in the capacity of the data-bits to be hidden with relation to the RGB image pixels. The effective of the proposed stego system has been estimated by Mean Square Error (MSE), Peak Signal to Noise Ratio (PSNR). This paper also illustrates how security has been enhanced using this algorithm.

Keywords: Steganography, Randomization, Triple-A Algorithm, Pixel Indicator Algorithm and Computer Security.

اخفاء الصورة المائية من المؤشر بكسل استنادا إلى التوزيع العشوائي

خلاصة

إخفاء المعلومات هو فن اخفاء حقيقي وان الاتصالات تجري عن طريق إخفاء المعلومات في غيرها من المعلومات. في هذا البحث لدينا وسيلة لتحقيق في إخفاء المعلومات صورة RGB على أساس تقنية مؤشر بكسل والثلاثي خوارزمية. انها تستخدم نفس مبدأ LSB، حيث يتم إخفاء سر في بت على الأقل أهمية من بكسل، مع مزيد من العشوائية في اختيار عدد البتات المستخدمة وقنوات الألوان التي يتم استخدامها. ومن المتوقع أن هذا التوزيع العشوائي لزيادة أمن النظام، وكذلك زيادة قدرته. ويمكن تطبيق هذه التقنيات لصور RGB حيث يتم تمثيل كل بكسل من ثلاثة بايت للدلالة على كثافة اللون الأحمر والأخضر والأزرق في تلك بكسل. وأظهرت نتائج هذا العمل جذابا خصوصا في قدرة بت البيانات إلى أن تكون مخفية مع يتعلق بكسل صورة RGB. وقد قدر من فعالية نظام stego المقترحة عن طريق مربع الخطأ (MSE)، وإشارة إلى الذروة نسبة الضوضاء (PSNR). هذا البحث كما يوضح كيف تم تعزيز الأمن باستخدام هذه الخوارزمية.

1. Introduction

Steganography is the process of hiding of a secret message within an ordinary message and extracting it at its destination. Anyone else viewing the message will fail to know that it contains secret/encrypted data. The word comes from the Greek word “steganos” meaning “covered” and “graphei” meaning “writing” [1, 2, 3].

The LSB method insertion is a very simple and common approach to embedding information in an image in special domain. The limitation of this approach is vulnerable to every slight image manipulation [4].

Some techniques have been used for image steganography such as LSB, SCC and image intensity .In LSB, the least significant bit of each pixel for a specific color channel or for all color channels is replaced with a bit from the secret data. Although it is a simple techniques, but the probability of detecting the hidden data is high. The Stego Color Cycle (SCC) technique is an enhancement [5].

2. Steganography

Steganography techniques require two files: cover media, and the data to be hidden [6]. When combined the cover image and the embedded message make a stegofile, which is in

our work for image steganography known as stego-image image [7]. One of the commonly used techniques is the *LSB,* its work by they pixel is replaced by bits of the secret till secret message finishes [5,8]. The risk of information being uncovered with this method as is, is susceptible to all 'sequential scanning' based techniques [7], which is threatening its security.

The random pixel manipulation technique attempts at overcoming this problem, where pixels, which will be used to hide data are chosen in a random fashion based on a stego-key. However, this key should be shared between the entities of communication as a secret key [9].

Image-based steganography techniques need an image to hide the data in. This image is called a cover media. Digital images are stored in computer systems as an array of points (pixels) where each pixel has three color components: Red, Green, and Blue (RGB). Each pixel is represented with three bytes to indicate the intensity of these three colors (RGB) [7].

The color channel, where the secret data will be hidden in, is cycling frequently for every bit according to a specific pattern [10]. For example, the first bit of the secret data is stored in the LSB of red channel, the second bit in the green channel, the third bit in the blue channel and so on. This technique is more secure than the LSB but still it is suffers detecting the cycling pattern that will reveal the secret data. Also it has less capacity than the LSB. StegoPRNG is also a different technique that uses the RGB images. However in this technique, a pseudo random number generator (PRNG) is used to select some pixels of the cover image. Then, the secret will be hided in the Blue channel of the selected pixels. Again this technique has the problem of managing the key, and problem of capacity since it uses only the Blue channel out of the three channels of their available channels [5].

3. The Proposed Technique

The proposed method takes advantage of psycho visual redundancy and the dependency of a pixel. A color image is generally formed by three different bands, such as red, green, and blue, in a color coordinate system. In the proposed algorithm, the data hiding procedure is performed on R, G, and B bands, respectively. The step-by-step procedure is stated as follows and Table (1) shows the Meaning of indicator values. The proposed algorithm was implemented in Matlab ver 7.1. The devised method consists of two main processes. First one deals

with the hiding data which passes some controls to matlab GUI for implementation of LSB hiding algorithm. The other process then returns back the reverse information in the cover RGB color image .we have implemented steganographic routines in matlab using the GUI toolbox. The suggested technique tries to solve the problem of the previous two techniques by using one of the channels as an indicator for data existence in the other two channels and the indicator is set randomly by nature.

Designing any stego algorithm should take into consideration the following three aspects (Figure 1):

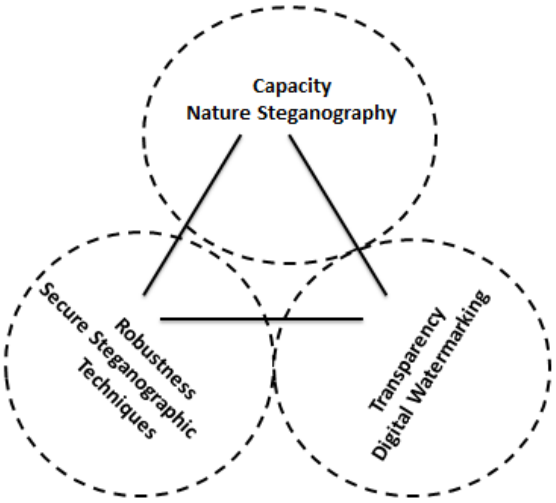

Figure 1. Steganography tradeoff parameters

• Capacity: The amount of data that can be hidden without significantly changing the cover medium.
• Robustness: the resistance for possible modification or destruction in unseen data.
• Invisibility (Security or Perceptual Transparency): The hiding process should be performing in a way that it does not raise any suspicion of eavesdroppers.
Figure 1, shows the relation between these three main parameters. If we increase the capacity of any cover to store more data than a practical possible threshold, then its transparency or robustness will be affect and vice versa. Similarly, transparency and robustness are related; if any of these two parameters are influenced, it can affect the performance in the other one. The capacity, robustness, and security parameters relation issues can be driven by the application need and its priorities [11].

Table 1. Meaning of indicator values.

indicator	K=0, $I_{LSB} \leftarrow I_{BIN}$	K=1, $I_{LSB} \leftarrow I_{BIN}$
KGB	**G**	**B**
RKB	**R**	**B**
RGK	**R**	**G**

3.1 Embedding Algorithm:

Algorithm for secret data embedding process:

Begin
Input : Color cover Image (Ic) and Secret Image (IS)
Output : Stego Cover Image
Step 1 : Read the Color cover image (Ic) and the Image data to be embedded
Step 2 : Generate a randomize Binary map key
Step 3 : Split the cover into RGB planes
Step 4 : choose which RGB plane to save map key
Step 5 : Repeat step5 for all row and column of cover image
Step 6 : Read each pixel in map key
If pixel =0 then embedded the secret pixel of image in channel one
Else
embedded the secret pixel of image in channel two
Step 7 : Combine the RGB plane to form stego cover
End

3.2 Reconstructed Algorithm:

Algorithm for secret data recovery process:

Begin
Input : Stego Cover Image (Is)
Output : Secret Image (IS)
Step 1 : Read the stego image (Is) and split to RGB planes
Step 2 : Split the cover into RGB planes
Step 3 : determine where randomize Binary map key
Step 4: Repeat step5 for all row and column of cover image
Step 5 : Read each pixel in map key

If pixel =0 then get LSB of the secret pixel of image in channel one
Else
Get LSB of the secret pixel of image in channel two
Step 6 : Save the secret Image (IS)
End

3.3 Error Metrics

The effectiveness of the stego process proposed has been studied by estimating the following four metrics for both cover images. Bit Error Rate (BER) evaluates the actual number of bit positions which are replaced in the stego image in comparison with cover image. It has to be computed to estimate exactly how many bits of the original cover image (I_c) are being affected by stego process. The BER for the Stego image (I_s) is the percentage of bits that have errors relative to the total number of bits considered in I_c.

Let I_{cbin} and I_{sbin} are the binary representations of the cover image and stego cover then [12],

The total number of bit errors,

$$T_e = \sum_{i=1}^{n} |I_{cbin} - I_{sbin}| \ldots \qquad \ldots\ldots\ldots\ldots\ldots\ldots\ldots\ldots\ldots\ldots\ldots\ldots(1)$$

and the bit error rate BER = T_e / T_n

T_n is the total number of bits considered for the gray image of size M × N pixels. T_n will be M × N × 8.

Peak Signal to Noise Ratio (PSNR):

The PSNR is calculated using the equation [12],

$$PSNR = 10log_{10}\left(\frac{I_{max}^2}{MSE}\right)\text{dB} \ldots\ldots\ldots\ldots\ldots\ldots\ldots\ldots\ldots\ldots\ldots\ldots(2)$$

Where I_{max} is the intensity value of each pixel which is equal to 255 for 8 bit gray scale images. Higher the value of PSNR better the image quality

Mean Square Error (MSE)

The MSE is calculated by using the equation [12],

For Gray scale Images: $$MSE = \frac{1}{MN}\sum_{i=1}^{M}\sum_{j=1}^{N}(x_{i,j} - y_{i,j})^2 \quad \ldots \quad \ldots(3)$$

For color Images: $$MSE = \left[\frac{MSE(R)+MSE(G)+MSE(B)}{3}\right] \ldots\ldots\ldots\ldots\ldots\ldots(4)$$

Where M and N denote the total number of pixels in the horizontal and the vertical dimensions of the image $x_{i,j}$ represents the pixels in the original image and $y_{i,j}$ represents the pixels of the stego-image.

4. Results and Discussion

By selected the three different images in (sizes, application field) to perform in the testing have shown in Table (2):

Table 2. The Size of Original Cover Image and the Binary Image of Three Tests.

Cover image	Size of cover image	Size of binary image
Lena	**512x512**	**400x333**
Sun	**280x210**	**2100x2100**
Colored	**246x165**	**1138x1508**

The Results of our method is shown in Table (3), and using Image Quality (In PSNR MSE) ,Then three digital images has been taken as cover images for the processed method are shown in the following Figures (2-4).

Table 3. Results in terms of Image Quality (In PSNR MSE) using RGB channel for different color images (for BPP=8/3).

Cover Image	Channel 1 Red		Channel 2 Green		Channel 3 Blue	
	MSE	PNSR	MSE	PNSR	MSE	PNSR
Lena	0.44056	51.6907	0.44042	51.6921	0.43972	51.6991
Sun	0.27425	53.7494	0.27464	53.7431	0.27322	53.7658
Colored	0.30999	53.2173	0.3098	53.22	0.31084	53.2054

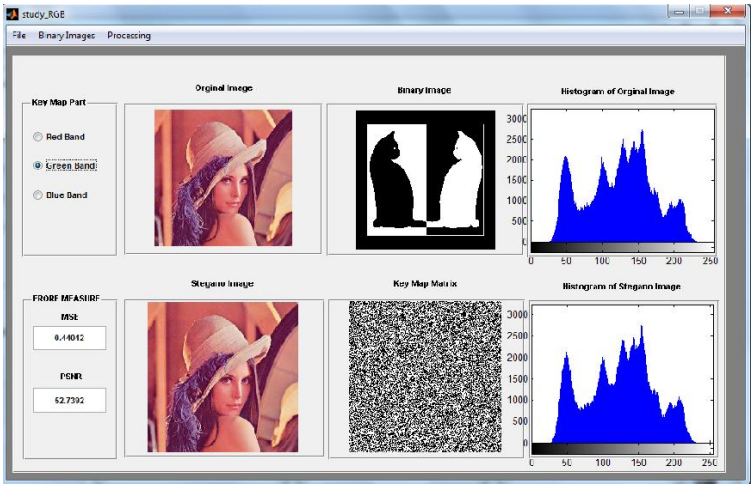

Figure 2. Original cover images and the binary image of Test1

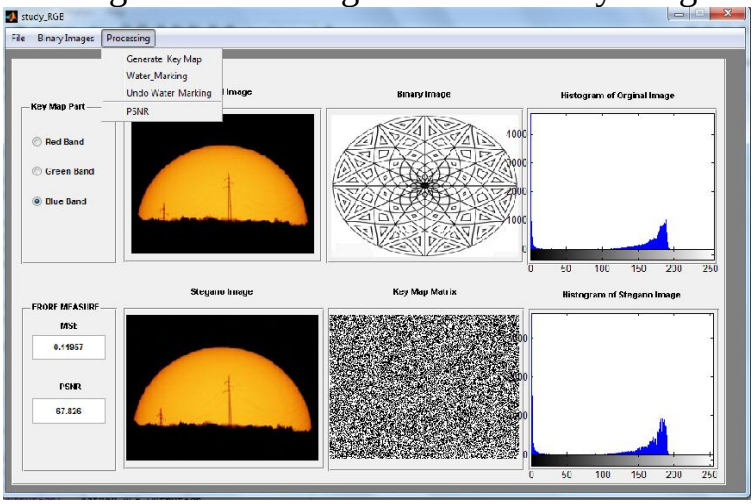

Figure 3. Original cover images and the binary image of Test2

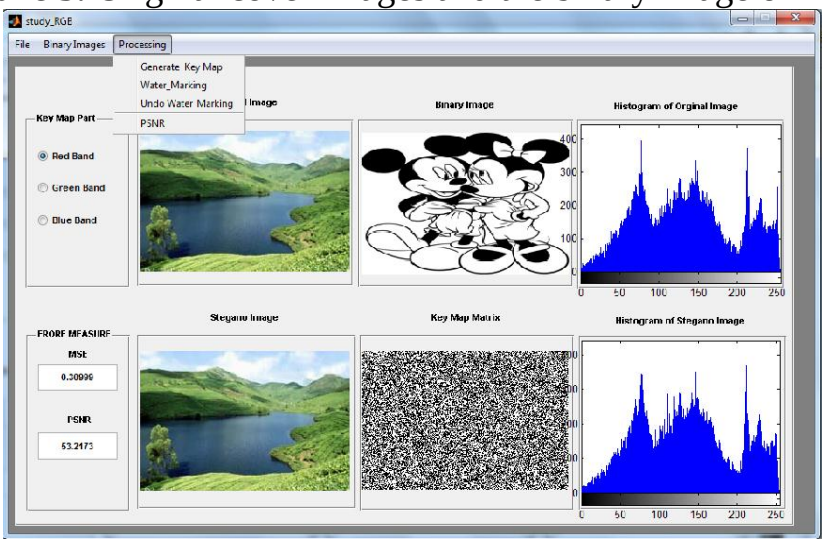

Figure 4. Original cover images and the binary image of Test3

5. Conclusions

Demonstrated a new watermarking technique that uses RGB band scheme to embed a copyright image or any binary image into original image. This technique works well with images of all sizes. This technique provides a Randomize key map embed in one channel and two other channels will content the copyright images or binary images are embedded into original image for copyright protection. Also, the embedded image is shared among n participants where all the n shares must be used to reconstruct the embedded image. This makes the system more secure. The method can with stand attacks like JPEG compression, resize and adding noise with less loss in quality of the image. In this work we can be used either symmetric key or public key and embed the hash value inside the image so that at the receivers end the authentication and integrity of the image can be verified by recalculating the hash and verifying it. Similarly digital signatures can be generated for images and can be verified. Also (k,n) threshold secret sharing schemes can be implemented for much security.

Experimental results have shown that the proposed method provides an efficient way for embedding large amount data into cover images without making noticeable distortions. Moreover, the proposed methods use less than half of the total number of pixels in an image where methods discussed in references [8,13] use almost all the pixels of an image for the same amount of hiding capacity.

References

1. N. F. Johnson and S. Katzenbeisser," .A Survey of Steganographic Techniques", in S. Katzenbeisser and F. Peticolas (Eds.): Information Hiding, Artech House, Norwood, MA, Page (43-78), 2000.
2. Lou, D. C. and Liu, J. L. "Steganography Method for Secure Communications", Elsevier Science on Computers& Security, 21, 5, Page (449-460), 2002.
3. J. Fridrich and M. Goljan, "Practical Steganalysis of Digital Images-state of the Art", Proc. SPIE Photonics West, Vol. 4675, San Jose, California, Page (1-13), January 2002.
4. C.K. Chan, L. M. Chen, "Hiding data in images by simple LSB substitution", Pattern Recognition, Vol. 37, Page (469–474), 2004.

5. K. Bailey, K. Curran, "An Evaluation of Image Based Steganography Methods", Multimedia Tools & Applications, Page (55-88), Vol. 30, No. 1, July 2006.
6. A. Gutub, L. Ghouti , A. Amin, T. Alkharobi, M.K. Ibrahim, "Utilizing Extension Character 'Kashida' With Pointed Letters for Arabic Text Digital Watermarking", Inter. Conf. on Security and Cryptography - SECRYPT, Barcelona, Spain, 28 - 31, July 2007.
7. N.F. Johnson, S. Jajodia, "Exploring Steganography: Seeing the Unseen", IEEE computer, Vol. 31, No. 2, Page (26-34), February 1998.
8. K. Hempstalk, "Hiding Behind Corners: Using Edges in Images for Better Steganography", Proceedings of the Computing Women's Congress, Hamilton, New Zealand, Page (11-19), February 2006.
9. A. Gutub, M. Ankeer, M. Abu-Ghalioun, A. Shaheen, and A. Alvi, "Pixel indicator high capacity technique for RGB image based Steganography", WoSPA 2008–5th IEEE International Workshop on Signal Processing and its Applications, University of Sharjah, Sharjah, U.A.E., Page (18-20), March 2008.
10. R. Chandramouli, N. Memon, "Analysis of LSB Based Image Steganography Techniques" Proc. IEEE ICIP, Page (1019-1022), 2001.
11. N. Tiwari1, M. Shandilya, "Secure RGB Image Steganography from Pixel Indicator to Triple Algorithm-An Incremental Growth", International Journal of Security and Its Applications, Page (53-62), Vol. 4, No. 4, October, 2010.
12. R. Amirtharajan, R. John, "Constructive Role of SFC & RGB Fusion versus Destructive Intrusion", International Journal of Computer Applications, Page (0975 - 8887) Vol. 1, No. 20, 2010
13. G.C. Kessler, "An Overview of Steganography for the Computer Forensics Examiner", Forensic Science Communications, Vol. 6, No. 3, July 2004.

Radiological Characterization of Destroyed Nuclear Reactor Tammuz-2 at Al-Tuwaitha Site

Yousif M. Zayir AL-BAKHAT, Assim OleIwi Mahdi, Fouzey H. Kitah,
Samir Nouri Marmardji, Anwar A.Ahmed, and
Nabeel H. A. AL-Tameemi

Radiation &Nuclear Safety Directorate, Ministry of Science &Technology
e-mail: yousif_zayir@yahoo.com

Abstract

In-situ measurement, sampling and analysis of destroyed nuclear reactor Tammuz-2, were implemented using portable monitors to determine the external exposure dose rates. The quantity and quality of radionuclides were determined using gamma spectrometry techniques. Results indicated that the maximum dose rates at bottom of reactor core were 10.8 mSv/h; many of the soil samples were contaminated by Cs-137and Co-60. Therefore, the workers, general public and environmental will be subjected to the principles of the optimization of radiation protection according to ALARA (As Low As Reasonable Achievable) principle during all phases of decommissioning nuclear reactor Tammuz-2 as recommended by International Atomic Energy Agency (IAEA).

Keyword: Decommissioning, Iraqi Decommissioning Program (IDP), Radiation Safety

التوصيف الاشعاعي لمفاعل تموز-2 المدمر في موقع التويثة

يوسف محسن زاير البخات وعاصم عليوي مهدي وفوزي حسن كاطع ومير نوري مرمجيو
وانور عبد الفتاح احمد ونبيل هاشم امين التميمي

خلاصة

لغرض تصفية مفاعل تموز -2، تم اجراء قياسات حقلية باستخدام الاجهزة المحمولة لتحديد مستوى التعرض الاشعاعي الخارجي لبناية المفاعل المدمرة وقد دلت نتائج المسح الاشعاعي الحقلي ان اعلى مستوى تعرض اشعاعي كان في حوض المفاعل والقنوات الافقية رقم 2 و3 حيث وصل حوالي 10.8 ملي سيفرت/ساعة في قعر الحوض. كذلك تم اجراء التحليل الطيفي لعينات التربة الماخوذة من مناطق مختلفة من بناية المفاعل المدمرة باستخدام منظومة التحليل الطيفي لاشعة كاما. دلت النتائج ان بعض العينات ملوثة بنظيري السيزيوم -137 والكوبلت-60. عليه يجب اتخاذ الاجراءات الوقائية الازمة لتامين سلامة العاملين والناس والبيئة اثناء مراحل التصفية للمفاعل وحسب مبدا الآرا (تقليل مستوى التعرض الاشعاعي الى اقل قدر ممكن) الموصى بة من قبل الوكالة الدولية للطاقة الذرية.

Introduction

Decommissioning is the final phase in the life-cycle of nuclear facilities, after siting, design, construction, commissioning and operation. It is a complex process involving activities such as decontamination, dismantling, demolition of equipment and structures, and management of resulting waste, while taking into account aspects of health and safety for the workers and the general public, as well as protection of the environment. The ultimate objective of decommissioning is unrestricted release or reuse of the site [1-8]. The decommissioning strategy for nuclear reactors can vary from case to case. Therefore the planning and implementation of decommissioning strategies for the destroyed nuclear facilities are very complex process. Characterization is an initial step in the decommissioning process and requires a logical approach in order to obtain the data necessary for planning a decommissioning program [8-10]. Characterization involves a survey of

existing data, calculation, in-situ measurement and/or sampling and analysis. Using this database the decommissioning planner may assess various options and their consequences [4, 7], considering:

- techniques; decontamination processes, dismantling procedures ,
- radiological operating protection of worker, general public and environment;
- Waste classifications; and resulting costs;
- Comparison and optimization of these factors will lead to the selection of a decommissioning strategy.

TAMMUZ-2 NUCLEAR REACTOR

Tammuz-2 nuclear reactor is located at Al-Tuwaitha site about (20 Km South of Baghdad), GPS Coordinates (North= 33°12.194″, East= 44°31.079″), it is a part of the nuclear complex built by France [1] , which consists of five facilities[1]:

1. Tammuz-1 reactor (40 MW) which was destroyed by Israel in 1981,
2. Tammuz -2 reactor (500 KW),
3. Radioactive Waste Treatment Station (RWTS),
4. Laboratory Workshop Building (LWB) and,
5. Lamma facility (LAMA).

Tammuz-2 reactor was operated in 1980, and destroyed in 1991. Tammuz Complex occupies service area of (270 m^2).Tammuz -2 reactor is utilized:

- As an exact mock – up of Tammuz -1 reactor for measurements on core characteristics (reactivity, control rods, efficiency, power calculation, flux measurement), and measurements on experimental devices, neutron source for neutrongraphy and various studies with neutrons. Primarily designed as a neutron mock-up, it offers the same operating facilities as Tammuz-1:

- Pool type with direct access to the core, Easy change of core configuration, Layout and easy handling of devices inside and outside core caisson, Post irradiation examination devices: neutrongraphy, hot cells. It is connected to the channels making easy underwater transfers between Tammuz-2 andTammuz-1 pools and hot cells [1].

OBJECTIVES

The objective is to determine the exposure dose rates and information on quantity and quality of radionuclides, their distribution in the building of destroyed nuclear reactor Tammuz-2, and for the purpose of protection the workers, general public and environment against radiation risks.

Material and Methods

For the purpose of determination the external exposure dose rates of the destroyed nuclear reactor Tammuz-2, the background was determined using different types of portable monitoring, then compare the results of measurements, with the result of measurements of Tammuz-2 reactor.

The background was determined, as in Table-1 by using hand held monitors type:

- Ludlum type for measuring Gamma (γ) dose rate, unit (μSv/h).Gamma Scintillation detector type NaI crystal size (5cm x5.1cm).

- Radiagem type for measuring high (γ) dose rates, unit (μSv/h), water proof, GM detector.

Surface soil samples were collected from building of Tammuz-2 reactor, crushed by grinding machine, sieved through a (1) mm mesh sieve, then dried in an oven at (80 – 100)^{0}C for 12 hours. Weight one kilogram and packed in marinelli beaker, closed and tightly sealed using parafilm and store about one month to allow U-238 and Th-232 decay series to reach radioactive equilibrium with it short live progeny. Gamma spectrometer (Canberra) system was used for measurements and analyses of samples, which consists of a detector, preamplifier and pulse-height analyzer (DSA 2000),lead shield, using vertical high purity germanium (HpGe) detector of efficiency 40 %, and resolution (2.0 keV) , based on the measurement of 1.332 MeV gamma ray photo peak of Co-60 source and Multichannel analyzer (MCA) with 8192 channel is used , Both high voltage supply and amplifier device are compact in one unit (DSA 2000), A detector shield are with a cavity adequate to accommodate large samples. Shield has walls 10 cm lead, thick lined inside with graded absorber of Cd ~ 1.6 mm Cu ~ 0.4 mm [11-13].

Calibration and efficiency of the system are carried out using multi – gamma ray standard source (MGS-5, Canberra) of Marinelli beaker geometry. A library of radionuclides which contained the energy of the characteristic gamma emissions of each nuclide was analyzed and their corresponding emission probabilities were built from the data supplied in the software (Genie-2000). The activity concentrations of Ra-226 was evaluated from the gamma ray 609 keV of Bi-214 peak indicated for U-238, while 911 keV gamma line of Ac-228 or 238.6 keV of Bi-212 indicated for Th-232, k-40 activity was determined from peak at 1460.8 keV and Cs-137 was determined from gamma line 661.6

keV peak. Data on activity concentrations of radionuclides ($Bq.kg^{-1}$) (assuming secular equilibrium between U-238 and their progenies) [13-16] the activity concentrations of Ra-226, Th-232 and k-40 in soil sample are given in table (10).

MEASURMENTS

Background Measurements (B.G)

Table-1 B.G dose rates measurements, GPS: N= 33 12 158, E= 44 31 106.

No.	Ludlum monitor (µSv/h) at hight 1m
1	0.080
2	0,066
3	0.089
4	0.070
5	0.079
6	0.077
7	0.073
8	0.080
9	0.079
10	0.072
11	0.075
12	0.071
13	0.078
14	0.080
15	0.078
16	0.077
17	0.079
18	o.o78
19	0.079
20	0.076
Min	**0.070**
Max	**0,089**
Average	**0.0771**

Table 2. Dose rates around Tammuz-2 building(Ludlum monitor).

N0.	Location	Dose rate at 1m height (µSv/h)
1	Office building entrance	0.085
2	10m from entrance	0.084
3	building Corner near chimney	0.094
4	Near reactor chimney	0. 101
5	15m from chimney at the edge of the road	0. 118
6	10m from office building chimney side	0.098
7	10 from hot shop building(h.s.b) gate	0.099
8	At hot shop building gate	0.107
9	10m from h.s.b in front of the cells	0.097
10	10m to the wall at end of h.s.b	0.097
11	20m from h.s.b wall near sewerage	0.087
12	10m from gallery	0.088
13	10m from the end wall of gallery	0.085
14	10m from the end wall ofTZ-1 building	0.090
15	10m from the middle of TZ-1 office	0.094
16	10m from the in front side of TZ-1 office	0.088
17	10m from the in front side of h.s.b	0.086
18	Near storage tanks	0.082
19	10m from the wall of TZ-2 in front side of offices building	0.086
20	10m from office corner	0.088

Table 3. Dose rates in Tammuz-2 buildings level 0.0 offices and reactor hall (Ludlum monitor)

No.	Location	Dose rate at 1m hight μSv/h
1	Entrance in side office building	0.070
2	Room 1 on left	0.068
3	Room2 on left	0.088
4	Entrance of reactor hall	0.064
5	Laboratory 1 on the right	0.046
6	Laboratory 2 on the right	0.052
7	Dark room	0.092
8	Inside reactor hall	0.098
9	Pool edge wall no3	6.84

Table 4. Dose rates inside reactor facility +3.80m office building (Ludlum monitor)

No.	Location	Dose rate at 1m μSv/h
1	Hot Shop Building(H.S.B) entrance	0.110
2	Near channel 3	0.096
3	Near channel 2 beside hot cells	0.083
4	H.S.B. near cell B	0.071
5	H.S.B. near middle hall	0.065
6	H.S.B. wall of cell B	0.076
7	H.S.B. the wall in the middle of the two cells	0.075
8	H.S.B. wall of cell A	073
9	Area in front of H.S.B	0.070

Table 5. Dose rates insideTammuz-2 buildings level -4m offices and reactor hall (Ludlum monitor)

No.	Location	Dose rate at 1m hight µSv/h
1	Entrance of the (-4 m) offices	0.080
2	Left side rooms	0.083
3	First room on Right side rooms	0.081
4	Second room on Right side	0.080
5	Third room on Right side	0.081
6	Last room on Right side	0.082

Table 6. dose rates inside hot shop building (H.S.B.)(Ludlum monitor)

No.	Location	Dose rate at 1m hight µSv/h
1	Area near air condition	0.068
2	Inside air condition room	0.096
3	Touch to smoke detectors	2.18
4	Room 1 on the right	0.065
5	Laboratories	0.070
6	Storage room near different irradiate objects	8.0
7	Primary cooling circuit and purification	0.051

Table 7. Dose rates at different levels of Channel No. 3 (Radgaim monitor).

No.	Location	Dose rate µSv/h
1	Edge of wall no3	0.456
2	Edge of wall no2	3.222
3	-4m inside Channel No 3	10.6
4	-5m inside Channel No 3	14.2
5	-6m inside Channel No 3	18.5
6	-7m inside Channel No 3	15.7

Table 8. Dose rates at different levels of Channel No. 2 (Radgaim monitor)

No.	Location	Dose rate µSv/h
1	Edge of wall no1	0.102
2	Edge of wall no4	0.081
3	-4m inside Channel No 2	0.24
4	-5m inside Channel No 2	0.23
5	-6.5m inside Channel No 2 near irradiated rod	5.8

Table No (9) dose rates measurements at different levels of reactor core chimney (Radgaim monitor).

No.	Location	Dose rate µSv/h
1	+1m above Edge of wall no3	3.35
2	+1m above pool stage	7.24
3	0.0 level at pool stage	6.16
4	-1m inside reactor pool near chimney	10.6
5	-2 m inside reactor pool near chimney	15.2
6	-3 m inside reactor pool near chimney	30.9
7	-4 m inside reactor pool near chimney	56.9
8	-5 m at the edge of top of reactor core beside chimney	141
9	-5.5 m reactor core beside chimney	751
10	-6m reactor core beside chimney	8990
11	-6.5m reactor core beside chimney -7 m reactor core beside chimney	6080 10800

Table 10. Gamma spectroscopy results (S= Soil, SC = mixed Soil and Concrete, BDL = Below Detection Limit)

No	Sample type	Location	Th^{232} Bq/kg	U^{238} Bq/kg	K^{40} Bq/kg	Cs^{137} Bq/kg	Co^{60} Bq/kg
1	S	Office building	42.5±8.1	22.3±5.9	682.6±72	BDL	BDL

		entrance					
2	S	Near chimney	14.7±1.8	9.4±5.9	434.6±42	BDL	BDL
3	S	10 m from chimney	31.3±5.2	28.2±4.2	584.8±56	7.8±1.5	BDL
4	S	10 from hot shop building(H.S.B) gate	20±2.4	17±4.3	596.7±58	BDL	BDL
5	S	10m from H.S.B. in front of the cells	30±4.5	24±4	546.3±54	BDL	BDL
6	S	20m from H.S.B. East	34.4±9.3	14.8±3.8	369.4±46	BDL	BDL
7	S	H.S.B. entrance	15.4±5.6	19.2±4.1	582.4±58	4.2±2.7	BDL
8	S	Near channel- 3	16.2±3.4	28.4±4.5	388±52.6	27.3±2.7	BDL
9	S	Near channel- 2 beside hot cells	13.7±7.8	20±6.2	520.2±69	18.5±2.7	BDL
10	S	In front of reactor building	17.8±2.3	15±3	529±54	BDL	BDL

11	S	20m from reactor building	18.9±7.6	18.5±3.5	488.9±50	3±0.9	BDL
12	S	10m from gallery	32.2±5.2	17.1±4.5	541.4±56	BDL	BDL
13	S	20m in front of H.S.B. near sewerage	22±2.6	29.8±3.5	622.1±61	BDL	BDL
14	SC	Inside reactor hall level 0.0m	24±8.6	25.6±2.4	350±44	15.6± 1.9	BDL
15	S	Level - 4m primary cooling room	25.4±4.8	7.7±2.1	318.7±42	17.8± 2	BDL
16	S	H.S.B near cell B	18.4±4.8	19±4.1	414.3±50	15.5± 2	63.3± 3.4
17	SC	H.S.B near middle hall	23.4±2.1	26.7±4.4	430±51	19.7± 2.2	BDL
18	SC	H.S.B near middle hall	24.4±8.9	24.6±3.8	486±54.4	18.1± 2.2	BDL

RESULT AND DISCUUSIONS

The results of gamma-dose rate levels of reactor core, channel (2&3) and the area around are found in excess of the background radiation levels ,while the maximum dose rates at the reactor core at depth (-7m) about 10.8 mSv/h. The activity concentrations of collected soil samples indicated that the area around reactor core and channel (2&3) are contaminated with Cs-137&Co-60. Individual doses expected from dismantling of the reactor pool are sufficiently high as compared with the occupational dose limit and the individual exemption dose criterion, warrant regulatory action, and must be subjected to the principles of the optimization of radiation protection safety according to ALARA principle as recommended by(IAEA).Access to this area should be controlled and restricted [3, 8].Radiation doses derived from the building debris/rubbles are considered "trivial" for the individuals involved in the management of these materials [10,1 1]. The building debris and rubbles can be handled without causing significant doses to the workers. All activities in the Tammuz-2 reactor decommissioning program have been proposed as generally acceptable/tolerable hazard", with the exception of the dismantling of the reactor pool, which has been proposed [12-15], as high hazard risk.

REFERENCES

1. Safety Report of France Complex at AL-Tuwaitha Site, 1974.
2. IAEA, characterization of radioactivity contaminated sites for remediation purpose, IAEA-TECDOC-1017, IAEA, Vienna, 1998.
3. IAEA, radiological characterization of shutdown nuclear reactors for decommissioning purposes, T.R series No. 389, IAEA, Vienna, 1998.
4. IAEA, “Standard format and content for safety related decommissioning document”, safety series No. 45, IAEA, Vienna, 2005.

5. IAEA, "characterization of radioactive waste forms and packages "T.R. series No. 383, IAEA, Vienna, 1997.
6. Application of the Concepts of Exclusion Exemption and Clearance, IAEA, safety guide No. RS-G-1.7, 2004.
7. International Basic Safety Standards for Protection against Ionizing Radiation and for the Safety of Radiation Sources, Safety Series No. 115, IAEA, Vienna (1996).
8. Decommissioning of Facilities Using Radioactive Material, IAEA Safety Standards Series No. WS-R- 5, IAEA, Vienna (2006) .
9. Decommissioning of Nuclear Fuel Cycle Facilities, IAEA Safety Standards, and Series No. WS-G-2.4, IAEA, Vienna (2001 11
10. Release of Site from Regulatory Control on Termination of Practices Safety Guide, WS-G- 5.1, IAEA, Vienna (2006).
11. Derivation of Activity Concentration Values for Exclusion, Exemption and Clearance, IAEA Safety Standards Series No. 44, IAEA, Vienna (2005).
12. Laboratory Procedure Manual for the Environment Survey Program -ORIS (OAK RIDGE ISTITUTE FOR SCIENCE AND EDUCATION) U.S.A, 2007.
13. ICRP (2000), protection of the public in situations of prolonged radiation exposure, ICRP publication 82; Ann, ICRP 29(1-2).
14. MOTTERSHEAD, C., ORR, C.H., "A gamma scanner for pre-decommissioning monitoring and waste segregation", Nuc. Eng. 371 (1996).
15. IAEA, (1990). Characterization of Radioactively Contaminated Sites for Remediation Purposes, IAEA- TECDOC-1017, Vienna.

Determination of Uranium Concentrations in Some Plants and Soils Samples from Baghdad-Iraq Using CN-85 Track Detector

Essam M.R. Drweesh, Lutfi M.M. Salih, and Roaa T. Abdulla

Department of physics, College of Science, Al-Nahrain University, Baghdad, Iraq

Abstract

The aim of this study is to measure the concentrations of uranium in17 samples of plants and soils collected from different areas in Baghdad city. The technique is based on the counting of α–particles by using the CN-85 track detector that is one of solid state nuclear track detectors (SSNTDs) and fission fragment track technique. The nuclear reaction used as source of uranium fission fragment is U-235 (n-f) obtained by the bombardment of U-235 with thermal neutrons emitted from Am-Be neutron source with thermal neutron flux of 5000 $n/cm^2.s$ for seven days. The concentration of uranium was calculated by comparison with the standard samples. The concentrations of uranium in plants sample ranged between 0.8 and 2.37 ppm with average of 1.59 ppm. The concentrations of uranium in soils samples ranged between 3.67 and 3.99 ppm with average of 3.82 ppm.

Keywords: SSNTDs**,** CN-85**,** uranium, Ra-226**,** Rn-222**,** track detector

قياس تراكيز اليورانيوم لنماذج من النباتات والتربة في مدينة بغداد باستعمال كاشف الأثر النووي CN-85

عصام درويش ولطفي صالح ورؤى عبدالله

خلاصة

قيست تراكيز اليورانيوم لسبعة عشر نموذجا من النباتات والتربة والتي جمعت من مناطق مختلفة في مدينة بغداد. حيث تم حساب تراكيز اليورانيوم من خلال الكشف عن جسيمات ألفا باستخدام تقنية كواشف الأثر النووي في الحالة الصلبة (SSNTDs) نوع CN–85 للكشف عن جسيمات ألفا وشظايا الانشطار. استخدمت تقنية عد أثار شظايا الانشطار النووي والناتج من أنشطار نواة اليورانيوم (U–235) من خلال قصفها بالنيوترونات الحرارية المنبعثة من المصدر النيوتروني (Am–Be) بفيض نيوتروني حراري يبلغ (5×10^{3}n.cm^{-2}s $^{-1}$) ولمدة سبعة أيام متتالية. تم حساب تراكيز اليورانيوم في العينات بالمقارنة مع تراكيز اليورانيوم في النماذج القياسية. تتراوحت تراكيز اليورانيوم في النباتات بين 0.8 و2.37 جزء بالمليون وبمتوسط 1.59 جزء بالمليون . أما تراكيز اليورانيوم في التربة فكانت ضمن المدى 3.67 – 3.99 جزء بالمليون وبمتوسط 382 جزء بالمليون.3.67–3.99 ppm. تعد هذه النتائج مقبولة بالمقارنة مع الحدود المسموح بها دوليا (11.7 ppm).

كلمات مفتاحية: SSNTDs، CN-85، uranium، Ra-226، Rn-222، كواشف الأثر النووي.

Introduction

Uranium is an element found in rocks since the earth was formed. Not all soils and plants contain uranium, but there are some places in the world where uranium is in the bedrock. Other related elements that may be found in association with uranium include Ra-226, Ra-228 and radon Rn-222. These isotopes are a part of a sequence formed through a transformation (decay) process that begins with the most prevalent form of “natural” (unprocessed) uranium U-238. Radioactive material is found

throughout nature. It is in the soils, water, and vegetation. Low levels of uranium, thorium, and their decay products are found everywhere. Some of these materials are ingested with food and water, while others, such as radon, are inhaled [1].

The dose from terrestrial sources also varies in different parts of the world. Locations with higher concentrations of uranium and thorium in their soil have higher dose levels. The major isotopes of concern for terrestrial radiation are uranium and thorium series and their decay products. Soils are made up of four basic components: minerals, air, water, and organic matter. In most soils, minerals represent around 45% of the total volume, water and air about 25% each, and organic matter from 2% to 5% [2].

The mineral portion consists of three distinct particle sizes classified as sand, silt, and clay. Sand is the largest particle that can be considered soil. Sand is largely the mineral quartz, though other minerals are also present. Quartz contains no plant nutrients, and sand cannot hold nutrients [3].

They are leached out easily with rainfall. Silt particles are much smaller than sand. The smallest of all the soil particles is clay. Clays are quite different from sand or silt, and most types of clay contain appreciable amounts of plant nutrients. Clay has a large surface area resulting from the plate-like shape of the individual particles [4].

Sandy soils are less productive than silts, while soils containing clay are the most productive and use fertilizers most effectively. Soil texture refers to the relative proportions of sand, silt, and clay. Loam soil contains these three types of soil particles in roughly equal proportions. sand, loam is a mixture containing relatively a larger amount of sand and a smaller amount of clay, while a clay loam contains a larger amount of clay and a smaller amount of sand. When cosmic radiation interacts with the gases in the atmosphere, it causes nuclear transformations that release particles such as neutrons and protons. These neutrons and protons interact with other nuclei in the atmosphere, producing radioactive nuclei, such as carbon-14 and tritium (hydrogen-3). Carbon-14 is responsible for less than 1 mrem per year of absorbed radiation in humans, and tritium only about 1 microrem. Long-lived radioisotopes in the earth's crust are also a source of absorbed radiation. One of these that is particularly significant is potassium-40, with a half life of 1.3×10^9 years and

making up only 0.019% of all potassium. It is significant because potassium is one of the most abundant elements and because it is an essential component of foods [5].

Experimental details

Seventeen samples of plants (leaf of short trees) and different of soils were collected from many places in Baghdad city as shown in Table 1.

Table 1: Type and location of samples code

Sample code	Type	location
A1	plant	Al-Hurriya square
A2	plant	Baghdad university intersection
A3	plant	Al-Sha'ab main street
A4	plant	Al-Talibiya
A5	plant	Kahramana square
A6	plant	Al-Karrada dakhil
A7	plant	Al-Alawee –al mathaf square
A8	plant	Al-Salhiya
A9	plant	Al-Tahrer square
A10	plant	Bab-al-Muadham
A11	plant	Al- Medan
A12	plant	Street of Dora refinery
A13	soil	Al- Hurriya square
A14	soil	Baghdad university intersection
A15	soil	Kahramana square
A16	soil	Al-Karrada dakhil
A17	soil	Street of Dora refinery

Leaf of trees samples were dried, crushed and sieved through sieve size 212micron, then stored for one month to get a radiological equilibrating. 0.5g was taken from each sample and pressed into a pellet 1cm diameter by using a piston, sheets of 200 µm thickness of CN-85 plastic 1x1cm^2 area were put behind each sample. The samples were irradiated using Am–Be neutron source for seven days with flux of thermal neutrons of 5000n/cm^2.s, which emits fast neutrons in (α,n) reaction, the irradiation time was seven days with influence of thermal neutrons as the following equations [6,7]:

$$^{235}U + {}^{1}_{0}n_{\text{ thermal}} \longrightarrow {}^{236}U \longrightarrow {}^{141}Br + {}^{92}Kr + 3\,{}^{1}_{0}n \quad \ldots\ldots\ldots\ldots\ldots(1)$$

$$^{9}Be + {}^{4}_{2}He \longrightarrow {}^{12}C + {}^{1}_{0}n_{\text{ fast}} + 5.76\ \text{MeV} \quad \ldots\ldots\ldots\ldots\ldots\ldots\ldots\ldots(2)$$

The neutron source was surrounded by a paraffin wax which is used for moderating fast neutrons with energy 10^6 eV to thermal neutrons of energy 0.025eV. (Figure 1).

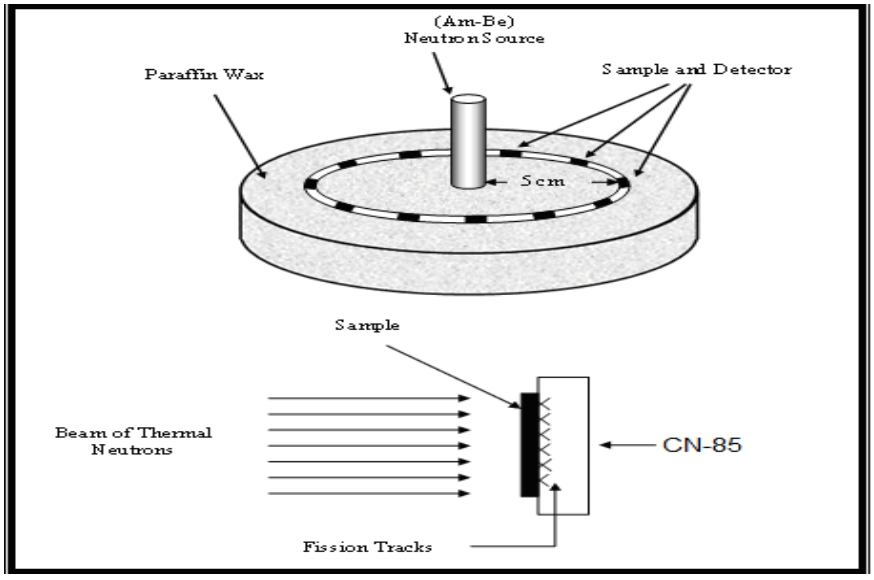

Fig 1: Irradiation of the detectors with samples for neutron source.

After irradiation, we used enchant solution, sodium hydroxide solution (6.25 Normality) for the etching process, which prepared as in the following equation: [8]

$$W = W_{eq} \times N \times V \quad \ldots\ldots\ldots\ldots\ldots\ (3)$$

Where:

W: weight of NaOH that needed to prepare the given normality = 62.5g

W_{eq} : equivalent weight of NaOH = (40g/mole)

V: volume of distilled water = (250 ml).

N: normality = 6.25

The enchant compartment has a volume of 250 mL contains the NaOH solution. This apparatus is closed assembly, except for small vent at the top of the condenser tube, which prevents any change of enchant normality concentration during the experiment due to evaporation. The enchant solution was placed in water bath as type of "Labsco" industrialization in Germany is used in this study. It includes a thermostat, which can be operated over a range of (10–100) ^{o}C. However, the water path was maintained at 60^{o}C and the etching time was 2:30 h, then we washed the detectors with distilled water. After that, the optical microscope type Motic industrialization in Malaysia was used for giving magnifications of up to 400X to measure the number of tracks. The tracks that observed in CN-85 track detector after etching is shown in (Figure 2).

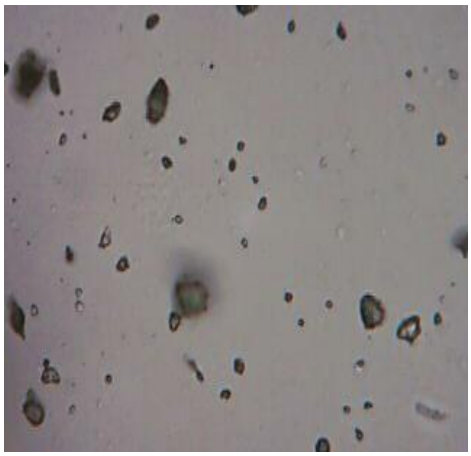

Fig 2: Image of tracks in CN-85 detector after etching

The tracks density is measured using the following equation **[**9**]**:

$$\text{Tracks density } (\rho) = \frac{\text{Average number of total pits (track)}}{\text{Area of field view}} \quad \ldots\ldots\ldots\ldots\ldots\ldots (4)$$

Results and Discussion

The uranium concentrations of the samples were measured by comparison between tracks density registered on the detectors of the samples and that of the standard samples by using the following relation: [10]

$$\frac{\rho_x}{\rho_s} = \frac{C_x}{C_s} \quad \ldots\ldots\ldots\ldots\ldots\ldots\ldots\ldots (5)$$

Where:

ρ_X: tracks density in the unknown sample (tracks/mm^2).

ρ_S: tracks density in the standard sample (tracks/mm^2).

C_S : concentration of uranium in the standard sample (ppm).

C_X : concentration of uranium in the unknown sample (ppm).

By plotting the concentrations of uranium with the tracks densities for the standard samples as shown in Figure 3, the slope of the straight line and equal to (ρ_S/ C_S) then Eq. 5 becomes:

$C_X = (\rho_X / \text{slope})$ ……. (6)

Uranium concentrations in plants and soils are shown in Tables 2 and 3.

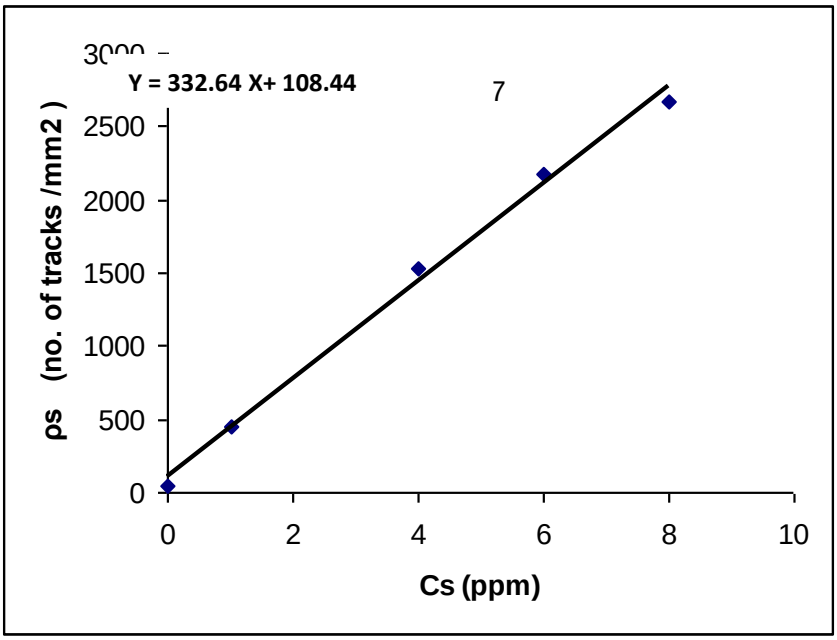

Fig 3: The relationship between the uranium concentrations and tracks densities in the standard samples .

Table 2. Uranium concentration in plants samples.

sample code	tracks density ρ tracks/mm^2)(	uranium concentration (ppm)
A1	616.29 ± 24.82	1.85 ± 1.33
A2	282.96 ± 16.82	0.86 ± 0.09
A3	460.74 ± 21.46	1.38 ± 0.17
A4	266.66 ± 16.32	0.80 ± 0.07
A5	334.81 ± 18.29	1.00 ± 0.10
A6	278.51 ± 16.68	0.83 ± 0.08
A7	791.11 ± 26.81	2.37 ± 1.53
A8	642.96 ± 25.35	1.93 ± 1.38
A9	589.62 ± 24.28	1.77 ± 1.23
A10	594.07 ± 24.37	1.78 ± 1.36
A11	762.96 ± 27.62	2.29 ± 1.51
A12	761.48 ± 27.59	2.29 ± 1.51
average	**529.09 ± 22.53**	**1.59 ± 1.25**

Table 3. Uranium concentration in soils samples.

sample code	tracks density ρ tracks/mm^2)(	uranium concentration (ppm)
A13	1328.88 ± 36.45	3.99 ± 1.99
A14	1220.74 ± 34.93	3.67 ± 1.91
A15	1293.33 ± 35.96	3.88 ± 1.96
A16	1250.37 ± 35.36	3.76 ± 1.93
A17	1274.07 ± 35.69	3.83 ± 1.95
average	**1273.47 ± 35.67**	**3.82 ± 1.94**

The uranium concentration of plants and soils are shown in Figures (4),(5).

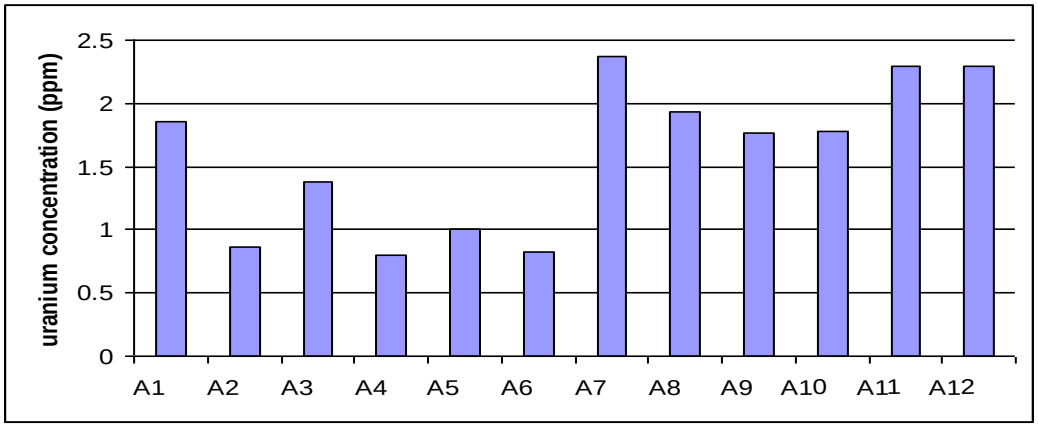

Fig 4: Uranium concentrations in plants samples

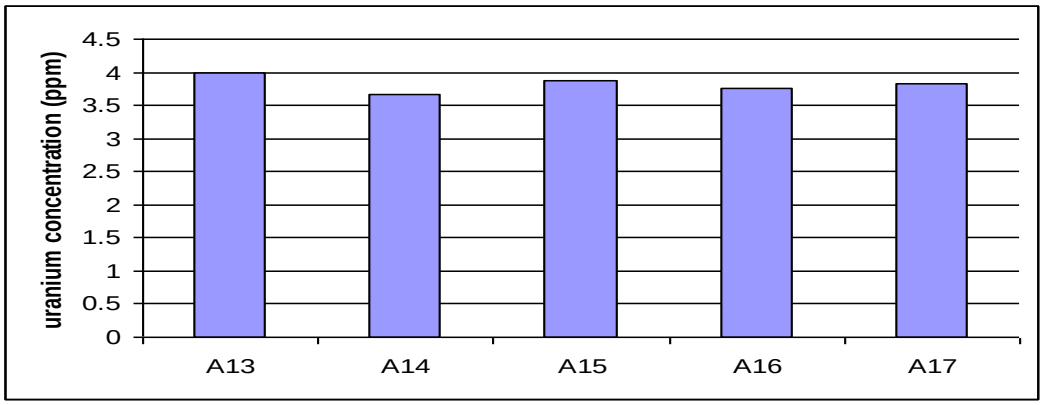

Fig 5: Uranium concentrations in soils samples

Table 2 shows the uranium concentrations of plants samples that vary from (0.8 ppm) to (2.37ppm), the minimum of uranium concentration was (0.8 ppm) in Al-Talibiya sample, and the maximum of uranium concentration was (2.37ppm) in Al-Alawee-almathaf -square sample. The average of the uranium concentrations of plants samples was (1.59ppm). Table (3) shows the uranium concentration of soils samples that vary from (3.67ppm) to (3.99ppm), the minimum of uranium concentration was (3.67ppm) in Baghdad university intersection sample, and the maximum of uranium concentration was (3.99ppm) in Al-Hurriya- square sample. The average of the uranium concentrations of soils samples was (3.82ppm). The average of the uranium concentration of soils was more than the average of the uranium concentration of plants because the soils are contained sands, slit and clay that comes from nature and air pollution such as smoke of cars, generators and factories. The results of the uranium concentration of plants and soils are quite low compared with the allowed limit (11.7 ppm) [11].

Reference

1. Natural radioactivity of rocks occurring in the contact zone of the karkonosze massif with the szklarska poreba schist belt Aleksandra BIEDA * and Grzegorz LIZUREK Acta Geodyn. Geomater., Vol. 5, No. 2 (150), 225-231, 2008.
2. [United Nations Scientific Committee on the Effects of Atomic Radiation. UNSCEAR 2000 report to the general assembly, with scientific annexes. Sources and effects of ionizing radiation. United Nations, New York, 2000.
3. UNSCEAR, Sources and Effects of Ionizing Radiation Report to the General Assembly, Scientific Committee on the Effects of Atomic Radiation UN, New York, p 34-52, 2000.
4. European Communities. ATLAS of Cesium deposition on Europe after the Chernobyl accident, 2001.
5. UNSCEAR "Sources, effects and risks of ionization radiation", United Nations Scientific Committee on the Effects of Atomic Radiation, Report to the General assembly, with Annexes, New York , 2005.
6. Azam A. Naqvl, A.H and Srivastava, D.S, Nucl.Geophys.Vol.9, No.6, 2006.

7. CIUFFO, Liliana E.C.; VELASCO, Hugo; BELLI, María; SANSONE, Umberto. soil-to-plant transfer for individual species in semi-natural grassland. Influence of potassium soil . *Journal Radiation Research*, vol. 44, no. 3, p. 277, 2003.
8. Al-Baidhani, Mustafa A., " Determination of the Radioactivity in Soil and Water samples in Baghdad, Karbala and Basrah ", M. Sc. Thesis, Al-Nahrain University, College of Science, 2006.
9. Lymburner, D. "Another Human Experiment", DU Education Project, Metal of Dishonor, International Action Center, NewYork, p 45,98, 2003.
10. Mazin M.Elias,N.F.Tawfiq and Doswer H.G., Conference On The Effect of Deepleted Uranium Weaponary on Human and Enviroment in Iraq ,2002.
11. United Nations Scientific Committee on the Effects of Atomic Radiation, UNSCEAR "Sources, Effect, and Risks of Ionizing Radiation", Report to the general Assembly with Scientific Annexes, United Nations, 1993.